MEDICAL UNIVERSITY OF VIENNA

Immune-microbe interactions in the context of the lung

Doctoral thesis at the Medical University of Vienna
for obtaining the academic degree

Doctor of Philosophy

Submitted by

Dr. med. univ. Martin Watzenböck

Supervisor:
Univ.-Prof. Dr. Sylvia Knapp, Ph.D.
Co-Supervisor:
Philipp Starkl, PhD
Medical University of Vienna,
Department of Internal Medicine 1,
Research Division of Infection Biology,
Währinger Gürtel 18-20, 1090 Vienna, Austria
&
Research Center for Molecular Medicine (CeMM) of the
Austrian Academy of Sciences

Vienna, 06/2022

Declaration

Martin Watzenböck, MD, conducted his PhD studies under the supervision of Prof. Dr. Sylvia Knapp, PhD at the (i) Department of Medicine I, Research Division of Infection Biology, Medical University of Vienna and (ii) the Research Center for Molecular Medicine (CeMM) of the Austrian Academy of Sciences. Additionally, parts of his PhD studies were conducted abroad, at the Service de Pneumologie, Centre Hospitalier Universitaire Vaudois (CHUV), Lausanne, Switzerland (three months) and the Department of Immunology and Pathology, Monash University, Melbourne, Australia (three months), where he analyzed critical data under the supervision of Prof. Dr. Benjamin Marsland. The work abroad was granted by the FWF-funded PhD program 'Cell Communication in Health and Disease' (CCHD) at the Medical University of Vienna and a Böhringer Ingelheim Foundation Travel Grant.

For the publication "Lipocalin 2 modulates dendritic cell activity and shapes immunity to influenza in a microbiome dependent manner" included in chapter 2.1 of this thesis, Martin Watzenböck conceptualized the project, conducted formal analysis, performed most experiments and wrote the original draft of the paper. Barbara Drobits and Philipp Starkl conceptualized the project, performed experiments and analyzed data. Sophie Zahalka performed experiments and helped with visualization. Anna-Dorothea Gorki, Asma Farhat, Federica Quattrone, Anastasiya Hladik, Karin Lakovits, Gabriel M. Richard and Therese Lederer contributed to experiments. Birgit Strobl, Gijs A. Versteeg provided resources and methodological advice. Sylvia Knapp conceptualized and administrated the project and acquired funding. Sylvia Knapp and Philipp Starkl were also involved in writing the original draft of the manuscript and jointly supervised the project. All authors reviewed the final draft of the manuscript.

For the publication "Multi-omics profiling predicts allograft function after lung transplantation" included in chapter 2.2 of this thesis, Martin Watzenböck conceived the project, analyzed data, performed bioinformatics analyses and wrote the manuscript. Anna-Dorothea Gorki, Federica Quattrone, Stefanie Widder and Sylvia Knapp conceived the project; Stefan Schwarz, Christopher Lambers, Peter Jaksch, Nina Rahimi and Konrad Hoetzenecker collected samples and clinical data, performed transplantations and managed patient follow-ups; Karin Lakovits, Federica Quattrone, Anna-Dorothea Gorki, Riem Gawish, Philipp Starkl, Sophie Zahalka, Dörte Symmank and Tyler Artner processed and analyzed samples; Kristaps Klavins performed

metabolomic and lipidomic analyses, Riem Gawish analyzed flow cytometry data; Florian Frommlet provided statistical expertise to the study design, Céline Pattaroni, Nikolaus Fortelny and Benjamin Marsland provided technical and analytical support; Stefanie Widder co-supervised the analytical part performed by me and contributed to the writing of the manuscript. Sylvia Knapp supervised the project, obtained ethical approval, acquired funding and wrote the manuscript. All authors approved the final version of the manuscript.

Table of contents

List of figures

List of tables

Abstract

The lung and airways are in constant contact with the environment and potential entry sites for various airborne pathogens. Due the crucial function of the lung, immune responses to these pathogens need to be of high efficiency. However, considering the delicate nature of lung tissue, they also need to be tightly regulated. Aberrant immune system activity and exaggerated immune responses contribute to various pathological processes. These can ultimately lead to pulmonary dysfunction, among them, immunopathology during viral infections and the development of chronic lung allograft dysfunction (CLAD) after lung transplantation.

The lung and airways harbor a unique microbiome, and recent evidence shows an important role of these microbiota in the regulation of the lung immune system. However, the precise regulatory mechanisms, the bacterial strains involved and their consequences for pulmonary health and disease are insufficiently understood. Furthermore, microbes colonizing distant body sites directly and indirectly influence pulmonary immune responses, as illustrated by the recently described 'gut-lung-axis'.

In the first part of this thesis, we investigated the role of Lipocalin-2 (LCN2), an antimicrobial protein, on the pulmonary immune system. Using RNA-sequencing of lung macrophages and dendritic cells (DCs) harvested from wild type (WT) and *Lcn2*$^{-/-}$ mice, we observed strong effects on lung CD103^{+} DC gene expression, with differential regulation of genes involved in antiviral immunity. These results could be validated in a mouse model of influenza infection, whereby LCN2 protected from excessive disease morbidity and mortality independent of the lung viral load. These effects could be attributed to increased numbers of CD8^{+} T cells in the lungs of *Lcn2*$^{-/-}$ mice after influenza infection, which we could link to increased antigen presentation by CD103^{+} DCs. Considering the absence of LCN2 on DC antigen presentation *in vitro*, and the antimicrobial effects exerted by LCN2, we speculated that the effects of LCN2 on antiviral immunity might be mediated via altered microbiota in *Lcn2*$^{-/-}$ mice. Using 16S rRNA gene sequencing, we found an effect of LCN2 on gut microbe composition. Interestingly, lung CD8^{+} T cell responses could be equalized by co-housing or antibiotic treatment of WT and *Lcn2*$^{-/-}$ mice, indicating that the effects of LCN2 on antiviral immunity are indeed modulated via the microbiome.

In the second part of the thesis, we investigated changes in the lung microbiome, metabolome, lipidome and broncho-alveolar lavage cell composition (BAL) after lung transplantation in a cohort of 78 lung transplant recipients. Each of the investigated

data-sets exhibited distinct temporal dynamics, and pulmonary microbial diversity rapidly increased after transplantation. By comparing the pre-transplant (donor) lung microbiome to matched samples after transplantation, we revealed a rapid divergence of microbial profiles with replacement of the donor microbiome. Interestingly, the established lung microbiome correlated with recipient factors, particularly the transplant indication, even after transplantation. Using a machine learning approach, we could predict future changes in lung function from microbial data, suggesting that the lung microbiome might be a biomarker for allograft dysfunction.

In summary, our data give further insights into the complex interplay between the microbiome and the pulmonary immune system, and reveal important roles of this interplay for antiviral immunity and allograft function after lung transplantation.

Zusammenfassung

Die Lunge und die Atemwege stehen in ständigem Kontakt mit der Umwelt und sind potenzielle Eintrittspforten für verschiedene über die Luft übertragene Krankheitserreger. Aufgrund der essentiellen Funktion der Lunge müssen die Immunreaktionen auf diese Krankheitserreger sehr effizient sein, aber angesichts der empfindlichen Natur des Lungengewebes auch streng reguliert werden. Eine abweichende Aktivität des Immunsystems und übertriebene Immunreaktionen tragen zu verschiedenen pathologischen Prozessen bei, die letztlich zu Lungenfunktionsstörungen führen, darunter Immunpathologie bei Virusinfektionen und CLAD (*chronic lung allograft dysfunction*) nach Lungentransplantation.

Die Lunge und die Atemwege beherbergen ein einzigartiges Mikrobiom und rezente Erkenntnisse zeigen, dass diese Mikroben eine wichtige Rolle bei der Regulierung des Lungenimmunsystems spielen. Die genauen Regulationsmechanismen, die beteiligten Bakterienstämme und ihre Auswirkungen auf die Gesundheit und Krankheit der Lunge sind jedoch unzureichend erforscht. Darüber hinaus beeinflussen selbst Mikroben, die entfernte Körperstellen (zum Beispiel den Darm) besiedeln, direkt und indirekt die Immunantwort der Lunge.

Im ersten Teil dieser Arbeit untersuchten wir die Rolle von Lipocalin-2 (LCN2), einem antimikrobiellen Protein, auf das pulmonale Immunsystem. Mit Hilfe der RNA-Sequenzierung von Lungenmakrophagen und dendritischen Zellen (DCs) aus wildtyp (WT)- und *Lcn2*$^{-/-}$ Mäusen konnten wir starke Auswirkungen auf die Genexpression von *CD103*$^{+}$ DCs in der Lunge feststellen, wobei Gene, die an der antiviralen Immunität beteiligt sind, unterschiedlich reguliert wurden. Diese Ergebnisse konnten in einem Mausmodell für Influenza-Infektionen bestätigt werden, wobei LCN2 unabhängig von der Viruslast in der Lunge vor übermäßiger Krankheitsmorbidität und Mortalität schützte. Diese Effekte konnten auf eine erhöhte Anzahl von CD8^{+} T-Zellen in der Lunge von *Lcn2*$^{-/-}$ Mäusen nach einer Influenza-Infektion zurückgeführt werden, was wir mit einer verstärkten Antigenpräsentation durch CD103^{+} DCs in Verbindung bringen konnten. In Anbetracht fehlender Effekte von LCN2 auf die DC-Antigenpräsentation *in vitro* und der antimikrobiellen Effekte von LCN2 spekulierten wir, dass die Auswirkungen von LCN2 auf die antivirale Immunität über ein verändertes Mikrobiom in *Lcn2*$^{-/-}$ Mäusen vermittelt werden könnten. Mithilfe von 16S rRNA-Gen Sequenzierung konnten wir eine Wirkung von LCN2 auf die mikrobielle Zusammensetzung des Darms feststellen. Interessanterweise konnte die Reaktion der

$CD8^+$ T-Zellen in der Lunge durch gemeinsame Haltung oder Antibiotikabehandlung von WT- und *Lcn2*$^{-/-}$ Mäusen ausgeglichen werden, was darauf schließen lässt, dass die Auswirkungen von LCN2 auf die antivirale Immunität tatsächlich über das Mikrobiom moduliert werden.

Im zweiten Teil der Arbeit untersuchten wir Veränderungen des Lungenmikrobioms, des Metaboloms, des Lipidoms und der Zellzusammensetzung der broncho-alveolären Lavage (BAL) nach Lungentransplantation in einer Kohorte von 78 Lungentransplantatempfängern. Jeder der untersuchten Datensätze wies eine ausgeprägte zeitliche Dynamik auf, und die mikrobielle Vielfalt in der Lunge nahm nach der Transplantation rasch zu. Durch den Vergleich des Lungenmikrobioms vor der Transplantation (Spender) mit den entsprechenden Proben nach der Transplantation konnten wir eine rasche Divergenz der mikrobiellen Profile mit Ersatz des Spendermikrobioms beobachten. Interessanterweise korrelierte das etablierte Lungenmikrobiom auch nach der Transplantation mit Empfängerfaktoren, insbesondere der Transplantationsindikation. Mithilfe eines „machine learning"-Ansatzes konnten wir künftige Veränderungen der Lungenfunktion aus mikrobiellen Daten vorhersagen, was darauf hindeutet, dass das Lungenmikrobiom ein Biomarker für Funktionsstörungen bei Allotransplantaten sein könnte.

Zusammenfassend lässt sich sagen, dass unsere Daten weitere Einblicke in das komplexe Zusammenspiel zwischen dem Mikrobiom und dem pulmonalen Immunsystem geben und eine wichtige Rolle dieses Zusammenspiels in der Regulation antiviraler Immunantworten und die Transplantatfunktion nach einer Lungentransplantation aufzeigen.

Publications arising from this thesis

Lipocalin 2 modulates dendritic cell activity and shapes immunity to influenza in a microbiome dependent manner

Martin L Watzenboeck, Barbara Drobits, Sophie Zahalka, Anna-Dorothea Gorki, Asma Farhat, Federica Quattrone, Anastasiya Hladik, Karin Lakovits, Gabriel M Richard, Therese Lederer, Birgit Strobl, Gijs A Versteeg, Louis Boon, Philipp Starkl*#, Sylvia Knapp*#

PLoS Pathog. 2021 Apr 27;17(4):e1009487. doi: 10.1371/journal.ppat.1009487.

Multi-omics profiling predicts allograft function after lung transplantation.

Martin L Watzenboeck*, Anna-Dorothea Gorki*, Federica Quattrone*, Riem Gawish*, Stefan Schwarz*, Christopher Lambers, Peter Jaksch, Karin Lakovits, Sophie Zahalka, Nina Rahimi, Philipp Starkl, Dörte Symmank, Tyler Artner, Céline Pattaroni, Nikolaus Fortelny, Kristaps Klavins, Florian Frommlet, Benjamin J Marsland, Konrad Hoetzenecker, Stefanie Widder*, Sylvia Knapp*#

Eur Respir J. 2022 Feb 3;59(2):2003292. doi: 10.1183/13993003.03292-2020.

*These authors contributed equally.

Corresponding authors.

Acknowledgments

I would like to thank my supervisor Sylvia for giving me the opportunity to undergo my PhD in her laboratory, for her continuous guidance and for her immeasurable support during the research that led to this thesis.
I thank my co-supervisor Philipp for his constant support and for teaching me not only countless experimental techniques and approaches, but also to think like a scientist.
I would also like to express my gratitude to all the Knapp lab members for their friendship, for their help and encouragement, and for making it a pleasure to come to work daily.
Lastly, I would like to thank my parents, Gudrun and Max, my brother Clemens, and my girlfriend Ines for your emotional support during this journey. This would not have been possible without you!

Abbreviations

AD: Alzheimer's disease

AFE: Alveolar fibroelastosis

AMR: Antibody-mediated rejection

APC: Antigen presenting cell

ASC: Apoptosis-associated speck-like protein

BAL: Bronchoalveolar lavage

BOS: Bronchiolitis obliterans syndrome

CD: Cluster of differentiation

CF: Cystic fibrosis

CLAD: Chronic lung allograft dysfunction

COPD: Chronic obstructive pulmonary disease

CXCR2: Chemokine (C-X-C motif) receptor 2

DAS: Donor-specific antibodies

DC: Dendritic cell

GPR: G protein coupled receptor

HA: Haemagglutinin

HFD: High fat diet

HMGB1: High mobility group box 1

ICAM1: Intercellular adhesion molecule 1

IFN: Interferon

IFTM: Interferon-induced transmembrane protein

IL: Interleukin

IL-10: Interleukin-10

IL-1beta: Interleukin-1beta

IL-6: Interleukin-6

IRF7: IFN-regulatory factor 7

ISG: IFN-stimulated gene

Iron: Fe3+

LCMV: Lymphocytic choriomeningitis virus

LRR: Leucine-rich repeat

Lipocalin 2: LCN2

Ly6C: Lymphocyte antigen 6 complex, locus C1

M1: Matrix protein

M2: Membrane protein
MAVS: Mitochondrial antiviral signalling protein
MC4R: Melanocortin 4 receptor
MHC: Major histocompatibility complex
MYD88 : Myeloid differentiation primary response 88
NA: Neuraminidase
NASH: Non-alcoholic steatohepatitis
NEP: Nuclear export protein
NF-kappaB: Nuclear factor-kappaB
NK cells: Natural killer cells
NLRP3: NOD-, LRR- and pyrin domain-containing 3
NOD: Nucleotide-binding and oligomerization domain
NS1: Non-structural protein
Nanomolar: nM
Neutrophil gelatinase-associated lipocalin : NGAL
OAS: 2′-5′-oligoadenylate synthase
PAMP: Pathogen-associated molecular pattern
PDGF-D: Platelet-derived growth factor receptor-D
PRR: Pattern-recognition receptor
RAS: Restrictive allograft syndrome
RIG-I: Retinoic acid-inducible gene I
RNA: Ribonucleic acid
RNase L: Ribonuclease L
S1P: Sphingosine-1-phosphate
SCFA: Short chain fatty acid
ssRNA: Single-stranded RNA
TIR: Toll/Interleukin-1 Receptor
TLR: Toll-like receptor
TNF: Tumor necrosis factor
TRIF: TIR-domain-containing adapter-inducing interferon-β
WT: wild type

1 Introduction

1.1 Lipocalin 2

Lipocalin 2 (LCN2), also referred to as neutrophil gelatinase-associated lipocalin (NGAL) or oncogene 24p3 is a ~25 kDa secreted protein (Figure 1) constituted of 178 amino acids, which belongs to the lipocalin family (Asimakopoulou et al., 2016). This family is comprised of small secreted proteins with a high level of functional and structural diversity. These proteins are generally distinguished by a wide array of molecular-recognition capabilities, including their binding to specific receptors located at the cell surface, their formation of macro-molecular complexes and, in particular, their capability to bind small hydrophobic molecules (Flower, 1996). LCN2 is expressed on a variety of tissues and cell types (Figure 2) and plays a role in multiple biological processes.

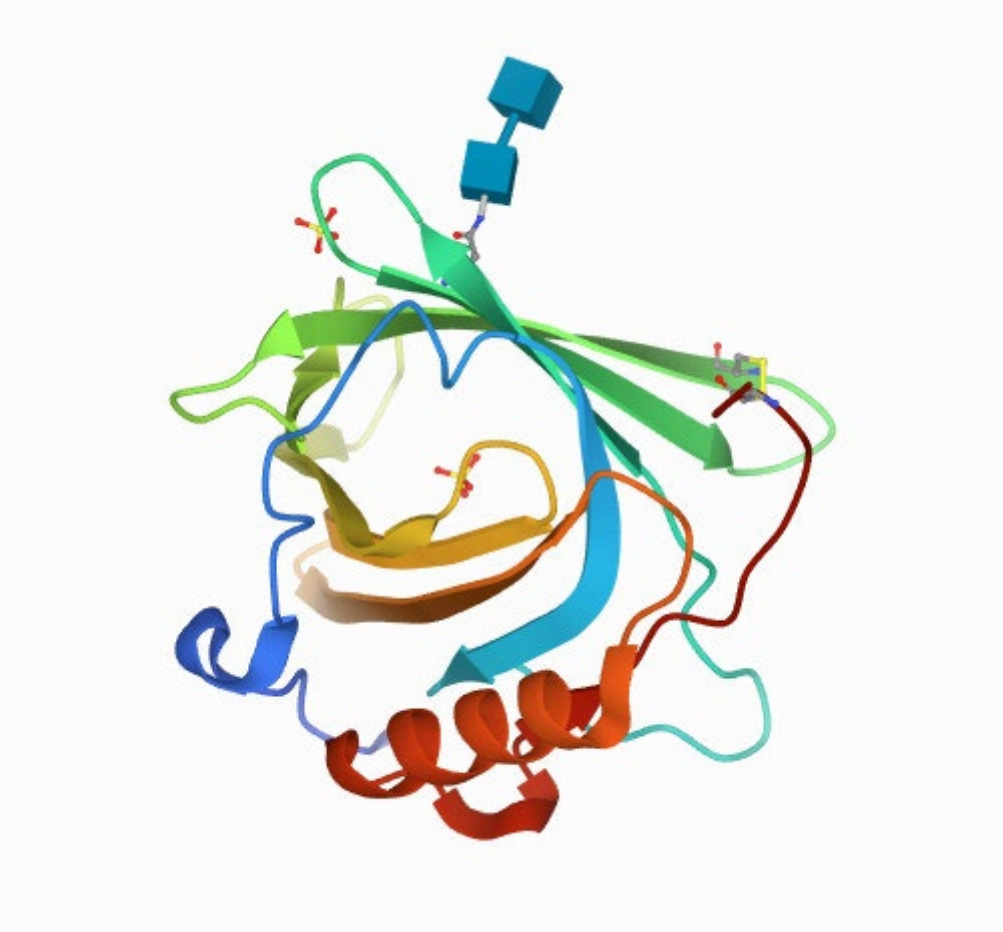

Figure 1: LCN2 structure. Adapted from RCSB Protein Databank (https://www.rcsb.org/, ID: 1DFV (Goetz et al., 2000))

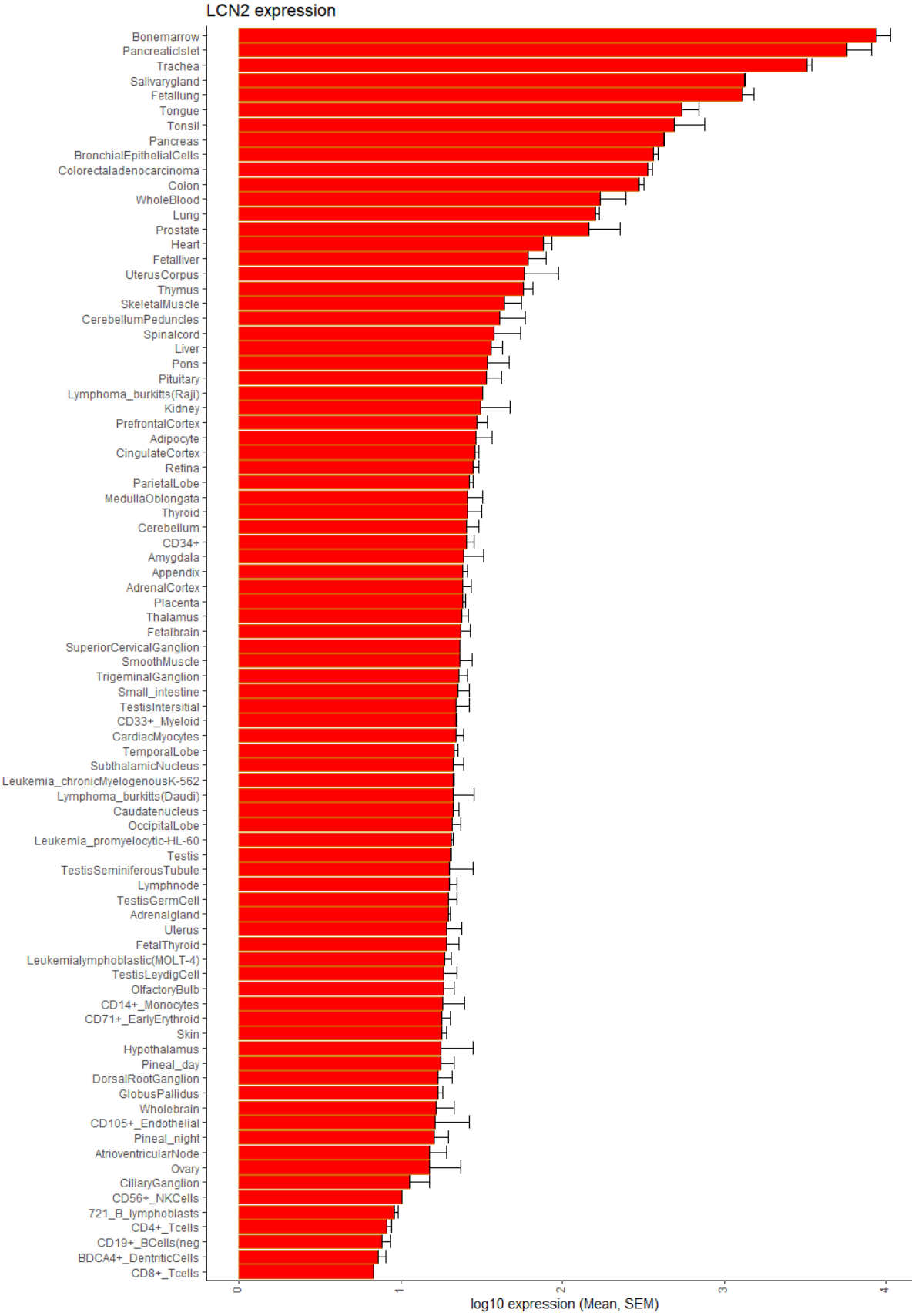

Figure 2: Lcn2 expression pattern (mean, SEM), adapted from biogps.org(Wu et al., 2009), Dataset: GeneAtlas U133A, gcrma.

1.1.1 The role of LCN2 during inflammation

Innate immune responses are the first line defense against pathogenic bacteria or viruses. The innate immune system consists of multiple interacting cellular and molecular components, including acute phase proteins, which are increased markedly during the early stages of infection and directly contribute to the elimination of pathogens by various mechanisms (Medzhitov, 2007). LCN2 is part of the acute phase reaction and plays an important role in innate immunity towards bacterial infections by inhibiting bacterial iron uptake. Free iron (Fe^{3+}) availability is tightly regulated through iron binding proteins such as transferrin and ferritin (Andrews, 2000). As a result, the concentration of free Fe^{3+} is as low as 10^{-18} M under physiological conditions (Ratledge and Dover, 2000). Therefore, the acquisition of iron is a remarkable challenge for all organisms. To prevent iron shortage, bacteria can produce and excrete siderophores (low-molecular weight molecules that bind iron with high affinity), which leads to the localization of iron complexes on the bacterial cell surface, where they can be internalized (Ratledge and Dover, 2000). LCN2 could be shown to bind to iron in association with siderophores, exerting bacteriostatic properties (Goetz et al., 2002). Additionally, being part of the acute-phase reaction, LCN2 is markedly increased upon Toll-like receptor 4 (TLR4) activation (Liu and Nilsen-Hamilton, 1995). As a consequence, *Flo et al* could show in 2004 that *Lcn2*$^{-/-}$ mice display a significantly greater bacterial burden and increased mortality after infection with *Escherichia coli (Flo et al., 2004)*. Following work demonstrated that these effects are not limited to *E. coli*: The siderophore-scavenging properties of LCN2 confer protection against infections with *Salmonella thyphimurium* (Nairz et al., 2009)*, Mycobacterium tuberculosis* (Saiga et al., 2008) and *Klebsiella pneumoniae* (Chan et al., 2009)*,* all of which are dependent on siderophores, or in the case of *M. tuberculosis*, carboxymycobactins, which are also bound by LCN2 (Holmes et al., 2005). In line with these effects, LCN2 demonstrates high expression in barrier tissues exposed to microorganisms, e.g. the lungs (Cowland and Borregaard, 1997).

While the effect exerted by LCN2 as a scavenger of bacterial siderophores is its best known biological function, recent work has shown that LCN2 has further immunomodulatory effects. Independent of its antibacterial properties, LCN2 could be shown to protect from lipopolysaccharide (LPS)-induced sterile endotoxemia, which was linked to an increased LPS-induced immune cell apoptosis and proinflammatory

gene expression in peritoneal exudate cells (Srinivasan et al., 2012). Another study, which found LCN2 to be the most substantially upregulated protein in the central nervous system after challenge with peripheral LPS also found increased levels of pro-inflammatory cytokines and worsened behavioral phenotypes after LPS-challenge in *Lcn2*$^{-/-}$ mice compared to their WT counterparts (Kang et al., 2018). LCN2 could also be shown to inhibit inflammation in murine nephrotoxic serum nephritis, by limiting cytokine production via Toll-like receptor 2 (TLR2) signaling (Eller et al., 2013). Contrary to its protective effects during infections with siderophore dependent pathogens, LCN2 exhibits detrimental effects in a mouse model of pneumonia caused by *S. pneumoniae*, a pathogen that does not depend on siderophores for iron uptake: Here, *Lcn2*$^{-/-}$ *mice* display decreased bacterial burdens and increased survival after infection, which is associated with LCN2-induced interleukin 10 (IL-10; an anti-inflammatory cytokine) production by macrophages and a deactivation of macrophages by LCN2 (Warszawska et al., 2013).

Another mechanism by which LCN2 can influence inflammatory processes is via shaping the intestinal microbiome. Moschen *et al.* could show that LCN2 decreased early-onset colitis and protected from colonic tumors resulting from IL-10 deficiency by altering the intestinal microbiome, specifically by preventing the bloom of facultative pathogenic *Alistipes sp*., which depend on siderophores for iron uptake (Moschen et al., 2016). Another study found that LCN2 can already alter intestinal microbial communities at baseline, and that upon IL-10 deficiency and dextran sulfate sodium (DSS)-exposure induced colitis, this resulted in exacerbated intestinal inflammation, which could be prevented by antibiotic treatment and transferred via cohousing of mice (Singh et al., 2016).

1.1.2 LCN2 in iron uptake and metabolism

Cellular iron uptake is of fundamental importance for cell metabolism, growth and development, which is why multiple proteins are involved in iron uptake and metabolism. While most tissues acquire iron via the uptake of iron-loaded transferrin (Wallace, 2016), inhibition of the transferrin pathway does not block organogenesis (Huggenvik et al., 1989). Since iron is essential for all cells and required for basic biological processes (Camaschella et al., 2020), this indicates the existence of additional proteins that can facilitate cellular iron uptake. One of these proteins is LCN2, which could be shown to bind iron and deliver it to the cytoplasm, where it acts

as an activator or repressor of iron-related genes (Devireddy et al., 2005). While the authors did not perform a precise characterization of the chemical bond between iron and LCN2, they reported that it might involve a mammalian siderophore. More recently, chemical siderophore equivalents were identified and characterized through their association with LCN2, which remains the only known mammalian siderophore-binding protein (Correnti and Strong, 2012).

To limit the pool of available iron to potential pathogens, mammalian hosts lower systemic iron levels through various mechanisms, which leads to hypoferrinemia (Ganz and Nemeth, 2009) and, thus, also ameliorates iron-dependent oxidative stress (Hentze et al., 2004). The importance of LCN2 as acute phase protein (which is overexpressed early during inflammatory conditions) (Liu and Nilsen-Hamilton, 1995) is highlighted by work using a mouse model of LPS-induced sterile inflammation, where *Lcn2*$^{-/-}$ mice show delayed hypoferremia (Srinivasan et al., 2012), increased oxidative stress, immune cell apoptosis and exaggerated inflammatory gene expression. Similar results could be found in the context of neuroinflammation induced by peripheral LPS injection, after which *Lcn2*$^{-/-}$ mice demonstrated exacerbated proinflammatory cytokines and transcriptional profiles in the central nervous system (Kang et al., 2018). The effects of LCN2-dependent iron trafficking can also promote iron export, reducing intracellular iron content and leading to an increased production of proinflammatory cytokines. This could be observed in mice infected with the intracellular pathogen *Salmonella enterica* Serovar Typhimurium, where elevated intracellular iron in *Lcn2*$^{-/-}$ macrophages was linked to increased expression of the anti-inflammatory cytokine IL-10 and decreased expression of the proinflammatory cytokines TNF (tumor necrosis factor) and IL-6 (Nairz et al., 2015). By promoting a proinflammatory macrophage polarization, LCN2 enhances bacterial killing and clearance in this model. It can be concluded that the effects of LCN2 on both iron homeostasis and inflammation are context and cell-type dependent.

The effects of LCN2 on iron homeostasis can also have detrimental effects. For example, in the J20 mouse model of Alzheimer's disease (AD), LCN2-deficiency improved AD-like behavioral, cognitive and histopathological changes (Dekens et al., 2018). The authors concluded that LCN2 likely contributes to brain iron dysregulation in AD.

1.2 Influenza infection

Influenza is an infectious disease of the respiratory tract caused by viruses belonging to the influenza A and B genera. All influenza viruses are single stranded negative-strand RNA viruses, which contain an envelope surrounding the capsid. Their genomes are comprised of eight RNA segments, which fulfill similar functions in influenza A and B viruses, encoding the viral RNA polymerase subunits (PB1, PB2 and PA), which are the largest of the RNA segments, the viral glycoproteins haemagglutinin (HA) and neuraminidase (NA), as well as the viral nucleoprotein (NP), matrix (M1) and membrane (M2) proteins and the nonstructural (NS1) and nuclear export protein (NEP). Both the RNA segments 7 and 8 encode two separate proteins: Segment 7 encodes M1 and M2, whereby segment 8 encodes NS1 and NEP (Figure 3) *(Krammer et al., 2018)*.

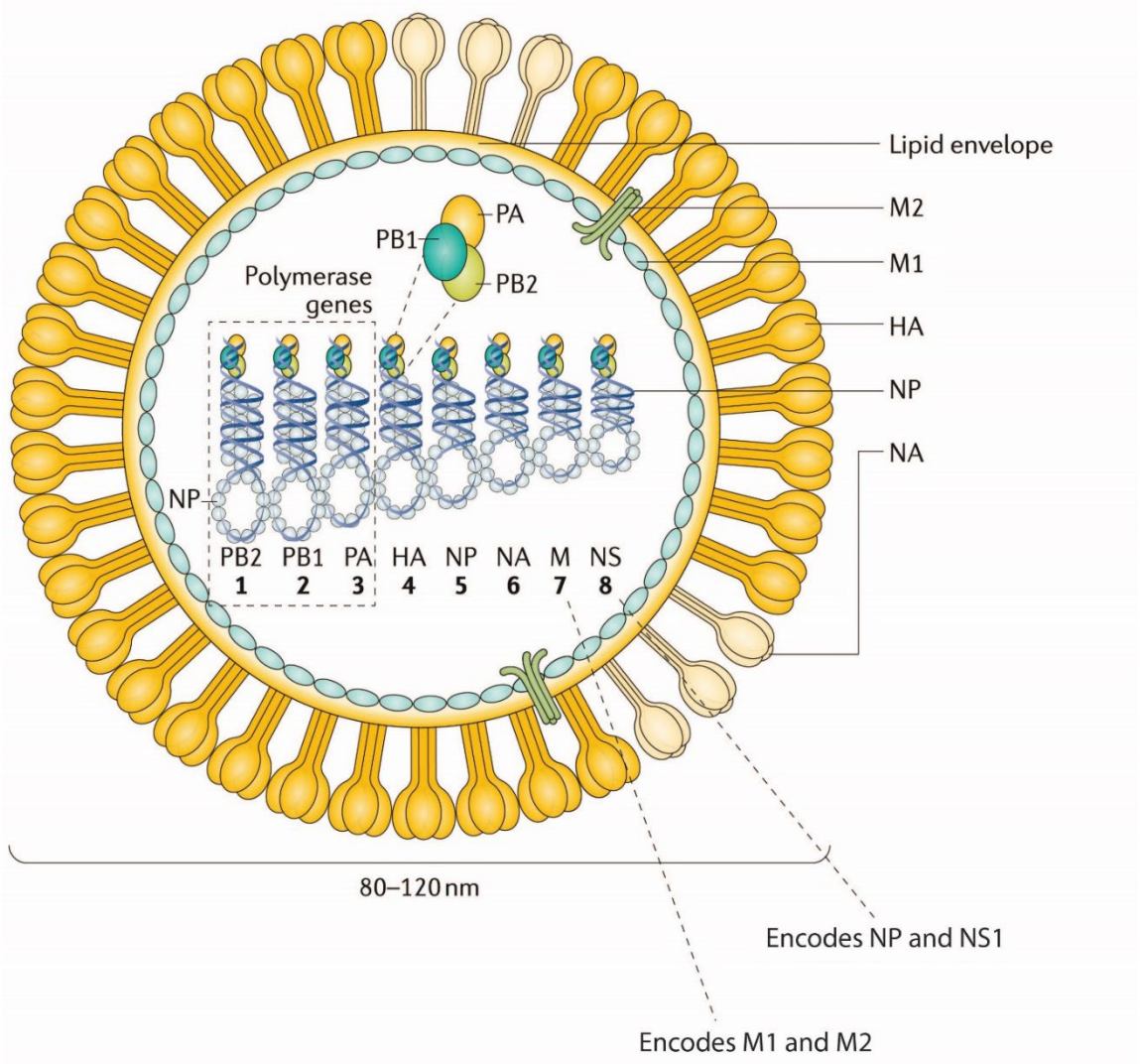

Figure 3: Influenza virus genome and structure. Adapted from (Krammer et al., 2018)

The glycoproteins HA and NA are located on the virion surface. HA mediates two functions: The binding of the virus to the target cell surface (Edinger et al., 2014), which is followed be internalization of the virus, and the fusion of the viral envelope with the endosomal membrane (Banerjee et al., 2013). NA enables cleaving from the host cell during viral release (Dou et al., 2018).

1.2.1 Epidemiology

Influenza occurs in seasonal epidemics, which cause the major burden of disease in humans, and sporadic pandemics. Most seasonal influenza cases occur in children, but the highest morbidity is found in the very young (Krammer et al., 2018), very old or immunocompromised (Kim et al., 2018). Age seems to play a particularly important role in seasonal influenza epidemics. For example, the United States Center for Disease Control and Prevention (CDC) reports a mortality rate of 1.2 per 100,000 for people aged 18-49 years, but a mortality rate of over 40 per 100,000 for people aged more than 65 years, for the 2018-2019 flu season (Centers for Disease Control and Prevention, 2021, September 29) (Figure 4).

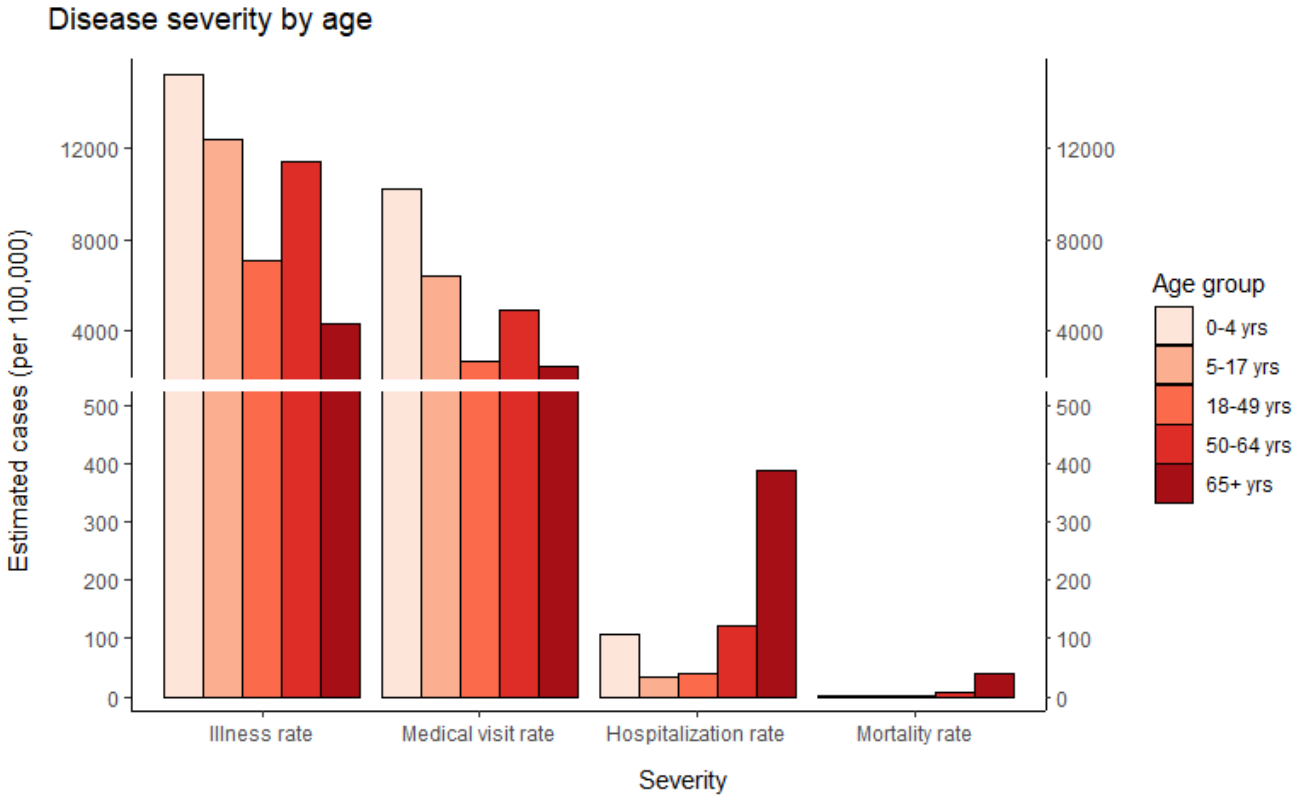

Figure 4: Estimated cases per 100,000 for the US 2018-2019 epidemic, grouped according to disease severity. Data from CDC (Centers for Disease Control and Prevention, 2021, September 29).

Influenza A has an extensive animal reservoir, primarily in aquatic birds (Dunning et al., 2020). Unlike influenza epidemics, influenza pandemics occur as a result of a novel influenza A virus crossing the species barrier and altering their surface antigens through antigenic shift, enabling efficient human-to-human transmission (Abadia-Molina et al., 2006). In the past 100 years, four influenza pandemics have occurred (Table 1), with the 1918 Spanish influenza causing between 17 and 100 million deaths the most severe.

Name	**Date**	**Virus subtype**	**Death toll**	**References**
Spanish influenza	1918-1920	H1N1	17-100 million	(Mills et al., 2004), (Spreeuwenberg et al., 2018), (Morens and Fauci, 2007)
Asian influenza	1957–1958	H2N2	1-4 million	(Viboud et al., 2016)
Hong Kong influenza	1968-1969	H3N2	1-4 million	(Jester et al., 2020)
Swine influenza	2009	H1N1	151,700–575,400	(Dawood et al., 2012)

Table 2: Influenza pandemics of the past 100 years

1.2.2 Immunity to influenza infection

The mucosal surface of the respiratory tract is in continuous contact with the environment, which leads to a constant exposure to potential pathogens and requires an efficient local defense system. To ensure the lung's crucial function of gas

exchange, the pulmonary immune system is maintained in a quiescent state during homeostasis. In case of infection, innate and adaptive immune responses are initiated for efficient pathogen recognition and removal. These responses need tight regulation to prevent excessive immunopathology and inflammation related lung damage (Iwasaki and Pillai, 2014).

1.2.2.1 The innate immune response to influenza infections

The airways harbor a specialized immune system, providing mechanisms to efficiently combat invading pathogens. In case of influenza viruses, these mechanisms involve recognition of viral RNA, which is sensed by plasmacytoid dendritic cells (pDCs) upon virus endocytosis and by macrophages in phagocytosed dying infected cells, leading to a complex signaling cascade to produce type I interferons (IFNs) and other proinflammatory cytokines, eicosanoids and chemokines at the site of infection (Iwasaki and Pillai, 2014). The latter promote the influx of further immune cells, which are responsible for viral clearance: Natural killer (NK) cells target and eliminate infected epithelial cells (Gazit et al., 2006), while recruited neutrophils and monocytes, together with alveolar macrophages, clear dead cells (Hashimoto et al., 2007).

The initial step required to activate the innate immune system is the recognition of the invading pathogen as foreign. This is achieved by specific pattern-recognition receptors (PRRs), which recognize pathogen associated molecular patterns (PAMPs), which are either part of the pathogen or are newly formed during infection (Medzhitov, 2001). Multiple members of at least three distinct classes of PRRs recognize influenza-associated patterns: The Toll-like receptors (TLR)3, -7 and -8, retinoic acid-inducible gene I (RIG-I) and the NOD-, LRR- and pyrin domain-containing 3 (NLRP3).

TLR3 is an endosomal sensor of double-stranded RNA (Alexopoulou et al., 2001). While influenza is a virus that contains single-stranded RNA and does not generate double-stranded RNA during replication (Pichlmair et al., 2006), influenza infection is nevertheless accompanied by substantial activation of TLR3 (Iwasaki and Pillai, 2014). This might be due to currently unidentified double-stranded RNA structures occurring in influenza-infected dying cells that are phagocytosed (Tatematsu et al., 2013). TLR3 activation induces the expression of interferon-regulatory factor 3 (IRF3), which prompts the production of type I IFNs (IFNα and -ß) and IFN-stimulated genes (ISGs). Additionally, TLR3 activation leads to the expression of nuclear factor-kappaB (NF-

kappaB), which in turn instigates the production of proinflammatory cytokines. TLR3 signals through TIR-domain-containing adapter-inducing interferon-β (TRIF).

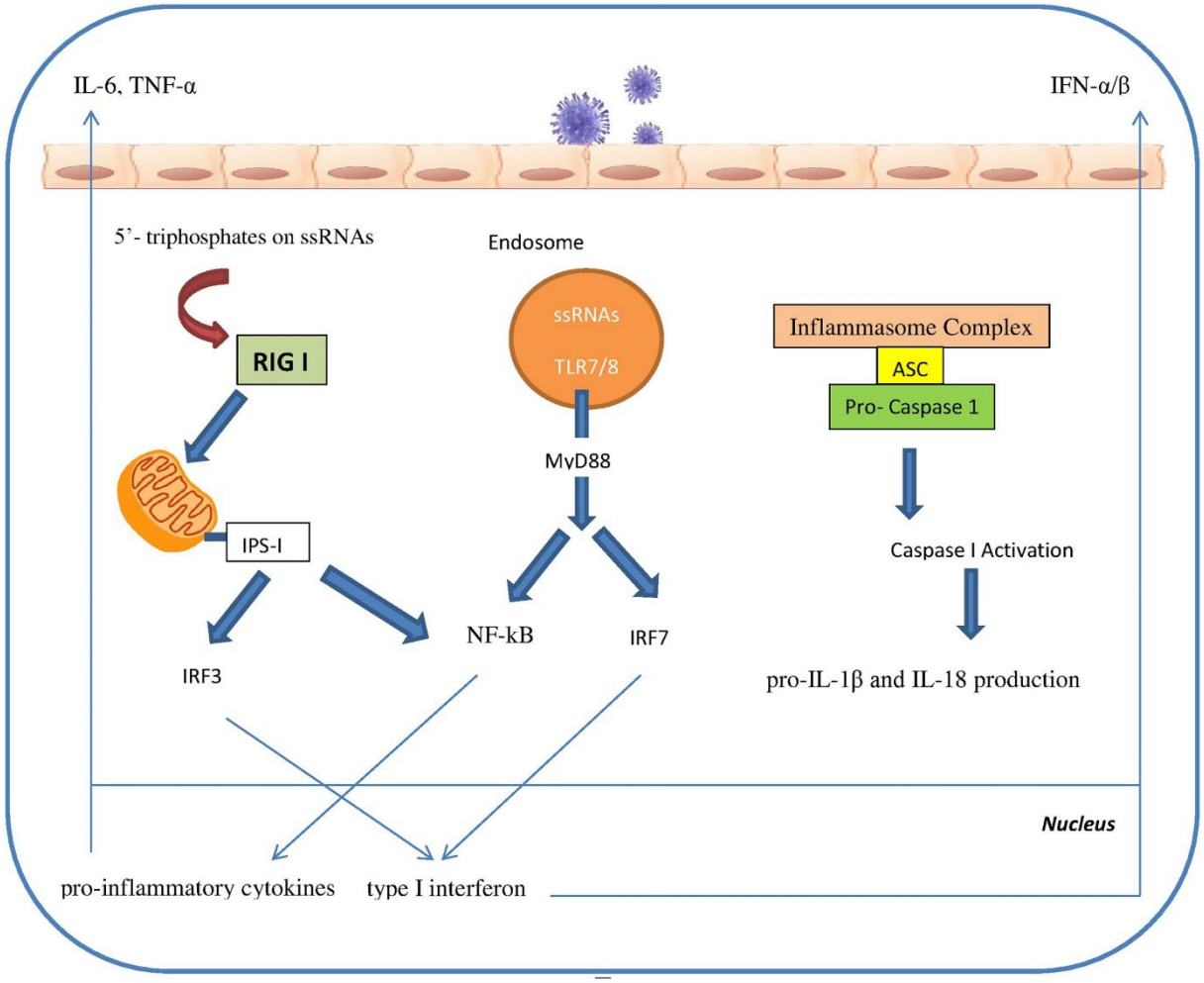

Figure 5: Innate immune response to influenza infection. Adapted from (Bahadoran et al., 2016)

TLR7 is another endosomal sensor, but recognizes single-stranded RNA (Petes et al., 2017). This receptor signals through the adaptor myeloid differentiation primary response 88 (MYD88) to activate NF-kappaB to induce proinflammatory cytokine production or IFN-regulatory factor 7 (IRF7), for type I IFN production (Figure 5).

TLR8 also recognizes ssRNA, but its precise relevance in influenza virus infections remains unclear. It does not lead to the production of IFNα (Ablasser et al., 2009).

RIG-I is a cytosolic sensor of the 5′-triphosphate viral ssRNA that is generated after viral replication (Pichlmair et al., 2006). This protein has a helicase domain, which binds to adenosine tri-phosphate (ATP) after activation, and a caspase recruitment domains which, after conformational changes, bind to the signaling adaptor

mitochondrial antiviral signaling protein (MAVS) (Pichlmair et al., 2006). Through MAVS signaling, IRF3 and NF-kappaB are activated, which in turn lead to the production of type I IFN and ISGs as well as proinflammatory cytokines, respectively (Jiang et al., 2011).

The NOD-like receptor family member NLRP3 is a PRR that in combination with the adaptor protein apoptosis-associated speck-like protein (ASC) and pro-caspase 1 forms the NLRP3 inflammasome (Lu and Wu, 2015). This complex is activated in two steps: priming and activation. The first step, which is referred to as signal 1, occurs after NF-kappaB expression, which is a consequence of inflammatory stimuli such as TLR-activation, and consists of the expression of NLRP3, IL-18 and pro-IL-1ß (Yang et al., 2019). The second step (signal 2) is initiated by host damage and leads to the cleavage and activation of caspase 1, together with the secretion of mature IL-1ß and IL-18. Ichinohe et al. observed in antibiotics-treated mice significantly reduced pro-IL1ß and pro-IL-18 expression after influenza infection (Ichinohe et al., 2011), which suggests that signal 1 in immune responses against influenza viruses is largely provided by commensals. While signal 2 can be provided by a multitude of different stimuli associated with cellular damage (Yang et al., 2019), at least three different stimuli associated with influenza infection and capable of delivering signal 2 have been identified: ssRNA (Thomas et al., 2009), proton flux through the influenza M2 ion channel in the trans-golgi network (Ichinohe et al., 2010) and, lastly, high-molecular-weight aggregates of the influenza virus virulence protein PB1-F2 in macrophage lysosomes, most likely in phagocytes that have engulfed dying infected cells which contain amyloid fiber-like structures of PB1-F2 (McAuley et al., 2013).

The activation of these receptors leads to downstream effector mechanisms that both provide antiviral resistance by reducing viral burden and increased disease tolerance, which, per definition, consists of the reduction of the negative impact on host fitness of a pathogen without reducing the pathogen burden (Medzhitov et al., 2012). Dysregulated, exaggerated signaling can, however, also lead to immunopathology.

Type I IFNs contribute to antiviral resistance by inducing a multitude of ISGs which block infection, degrade viral constituents and limit virus reproduction (Iwasaki and Pillai, 2014). Certain myxovirus resistance (MX) proteins, which are among the first identified antiviral ISGs, are potent inhibitors of viral infection (Iwasaki and Pillai, 2014). In humans, the MXA protein is located in the cytosol and provides resistance to the influenza A virus, among other viruses (Hefti et al., 1999). IFN-induced transmembrane

proteins (IFITMs) exhibit antiviral functions by limiting the membrane fusion between host cells and viral particles after viral attachment and endocytosis. As a consequence, IFITM3-deficient mice are highly susceptible to influenza virus infection (Bailey et al., 2012). Further antiviral ISGs include the 2′-5′-oligoadenylate synthase (OAS) family and ribonuclease L (RNase L), which degrade cytosolic viral RNA (Silverman, 2007), and protein kinase R which protects against viral infections by binding viral RNA and inhibiting translation (Balachandran et al., 2000).

Further innate immune cytokines, including IL-1, which promotes DC migration from the lungs to the mediastinal lymph nodes (Pang et al., 2013), IL-6 (Lauder et al., 2013) and IL-18 (Denton et al., 2007) are involved in viral clearance by boosting adaptive immunity.

The regulatory mechanisms behind disease tolerance to influenza infection are less well studied. A key cell type involved are innate lymphoid cells, which secrete amphiregulin in response to IL-33, a mechanism that could be shown to reduce tissue damage and improve lung function during influenza infection (Monticelli et al., 2011).

1.2.2.2 The adaptive immune response to influenza infection

In order to be able to react to a broad variety of molecules, the germline-encoded receptor structures of the innate immune system are inherently limited in specificity. The adaptive immune system is able to overcome this limitation through somatic recombination of germline-encoded elements which form the B- and T cell receptor repertoire. Additionally, the adaptive immune system is capable of forming long-lasting memory of previously encountered antigens, with the potential to be quickly reactivated upon recurring exposure. While innate responses occur within short time frames, adaptive immunity takes several days to become effective (Chaplin, 2010).

To be activated, effector cells of the adaptive immune system require antigen presentation by specialized cells, so called antigen presenting cells (APCs). While several cell types are capable of antigen presentation *in vitro* (Hughes et al., 2016), conventional dendritic cells (cDCs) are considered the classical example of dedicated professional APCs (Kambayashi and Laufer, 2014). Mature cDCs are defined by their high surface expression of the major histocompatibility complex class II (MHCII) and CD11c (Vivier and Malissen, 2005).

The two main respiratory mature cDC subsets resident in the lung are characterized as $CD103^{+}$ and $CD11b^{hi}$ $CD103^{-}$ respiratory DCs, both of which are critical for the

induction of adaptive immune responses (Sung et al., 2006). While CD103^{+} DCs are found at the mucosal surface, CD11b^{hi} respiratory DCs are located in the lung interstitial space (del Rio et al., 2007).

Innate immune system activation, such as influenza infection, lead to activation and antigen uptake by respiratory dendritic cells, which subsequently migrate from the inflamed lungs to the draining lymph nodes (Hammad and Lambrecht, 2008). The mechanisms leading to this migration are incompletely understood, but could be shown to involve multiple proinflammatory cytokines, including IL-1ß, IL-18, IL-12, TNF and tumor growth factor (TGF)-ß as well as chemokines such as chemokine ligand (CCL) 2 and CCL20. DCs migrate along the chemokine gradients of CCL21 and sphingosine-1-phosphate (S1P) (Figure 6). Activation of DCs also induces the expression of costimulatory molecules, including CD80, CD86, CD40 and intercellular adhesion molecule 1 (ICAM1), which are required to unleash their full potential as APCs (Braciale et al., 2012).

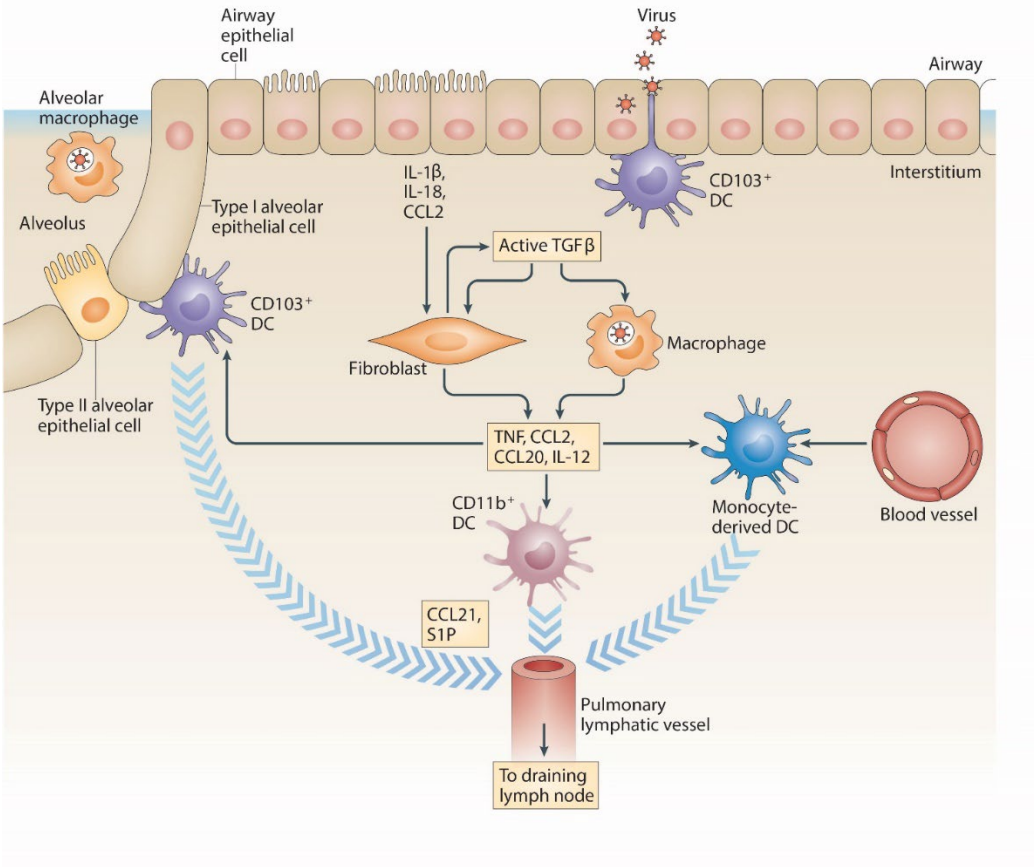

Figure 6: Dendritic cell activation and migration. Adapted from (Braciale et al., 2012).

Lung DCs then migrate to the draining lymph nodes to enable the encounter of both specific naïve antiviral T cells (which are extremely rare) (Lawrence and Braciale,

2004) and memory T cells (in case of previously encountered antigens) (Kim et al., 2010) to their cognate antigen.

The first respiratory DC subset to reach peak numbers in the draining lymph nodes are CD103$^+$ respiratory DCs (Braciale et al., 2012). This cell type could also be shown to be the most potent APC for presentation of viral antigens to naïve virus-specific CD8$^+$ T cells during the early response to influenza virus infection (Kim and Braciale, 2009). In particular, they are the most potent cross-presenting DC subset (Ho et al., 2011). Cross-presentation is the process of internalizing an exogenous antigen, which is then re-routed to the MHCI pathway of antigen presentation, rather than the MHCII pathway, and is of importance for the initiation of CD8$^+$ T cell responses.

Unlike CD103$^+$ DCs, which produce only low levels of pro-inflammatory mediators, CD11b^{hi} DCs produce large amounts of chemokines in response to inflammatory stimuli in the respiratory tract (Beaty et al., 2007). Their numbers in the draining lymph nodes peak at later time points (five to seven days) after influenza infection, and it has been suggested that they serve to expand the pool of already activated CD8$^+$ T cells (Braciale et al., 2012).

Both CD103$^+$ and CD11b^{hi} DCs also present antigen to activate CD4$^+$ T cells (Braciale et al., 2012). In contrast to activation of CD8$^+$ T cells, antigens are presented to CD4$^+$ T cells through MHCII (Bulte and Shakeri-Zadeh, 2022) (Figure 7).

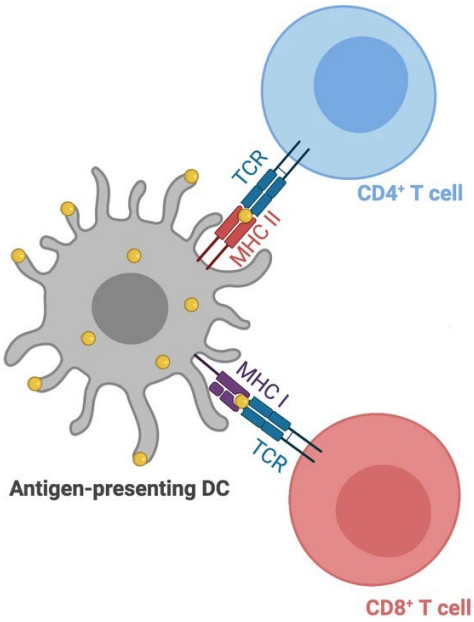

Figure 7: Antigen presentation via MHCI and MHCII. Adapted from (Bulte and Shakeri-Zadeh, 2022)

While they are more abundant than CD103$^+$ DCs and CD11b^{hi} DCs, phenotypically immature (MHCII^{low} CD11c^{low}) monocyte-derived DCs are poor activators of naive T

cells, eventhough they can also migrate to the draining lymph nodes after taking up antigens in the infected lung (Kim and Braciale, 2009). However, they may be able to differentiate into mature DCs, which increases their potential to present antigen (Jakubzick et al., 2008).

The crucial role of antigen-specific $CD8^+$ (also referred to as cytotoxic) T cells in the antiviral response to influenza infection is their ability to lyse virus-infected cells, after recognizing processed viral antigens, which are presented on the infected cell surface via MHCI, through their T cell receptors (Hufford et al., 2011). However, their cytolytic ability can also substantially contribute to immunopathology (Rouse and Sehrawat, 2010).

While $CD8^+$ T cells exhibit antiviral activity by killing virus-infected cells, the key role of $CD4^+$ T cells during influenza infection is the support of the activation and differentiation of antibody-producing B cells, which is why $CD4^+$ T cells are also termed T-helper cells (Topham and Doherty, 1998). Antibodies are large proteins employed by the immune system to identify and potentially neutralize foreign entities, including bacteria and viruses. These proteins are composed of a constant (Fc) region, which is encoded in the genome and required for increased stability and receptor-mediated functions, and a variable region, whose amino acid sequence randomly generated through a process termed somatic recombination, and which binds antigens (Murphy and Weaver, 2016). B cells express these randomly generated peptides on their surface as B cell receptors. Upon recognition of viral particles through these receptors, B cells are activated and the viral particles are endocytosed. Subsequently, these particles are expressed on the B cell surface via on MHCII complexes. $CD4^+$ T cells can recognize these molecules and subsequently further stimulate activated B cells through Inducible T-cell Costimulator (ICOS) and CD40-ligand. This additional activation is required for differentiation of B cells into antibody-secreting plasma cells (Murphy and Weaver, 2016).

The specific antibodies which are produced after influenza infection against most of the viral proteins differ in their kinetics and abundance (Sealy et al., 2003). Particularly strong and often neutralizing antibody responses are directed against the HA protein (Clarke et al., 1990). Antibodies promote elimination of the virus and are also an important component of immunological memory, since they protect from repeated infection with the same strain (Wrammert et al., 2008). Unpublished data from our lab indicate that both WT and *Lcn2*$^{-/-}$ induce robust responses to a murine strain of

influenza virus after intramuscular injection of inactivated viral particles, which is sufficient to protect from subsequent infections, indicating that LCN2 is not required for an effective B cell response.

Since neutralizing antibodies mainly target the HA and NA proteins (Li et al., 2019), influenza viruses employ evolutionary strategies to evade immunological memory. Two major processes drive influenza virus evolution: antigenic shift and antigenic drift (Krammer et al., 2018). Antigenic shift occurs as a result of interchange of RNA segments, after antigenically different viral strains of the same genus (influenza A or influenza B) have infected the same cell. This process, which is mainly limited to influenza A viruses due to their extensive animal reservoir (Abadia-Molina et al., 2006), leads to a sudden, drastic change of an influenza virus's antigenicity. Influenza pandemics are associated with novel influenza A virus antigens that are derived from animals strains of influenza virus, which cross the species barrier and acquire the ability to transmit between humans (Krammer et al., 2018).

Antigenic drift is the gradual accumulation of mutations in the antigens HA and NA, which enables influenza viruses to evade antibody-mediated immunity acquired by the host during vaccinations or previous infections (Webster et al., 1992). This process is responsible for the requirement of frequent influenza vaccine updates. While both the HA and NA gene can be affected by antigenic drift, it is most common for the HA gene, where only few amino acid changes can be sufficient (Kim et al., 2018). Unlike antigenic shift, which is exclusively observed in the influenza A genus, antigenic drift can be found in all influenza genera, but appears to be fastest in influenza A (Kim et al., 2018).

1.3 Immune-microbe interaction in the context of the lung

The term 'human microbiome' refers to the combination of all microorganisms (bacteria, archaea, viruses, protists and fungi) inhabiting the human body, their corresponding anatomical localization and the environmental conditions under which they reside (Marchesi and Ravel, 2015). Historically, it was estimated that bacteria colonizing the human body outnumber human cells by a factor of 10 or more (Savage, 1977), however more recent estimates suggest that the true bacteria to human cell ratio is likely closer to 1:1 (Sender et al., 2016a, Sender et al., 2016b). Nevertheless, the total number of microorganisms living on the human body is vast, as 3.8×10^{13}

bacteria are estimated to live on and in the body of a 70 kg male (Sender et al., 2016b). The composition of the microbiome is highly diverse, as illustrated by the results of the human microbiome project, which yielded >70 million 16S ribosomal gene sequences defining the microbial composition across 15 body sites (Human Microbiome Project, 2012). The microbiome of humans, as in other multicellular organisms, likely co-evolved with its host (Malla et al., 2018) and plays a critical role in many physiologic processes, including the development of the immune system (Belkaid and Harrison, 2017).

While the lung was traditionally considered a sterile body site, more recent investigations revealed the existence of a unique microbiome, which influences the local respiratory immune system (Wypych et al., 2019). The main genera present in the lungs under homeostatic conditions appear to be *Prevotella*, *Streptococcus*, *Veillonella*, *Fusobacterium* and *Haemophilus* (Dickson et al., 2016).

Furthermore, recent data indicates that the intestinal microbiome can influence respiratory immune responses, highlighting the existence of a gut-lung axis (Enaud et al., 2020). Therefore, the microbiome can influence the respiratory immune system both directly, by interactions between the lung microbiome with local immune cells, and indirectly, via the gut-lung axis. These interactions play important roles in respiratory health and disease, among them defense mechanisms against viral infections, and allograft (dys)function after lung transplantation.

1.3.1 The role of the microbiome in antiviral immunity

Over the last 15 years, multiple independent studies highlighted important roles of the microbiome in host defense against viral infections. Mechanistically, most of these studies identify a link between the gut microbiome and the respiratory immune system. Several different mechanisms, via which the gut microbiome influences pulmonary immunity have been identified. In one of the first studies to showing the important contribution of the gut microbiome to antiviral lung immunity, Ichinohe *et al.* reported that antibiotics-treated mice develop an impaired immune response to influenza, with reduced virus-specific $CD4^+$ and $CD8^+$ T cells (Ichinohe et al., 2011). This could be rescued by injection of TLR ligands. They concluded that intestinal microbes promote the expression of pro-IL-1ß and pro-IL-18 mRNA, which, after influenza infection, induces migration of DCs to the peripheral lymph nodes via inflammasome activation.

Abt *et al*. observed decreased viral clearance and increased mortality in antibiotics-treated mice after both, influenza and lymphocytic choriomeningitis virus (LCMV) infection, which they linked to decreased expression of antiviral genes and defective type I and type II IFN responses in macrophages (Abt et al., 2012).

The link between the microbiome and antiviral type I IFN production and signaling has since been confirmed by multiple other studies. Microbial metabolites could be shown to play an important messenger role in this setting. Desaminotyrosine, a small molecule which is produced via flavonoid metabolism by *Clostridium orbiscindens*, a human gut microbe, exerts a protective role in antiviral immunity by boosting type I IFN signaling, and by limiting lung immunopathology. Indeed, desaminotyrosine administration was sufficient to rescue antibiotics-treated mice that were infected with influenza (Steed et al., 2017). Short chain fatty acids (SCFAs), which are end products of dietary fiber fermentation by multiple commensal bacteria (Silva et al., 2020), are another class of bacterial metabolites that evidently play a role in promoting type I IFN response and ISG expression. The SCFA acetate was found to be able to promote G protein coupled receptor 43 (GPR 43, also known as free fatty acid receptor 2) signaling during respiratory syncytial virus infection in stromal cells, which in turn leads to increased type I IFN responses and ISG expression (Antunes et al., 2019). Microbiota can also drive the ISG signature during steady state in lung stromal cells, which is of crucial importance for early antiviral immunity to influenza (Bradley et al., 2019).

Beyond their effect on increasing type I IFN responses, SCFAs have additional protective effects during influenza infection (Trompette et al., 2018). High-fiber diet fed mice, which exhibit increased systemic SCFA levels due to pronounced intestinal fermentation of fibers have, show higher bone marrow production of $Ly6C^-$ patrolling monocyte. These cells alternatively activate macrophages, which lowers the expression of CXCL1 in the airways. During influenza infection, this reduces tissue immunopathology by limiting neutrophil recruitment to the lung. Additionally, SCFAs enhanced $CD8^+$ T cell function by promoting the metabolism of these cells. These effects could be shown to be dependent on the GPR41 (also known as free fatty acid receptor 3). Interestingly, oral administration of the SCFA butyrate could induce the same effects in mice that were not fed a high-fiber diet, highlighting the importance of this metabolite in antiviral immunity.

1.3.2 The microbiome in lung transplant function and dysfunction

In patients with irreversible end-stage pulmonary disease, such as end-stage cystic fibrosis (CF), chronic obstructive pulmonary disease (COPD) and idiopathic interstitial pneumonia, lung transplantation is the only life-saving treatment option (Inci, 2020). Lung transplantation can involve the replacement of one (single) or both (double) pulmonary lobes. The first lung transplantation was performed in 1963 by James Hardy (Hardy et al., 1963), and the patient survived for 18 days. Since then, substantial technological and medical advances have been made, but while the survival rate has drastically increased, the five-year survival rate remains at 59%, which is the lowest among all solid organ transplants (Bos et al., 2020).

While infections are the leading cause of death within the first year after lung transplantation (Bos et al., 2020), the primary cause of post-transplant morbidity and mortality overall and after the first year is chronic lung allograft dysfunction (CLAD), which is responsible for more than 40% of deaths after the first year post transplantation (Verleden et al., 2019). Both, predominantly obstructive and restrictive ventilatory patterns, as well as mixed patterns can occur, and CLAD functions as an umbrella term to describe the range of pathophysiological processes in the lung allograft that lead a functional deterioration. While many of these processes remain to be elucidated, they could be linked to a variety of triggers, among them the lung microbiome.

1.3.2.1 Definitions of CLAD, BOS and RAS

Per definition, CLAD is a persistent and substantial (>20%) decline in the measured forced expiratory volume during one second (FEV_1), that occurs later than three months after transplantation. As a reference, the best two postoperative values are taken. To fulfill the definition of CLAD, reversible causes of allograft dysfunction must be excluded, such as infection, acute rejection and aspiration (Verleden et al., 2019). CLAD is subdivided into different phenotypes: The most common manifestation is caused by obstruction of the airways by bronchiolitis obliterans syndrome (BOS), which presents as an isolated drop in FEV_1. However, a restrictive deficit in lung function is also present in up to 30% of patients (Sato et al., 2011), this manifestation is termed restrictive allograft syndrome (RAS) and is defined as a persistent decrease in FEV_1 combined with a decrease in total lung capacity, as well as the presence of radiological

pulmonary opacities (which are typically absent in BOS). RAS shows an even worse prognosis than BOS (Verleden et al., 2019).

1.3.2.2 Treatment and pathophysiology of CLAD

Treatment options for CLAD are scarce and have only shown a limited efficacy in clinical studies. When patients receive cyclosporine A-based immunosuppression, conversion of cyclosporine to tacrolimus could be shown to slow lung function decline in a series of cases (Meyer et al., 2014). The macrolide antibiotic azithromycin was reported to positively affect lung function in up to 40% of lung transplant recipients, and complete reversal of FEV_1 decline was observed in some patients, particularly when BAL neutrophilia was present (Vos et al., 2010). Nevertheless, no targeted therapy for CLAD is available.

The lack of specialized treatments for CLAD is due to an insufficient understanding of the pathophysiology, and the interplay between BOS, RAS and antibody-mediated rejection (AMR) (Verleden et al., 2020a). AMR is caused by the production of antibodies against donor antigens present on the transplanted lung. This clinical entity is well defined in heart and kidney transplant recipients, but less well understood in the context of lung transplantation (Levine et al., 2016).

BOS, the most prevalent and most well studied subtype of CLAD, is characterized by abundant small airway obstruction. Pathophysiologically, this is assumed to be the consequence of persistent microinjuries to the epithelium (Figure 8, left panel), which leads to inflammation and the recruitment of inflammatory macrophages and neutrophils as well as the accumulation of (myo-)fibroblasts (Figure 8, middle panel) and mesenchymal transition of epithelial cells.

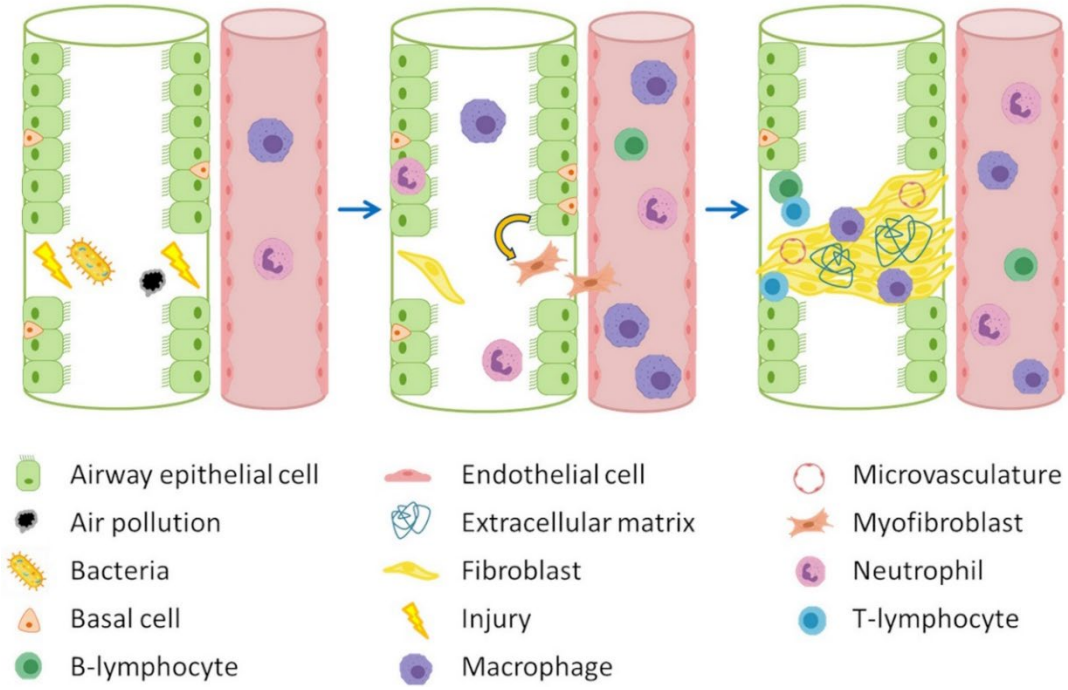

Figure 8: The pathophysiology of BOS, adapted from (Verleden et al., 2020a)

The histological pattern characteristic of RAS is alveolar fibroelastosis (AFE). Like obliterative bronchiolitis, AFE can arise following injury of the small- and mid-sized airways, which, in case of RAS, leads to fibrinous intra-alveolar deposition, the infiltration of aberrant macrophages and failed degradation of fibrous exsudates (Figure 8, right panel). The prevalence of donor-specific antibodies is higher in RAS than in BOS (Verleden et al., 2017), and AFE is associated with the presence of B-cell dominant lymphoid follicles, which likely arise due to the recognition of donor-specific antigens (Watanabe et al., 2019).

1.3.2.3 Radiological patterns associated with BOS and RAS

Radiological imaging plays a key role in monitoring the lung transplantation, both in the early phase after transplantation, to identify potential surgical complications or infections, but also during the later stage (>3 months) after transplantation, when early detection and potential initiation of treatment of CLAD is crucial (Madan et al., 2014). The most precise computed tomography (CT) finding of BOS is airtrapping on expiratory images. When more than 32% of the lungs are involved, this pattern reaches an accuracy of 88% (Bankier et al., 2001). This finding is typically associated with mosaic perfusion, due to hypoxic vasoconstriction in the affected area (Hota et al., 2018). Airtrapping is identified by acquiring and comparing both inspiratory and

expiratory CT-scans, and searching for areas with a reduced increase in attenuation on the expiratory scan (Figure 9). A major limitation of this technique is that it depends on the patient effort to produce sufficient inspiration and expiration (Byrne et al., 2021).

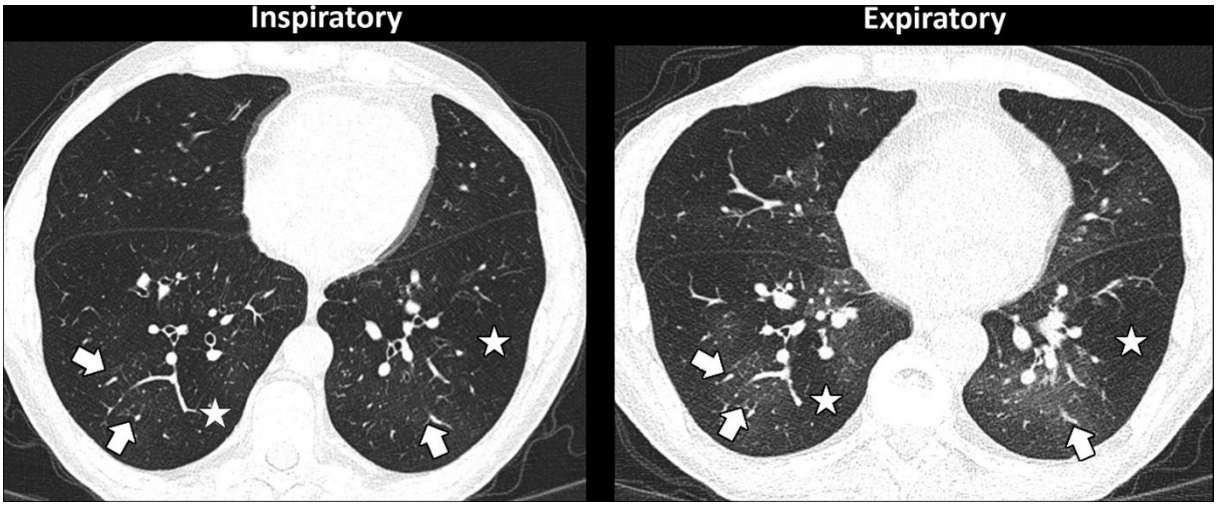

Figure 9: Airtrapping on thoracic CT-scans as a manifestation of BOS, adapted from (Byrne et al., 2021). Asterisks highlight areas of relative lucency on exspiratory images due to airway obstruction, arrows point to areas with reduced pulmonary vasculature and increased attenuation.

RAS, due to its pathophysiological and histological similarity to forms of pulmonary fibrosis, produces CT patterns that are considerably more striking than those associated with BOS, and include peripheral consolidations, pleural thickening, bronchiectasis as well as pulmonary volume loss, which typically shows an upper lobe dominance (Figure 10) (Verleden et al., 2014).

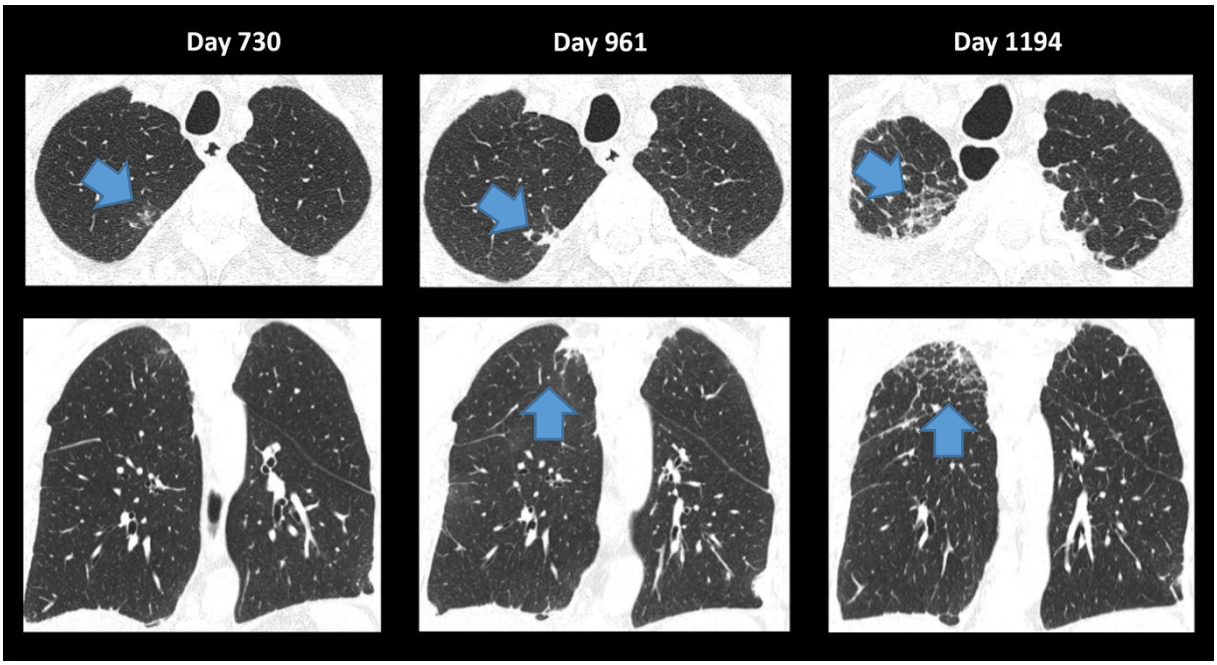

Figure 10: Presentation of RAS on chest CT. Patchy consolidation in the right upper lobe, which shows progression to interlobar septal thickening, pleuroparenchymal consolidation and fissural retraction (highlighted with an arrow). Timepoints refer to days after transplantation. Adapted from (Byrne et al., 2021).

While these findings can aid in the early detection of RAS, they show a high degree of overlap with other pathologic pulmonary conditions, such as infections, and are therefore non-specific (Byrne et al., 2021). The nature and localization of these findings, if RAS diagnosis is confirmed, also has prognostic significance: Diffuse or basal predominance of fibrotic patterns is linked to significantly shorter survival, when compared to predominantly upper-lobe-associated patterns (Verleden et al., 2016).
Mixed obstructive and restrictive phenotypes of CLAD typically present as apically predominant pleuroparenchymal fibroelastosis and interstitial and pleural opacities (Verleden et al., 2020b).

1.3.2.4 The role of the microbiome in CLAD development

Multiple studies have identified the microbiome of the transplanted lung as both an independent predictor and a potential mechanistic factor for the development of CLAD. The post-transplantation lung microbiome, compared to the microbiome observed in healthy, non-transplanted lungs, is characterized by increased microbial biomass (Charlson et al., 2012), and relative dysbiosis, as measured by a decreased alpha-diversity and alterations in the composition of bacterial communities (Petersen and Round, 2014). These alterations include an expansion of lung commensals, but also

of potential pathogens, including *Pseudomonas*, *Enterobacteriaceae*, *Staphylococcus* and anaerobes, in the transplanted lung (Charlson et al., 2012). Longitudinal studies have indicated that these changes are subject to a high degree of temporal heterogeneity, particularly within the first year after transplantation (Snell et al., 2019). This can be influenced by recipient-factors, for example, in CF, recipient-derived *Pseudomonas* strains populated the allograft within days after transplantation (Syed et al., 2016). The correlation of different taxa with BOS development has been reported by several studies. Interestingly, these studies differ with regards to the specific genera associated with BOS development, and the time of the association. Using metagenomics shotgun sequencing, Schott *et al.* observed lower rates of acute cellular rejection and BOS development in transplant recipients with *Actinobacteria*-dominant pulmonary microbial profiles at three months after transplantation. This was not observed at later timepoints, indicating that the observation was time-dependent (Schott et al., 2018). In another small, uncontrolled study, *Actinomyces* and *Xanthomonadaceae* were found enriched in patients with BOS (Borewicz et al., 2013). In a recent prospective cohort study of 134 patients, Combs *et al.* identified total bacterial DNA burden (collected during surveillance bronchoscopy one year after transplantation) as independent predictor of CLAD development or death within 500 days of follow-up (Combs et al., 2021). While they found lung bacterial communities to be significantly different between patients who survived without CLAD and those who developed CLAD or died, no individual bacterial taxa were found to be definitively associated. This important study suggests that overall bacterial biomass, rather than specific taxa, may contribute to the airway injury subsequently leading to BOS or RAS development. Mechanistically, the post-transplant lung microbiome could be linked to inflammatory cytokine signatures (Shankar et al., 2016) and myeloid cell responses (Sharma et al., 2017), factors that are known to be involved in the development of CLAD. Additionally, studies by the SysCLAD Consortium revealed associations between the microbiome of lung allografts and host gene expression profiles (Bernasconi et al., 2016). Bernasconi *et al.* distinct gene expression profiles in BAL samples, whereby inflammatory profiles with elevated expression of *Tnf*, *Cox2*, as well as t tissue remodeling genes were linked to bacterial dysbiosis (Bernasconi et al., 2016). In another study by Moraux *et al.*, these findings were extended to show that anabolic and catabolic gene expression profiles, determined by the expression of the genes thrombospondin-1 and platelet-derived growth factor receptor-D (PDGF-D)

(anabolic) or matrix metalloproteinases, collagen-V1 A-2, fibronectin-1 and insulin-like growth factor 1 (catabolic), respectively, correlated with diverging microbial profiles (Mouraux et al., 2018). Interestingly, in both of these studies, causative links between certain microbes and gene expression profiles could be established through *in vitro* assays. In summary, these data clearly show that the composition and biomass of the post-transplant microbiome is a potential biomarker and represent potential therapeutic targets for CLAD.

1.4 Thesis aims

The respiratory tract performs the crucial function of gas exchange and is in permanent direct contact with inhaled, potentially dangerous environmental factors. Therefore, pulmonary immune responses need to be highly efficient in removing such threats, but also tightly regulated given the delicate nature of the lung (alveolar) tissue. Recent evidence suggests that host-microbiome interactions, involving commensals of the respiratory tract or other sites, are required for efficient immune responses against pulmonary pathogens and play key roles in immune-regulation. However, we are only beginning to grasp the complexity of this interplay and its consequences during health and disease.

In the first part of this thesis, we investigated the role of LCN2, a small secreted glycoprotein, in the regulation of lung myeloid cell function and antiviral immune responses. This protein was of particular interest to us in the context of interactions between the host immune system and the microbiome for two reasons: First, it can directly inhibit the growth of many bacterial strains by preventing siderophore-dependent iron uptake. While this antibacterial activity is highly relevant for host defense against bacterial pathogens, it likely also affects microbiome composition. Second, several recent studies have highlighted an immunomodulatory role of LCN2 that goes beyond its antibacterial effects, and it is tempting to speculate that this role of LCN2 may be, at least partly, related to its potential effects on the microbiome. Using RNA-sequencing, 16S-rRNA gene sequencing, mice deficient for LCN2 (*Lcn2*$^{-/-}$), a mouse model of influenza infection and two different strategies to perturb the microbiome (antibiotic treatment and co-housing of mice with different genotypes), we here aimed to determine the role of LCN2 in host-microbiome interactions, and its consequences for the regulation of pulmonary antiviral immune responses.

In the second part of the thesis, we focused on the dynamics of the broncho-alveolar microbiome, cellular composition, metabolome and lipidome after lung transplantation. In the context of CLAD pathogenesis, the transplanted (donor-derived) microbiome may be a trigger for the immune responses that mediate rejection of the transplant. By comparing the pre-transplantation (donor) microbiome to the lung microbiome after transplantation, we aimed to get insights into the fate of the donor microbiome after transplantation. In a machine learning approach, we further assessed whether the lung microbial profile at a given time point could predict subsequent changes in lung

function, and compared the accuracy of these predictions to those based on metabolomic or lipidomic profiles or clinical data.

2 Results

2.1 Lipocalin 2 modulates dendritic cell activity and shapes immunity to influenza in a microbiome dependent manner

In the first part of this chapter, I will present the paper “Lipocalin 2 modulates dendritic cell activity and shapes immunity to influenza in a microbiome dependent manner”. In this study, we aimed to determine the effect of LCN2 on the transcriptome of macrophages and dendritic cells, to evaluate immunological effects of LCN2 in the lung that go beyond direct antibacterial effects. Our results revealed that, particularly in dendritic cells, the expression of a substantial number of genes involved in antigen processing and presentation, as well as antiviral immunity were altered during homeostasis in *Lcn2*$^{-/-}$ mice. We validated the importance of these pathways in a mouse model of influenza infection, whereby we found LCN2 to be protective of excessive morbidity and mortality, independent of the viral load. This correlated with increased numbers of CD8^{+} T cells in the lungs of influenza infected *Lcn2*$^{-/-}$ mice. Depletion of these cells protected from excessive weight loss during influenza infection. We could show that increased T cell counts were linked to an increased potential of CD103^{+} dendritic cells to cross present antigen to CD8+ T cells. Finally, we could show that the effects of LCN2 on antiviral immunity were dependent on the microbiome, as we observed differences in the intestinal microbial composition of WT and *Lcn2*$^{-/-}$ mice, which when equalized by co-housing and antibiotic treatment, protected *Lcn2*$^{-/-}$ mice from exagerrated CD8^{+} T cell responses. This work shows that a single gene can influence pulmonary antiviral immunity through microbiome-dependent mechanisms.

PLOS PATHOGENS

RESEARCH ARTICLE

Lipocalin 2 modulates dendritic cell activity and shapes immunity to influenza in a microbiome dependent manner

Martin L. Watzenboeck[1,2], Barbara Drobits[1,2], Sophie Zahalka[1,2], Anna-Dorothea Gorki[1,2], Asma Farhat[1,2], Federica Quattrone[1,2], Anastasiya Hladik[1,2], Karin Lakovits[1,2], Gabriel M. Richard[1,2], Therese Lederer[3], Birgit Strobl[3], Gijs A. Versteeg[4], Louis Boon[5], Philipp Starkl[1,2‡*], Sylvia Knapp[1,2‡*]

1 Research Laboratory of Infection Biology, Department of Medicine I, Medical University of Vienna, Austria, **2** CeMM, Research Center for Molecular Medicine of the Austrian Academy of Sciences, Austria, **3** Institute of Animal Breeding and Genetics, Department of Biomedical Science, University of Veterinary Medicine Vienna, Vienna, Austria, **4** Department of Microbiology, Immunobiology, and Genetics, Max Perutz Labs, University of Vienna, Vienna Biocenter (VBC), Vienna, Austria, **5** Polpharma Biologics, Utrecht, The Netherlands

‡ These authors jointly supervised this work.
* philipp.starkl@meduniwien.ac.at (PS); sylvia.knapp@meduniwien.ac.at (SK)

Citation: Watzenboeck ML, Drobits B, Zahalka S, Gorki A-D, Farhat A, Quattrone F, et al. (2021) Lipocalin 2 modulates dendritic cell activity and shapes immunity to influenza in a microbiome dependent manner. PLoS Pathog 17(4): e1009487. https://doi.org/10.1371/journal.ppat.1009487

Editor: Mehul Suthar, Emory University, UNITED STATES

Received: August 12, 2020

Accepted: March 19, 2021

Published: April 27, 2021

Data Availability Statement: Raw and processed RNA sequencing data are available from the NCBI Gene Expression Omnibus database (accession number GSE156079).

Funding: Funding was provided by the Austrian Science Fund (FWF, www.fwf.ac.at), DK Cell Communication in Health and Disease (W 1205-B09) and the Special Research Program Chromatin Landscapes (L-Mac: F 6104-B21) (to S.K.). P.S. acknowledges funding by the European Research Council (erc.europa.eu, Marie Skłodowska-Curie

Abstract

Lipocalin 2 (LCN2) is a secreted glycoprotein with roles in multiple biological processes. It contributes to host defense by interference with bacterial iron uptake and exerts immunomodulatory functions in various diseases. Here, we aimed to characterize the function of LCN2 in lung macrophages and dendritic cells (DCs) using *Lcn2*$^{-/-}$ mice. Transcriptome analysis revealed strong LCN2-related effects in CD103^{+} DCs during homeostasis, with differential regulation of antigen processing and presentation and antiviral immunity pathways. We next validated the relevance of LCN2 in a mouse model of influenza infection, wherein LCN2 protected from excessive weight loss and improved survival. LCN2-deficiency was associated with enlarged mediastinal lymph nodes and increased lung T cell numbers, indicating a dysregulated immune response to influenza infection. Depletion of CD8^{+} T cells equalized weight loss between WT and *Lcn2*$^{-/-}$ mice, proving that LCN2 protects from excessive disease morbidity by dampening CD8^{+} T cell responses. *In vivo* T cell chimerism and *in vitro* T cell proliferation assays indicated that improved antigen processing by CD103^{+} DCs, rather than T cell intrinsic effects of LCN2, contribute to the exacerbated T cell response. Considering the antibacterial potential of LCN2 and that commensal microbes can modulate antiviral immune responses, we speculated that LCN2 might cause the observed influenza phenotype via the microbiome. Comparing the lung and gut microbiome of WT and *Lcn2*$^{-/-}$ mice by 16S rRNA gene sequencing, we observed profound effects of LCN2 on gut microbial composition. Interestingly, antibiotic treatment or co-housing of WT and *Lcn2*$^{-/-}$ mice prior to influenza infection equalized lung CD8^{+} T cell counts, suggesting that the LCN2-related effects are mediated by the microbiome. In summary, our results highlight a novel regulatory function of LCN2 in the modulation of antiviral immunity.

Individual Fellowship H2020-MSCA-IF-2014 655153) and the Austrian Science Fund (FWF) (P31113-B30). The funders had no role in study design, data collection and analysis, decision to publish, or preparation of the manuscript.

Competing interests: The authors have declared that no competing interests exist.

Author summary

Outcome from infectious diseases is determined by the adequacy of the immune response, with efficient clearance of the causative pathogen, while keeping the inflammatory response in check to avoid excessive inflammation, tissue damage and resulting mortality. The regulation of immunity is shaped by multiple players. As such lipocalin (LCN) 2 exhibits immune-modulatory properties and for instance deactivates alveolar macrophages, but the precise mode of action remains unclear. Here, we explored the precise effects of LCN2 on cellular lung immunity, and discovered that LCN2 markedly impacted homeostatic expression of pulmonary dendritic cell (DC) genes related to anti-influenza immunity. In agreement with this finding, LCN2-deficient mice infected with influenza virus showed a higher mortality and more pronounced immune response, despite an unaltered viral clearance. Mechanistically, we found the presence of LCN2 associated with dampened DC functions, ultimately preventing exuberant T cell activation during influenza infection. Considering LCN2's antibacterial effects as a siderophore-binding protein, we speculated that an indirect, microbiome-dependent effect might explain these findings. In fact, LCN2 remarkably shaped the microbiome composition, and interference via antibiotics or cohousing erased the protective effects of LCN2 on the anti-viral immune response.

Introduction

Lipocalin 2 (LCN2) is a 25-kDa secreted glycoprotein involved in a variety of biological processes, including immune responses, iron homeostasis and metabolism [1–3]. Acting as scavenger of bacterial siderophores, LCN2 is known as host defense molecule with potent antibacterial activity against siderophore-dependent bacteria, such as *Escherichia coli* and *Klebsiella pneumonia* [4,5]. In line with this function, LCN2 is highly expressed in barrier tissues exposed to microorganisms including the lungs [6] and further induced upon Toll-like receptor (TLR) stimulation [4].

Multiple studies have uncovered immunoregulatory effects of LCN2 beyond scavenging bacterial siderophores, and LCN2 has been found to protect from excessive inflammation-related morbidity in sterile endotoxemia [7], neuroinflammation [8] and non-alcoholic steatohepatitis (NASH) [9]. Intriguingly, all these observations are linked to effects of LCN2 on myeloid cells, such as macrophages or, in the context of NASH, macrophage-neutrophil interplay. Our group could previously show that LCN2 deactivates lung macrophages and worsens disease outcome from pneumonia caused by the siderophore-independent pathogen *Streptococcus pneumoniae* [10]. These studies highlight effects of LCN2 on myeloid cell function and plasticity, with important consequences in various infectious and non-infectious diseases. Given the expression pattern at mucosal surfaces including the intestine and LCN2's potential to alter the availability of microbial nutrients, it is tempting to speculate that LCN2 might shape the composition of the microbiome. Since the microbiome can strongly influence many aspects of the host immune system [11], this could be a major relay mediating LCN2-related immunomodulatory effects.

While immune responses need to be of sufficient intensity for pathogen clearance, inflammatory responses can cause substantial damage to the host. Indeed, certain pulmonary viral infections, including influenza and SARS-CoV-2 [12,13], are associated with particularly severe degrees of inflammation, which, considering the delicate architecture of lung tissue,

require complex and efficient regulatory mechanisms [14]. Immunopathology during viral infections can be caused by both innate and adaptive immune activity, for instance by dysregulated production of proinflammatory cytokines, or exuberant cytolytic activity of $CD8^+$ T cells [15]. Pulmonary dendritic cells (DCs) represent the interface between the innate and adaptive immune systems in the lungs by uptake, processing and presentation of antigens leading to initiation of specific T cell responses. In particular, $CD103^+$ DCs contribute substantially to the cytotoxic T lymphocyte response during influenza infection [16]. Potential effects of LCN2 on DCs could consequently influence adaptive anti-viral immune responses. Here, we aimed to examine the role of LCN2 as modulator of lung immunity in the context of homeostasis and viral infections. Since previous studies [7–10] suggested an immunomodulatory effect of LCN2 on myeloid cells, we focused our studies on alveolar macrophages and $CD103^+$ dendritic cells.

Results

Lipocalin 2 shapes the transcriptome of pulmonary myeloid cells during homeostasis

To assess if LCN2 exerts any effects on the homeostatic transcriptome of lung-resident myeloid immune cells that could impact acute immune responses [17], we performed RNA sequencing of pulmonary $CD103^+$ DCs and alveolar macrophages (AMs) isolated from wild type (WT) and *Lcn2*$^{-/-}$ mice (Fig 1A). Using principal component analysis on all expressed genes, we revealed a clear separation of $CD103^+$ DCs according to genotype (Fig 1B), and a tendency for AM samples (Fig 1C). Differential gene expression analysis identified 56 upregulated and 54 downregulated genes in *Lcn2*$^{-/-}$ AMs (S1A Fig), and 205 upregulated and 142 downregulated genes in *Lcn2*$^{-/-}$ $CD103^+$ DCs (S1B Fig). While showing little overlap with AMs (S1C Fig), the LCN2-related differentially expressed genes of $CD103^+$ DCs mapped to different KEGG (Kyoto Encyclopedia of Genes and Genomes) pathways (Fig 1D and S1 Table) see S1D Fig and S2 Table for differentially impacted KEGG pathways in AMs, with *antigen processing and presentation* (based on 11 differentially expressed genes) affected the most. Remarkably, three pathways related to infections (*Legionellosis* [9 genes], *Measles* [11 genes] and *Influenza A* [11 genes]), were among the 10 most significantly impacted (Fig 1D). Focusing on *antigen processing and presentation* and *Influenza A*, we identified three heat-shock proteins (*Hspa8*, *Hspa1b*, *Hspa1a*), the M alpha chain of the MHC-II complex (*H2-DMa*) and *Tnf* (Fig 1E) to be differentially regulated. The genes related to *antigen processing and presentation* further included the nonclassical MHC class I molecule H2-M3, highlighting that LCN2 affected expression of both, MHC class I and II associated genes. Interestingly, the *Influenza A* pathway was related to six additional differentially regulated genes, including *Il1b* and *Nlrp3*. These results reveal that LCN2 shapes pulmonary $CD103^+$ DC gene expression profiles in homeostasis and suggest potential effects of LCN2 on antigen processing and presentation by DCs in the context of antiviral immune responses.

Lipocalin 2-deficient animals show increased disease morbidity and lung T cell numbers upon influenza infection

Considering the importance of $CD103^+$ DC in cross presenting antigen during influenza infection [16], and the obvious impact LCN2 has on homeostatic $CD103^+$ DC signatures, we tested the functional implications of these findings. Using a mouse model of influenza infection based on intranasal inoculation with PR/8 (a mouse-adapted H1N1 influenza strain [18]) we determined the potential functions of LCN2 in antiviral immunity. LCN2 deficiency was

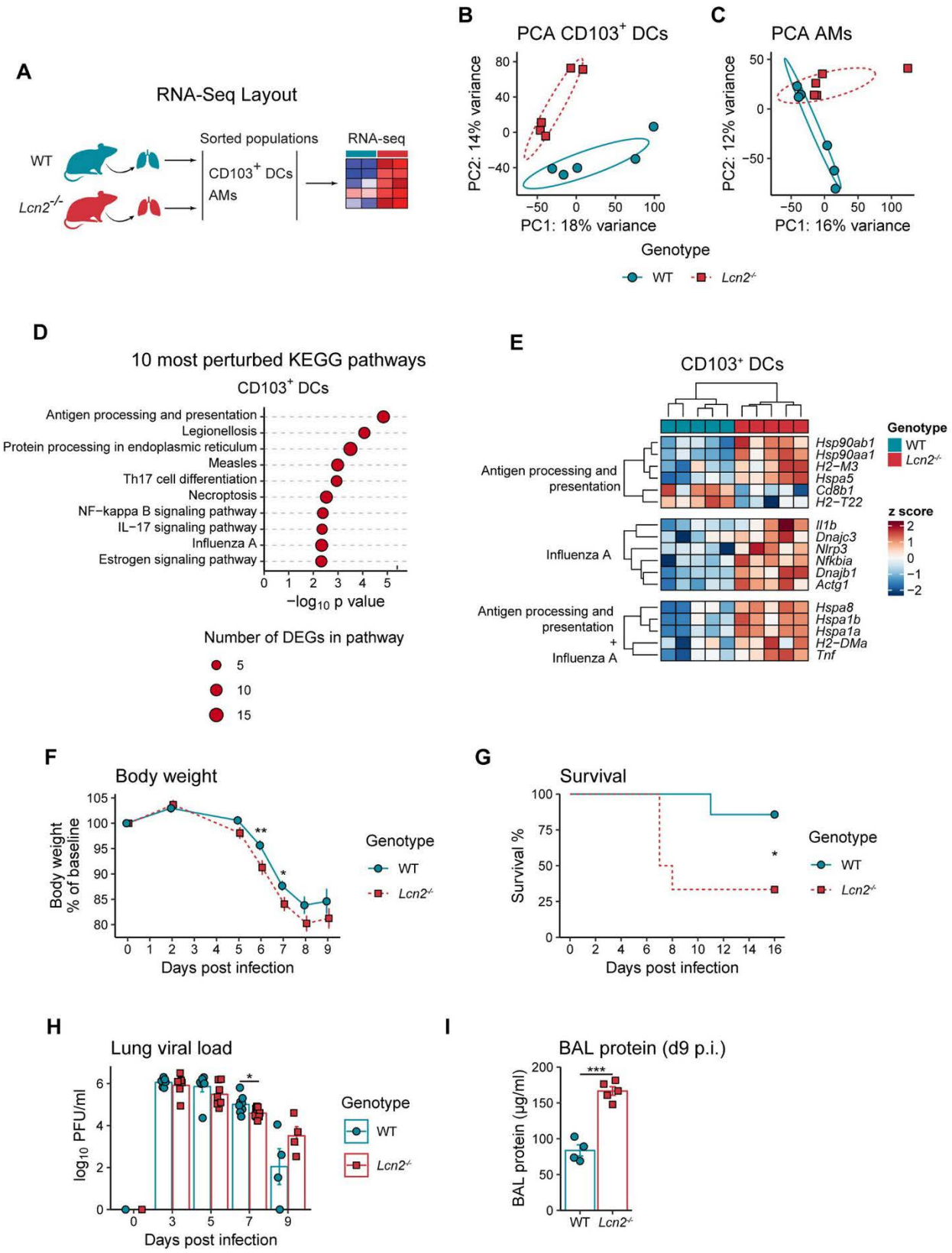
A
RNA-Seq Layout
WT
Lcn2-/-
Sorted populations
CD103+ DCs
AMs
RNA-seq
B
PCA CD103+ DCs
PC2: 14% variance
PC1: 18% variance
C
PCA AMs
PC2: 12% variance
PC1: 16% variance
Genotype
WT
Lcn2-/-
D
10 most perturbed KEGG pathways
CD103+ DCs
Antigen processing and presentation
Legionellosis
Protein processing in endoplasmic reticulum
Measles
Th17 cell differentiation
Necroptosis
NF−kappa B signaling pathway
IL−17 signaling pathway
Influenza A
Estrogen signaling pathway
−log10 p value
Number of DEGs in pathway
5
10
15
E
CD103+ DCs
Antigen processing and presentation
Influenza A
Antigen processing and presentation + Influenza A
Hsp90ab1
Hsp90aa1
H2−M3
Hspa5
Cd8b1
H2−T22
Il1b
Dnajc3
Nlrp3
Nfkbia
Dnajb1
Actg1
Hspa8
Hspa1b
Hspa1a
H2−DMa
Tnf
Genotype
WT
Lcn2-/-
z score
F
Body weight
Body weight % of baseline
Days post infection
Genotype
WT
Lcn2-/-
G
Survival
Survival %
Days post infection
Genotype
WT
Lcn2-/-
H
Lung viral load
log10 PFU/ml
Days post infection
Genotype
WT
Lcn2-/-
I
BAL protein (d9 p.i.)
BAL protein (µg/ml)
WT
Lcn2-/-

Fig 1. LCN2 shapes myeloid cell transcriptome during homeostasis and limits disease morbidity during influenza infection. (A) Experimental layout to assess the influence of LCN2 on the transcriptome of pulmonary myeloid immune cells. $CD103^+$ dendritic cells (DCs) and alveolar macrophages (AMs) were isolated by FACS and processed for RNA sequencing. (B-C) Principal component analysis of $CD103^+$ DCs (B) and AMs (C) derived from lungs of WT and *Lcn2*$^{-/-}$ mice. (D) Top ten KEGG pathways with lowest SPIA (Signaling Pathway Impact Analysis) p values in $CD103^+$ DCs. Circle sizes indicate the number of differentially expressed genes (DEGs) associated with the respective pathway. (E) Heatmap of DEGs in *antigen processing and presentation* or *Influenza A* KEGG pathways. Raw counts are *rlog* transformed followed by z-score scaling. (F) Comparison of relative body weight (normalized to baseline) between WT and *Lcn2*$^{-/-}$ mice after infection with 10 PFU PR/8, shown as group means +/- SEM. Pooled data from three independent experiments are shown, n = 17 mice per genotype. (G) Survival of WT and *Lcn2*$^{-/-}$ mice after infection with 15 PFU PR/8. n = 7 (WT) and 6 (*Lcn2*$^{-/-}$). Data are representative of two independent experiments. (H) Viral load, assessed by plaque assay on MDCK cells, in lung homogenates of WT or *Lcn2*$^{-/-}$ mice after infection with 10 PFU PR/8. n = 4–10 mice per genotype and timepoint. (I) Total protein concentration in bronchoalveolar lavage (BAL) 9 days after infection with 10 PFU PR/8. n = 4 (WT) and 5 (*Lcn2*$^{-/-}$). Data are representative of two independent experiments. (E) Columns represent samples collected from individual mice. Bar diagrams (H, I) show group means +/- SEM. Significance was assessed using Student's t test for (F), (H) and (I), or asymptotic two-sample logrank test for (G). $^*p < 0.05$, $^{**}p < 0.01$, $^{***}p < 0.001$.

https://doi.org/10.1371/journal.ppat.1009487.g001

associated with increased body weight loss over nine days after infection (Fig 1F), which led to higher mortality in *Lcn2*$^{-/-}$ mice (Fig 1G). Interestingly, this impaired disease phenotype was not associated with increased lung viral loads in *Lcn2*$^{-/-}$ mice (Figs 1H and S1E). In contrast, LCN2 deficiency was associated with increased bronchoalveolar lavage (BAL) levels of proinflammatory cytokines (i.e. IL12, interferon [IFN]γ, IP-10, IL6, MCP-1, BAFF and IFNα) three days after influenza infection (S1F Fig). Furthermore, *Lcn2*$^{-/-}$ animals showed higher BAL protein levels at the peak of inflammation (nine days after influenza infection; Fig 1I), indicating increased lung vascular permeability and inflammation [19,20]. We conclude from these results that LCN2 attenuated influenza infection-related inflammation and disease morbidity independent of viral clearance, suggesting a role for LCN2 in limiting virus-related immunopathology.

To characterize the regulatory function of LCN2 on immunological processes during influenza infection, we analyzed the influenza-induced lung T cell response by flow cytometry (S2A Fig). We observed more $CD4^+$ T helper cells (Fig 2A) and $CD8^+$ cytotoxic T cells (Fig 2B) in lungs of *Lcn2*$^{-/-}$ mice seven, nine and 16 days after infection. Furthermore, LCN2 deficiency was associated with elevated proportions of $CD69^+$ activated pulmonary $CD4^+$ (S2B Fig) and $CD8^+$ T cells (Fig 2C) and higher numbers of IFNγ-expressing (Fig 2D) and of antigen-specific $CD8^+$ T cells (Fig 2E). This enhanced adaptive immune response was further reflected by increased influenza-specific serum IgG antibody levels in *Lcn2*$^{-/-}$ mice (Fig 2F). Apart from an increase in lung neutrophils (day nine) and B cells (day 16 after infection) in *Lcn2*$^{-/-}$ mice, we observed no significant differences in the composition of lung immune cells (S2C–S2E Fig). However, the enlarged mediastinal lymph nodes (mLNs), which are considered the primary sites of early T cell proliferation after influenza infection [21], and increased mLN cell numbers nine and 16 days after influenza infection underline the increased adaptive immune response in *Lcn2*$^{-/-}$ animals (Fig 2G). We next depleted $CD8^+$ T cells to assess their contribution to the increased morbidity of *Lcn2*$^{-/-}$. This depletion protected *Lcn2*$^{-/-}$ mice from exaggerated weight loss between day 4 and 7 post infection (Fig 3C–3E), indicating that $CD8^+$ T cells mediate the increased weight loss during this time period. Taken together, these results suggested that LCN2 influenced disease morbidity during influenza infection by regulation of T cell-related adaptive immunity.

LCN2 alters the antigen presentation efficiency of $CD103^+$ DCs, but not intrinsic T cell proliferation

We next aimed to determine whether the increased lung T cell numbers in *Lcn2*$^{-/-}$ mice were related to an increased intrinsic T cell proliferation potential. To do so, we applied a competitive T cell chimera tracing strategy based on transfer of equivalent numbers of $CD45.2^+$ splenic T cells isolated from green fluorescent protein (GFP) expressing WT mice and GFP^- *Lcn2*$^{-/-}$

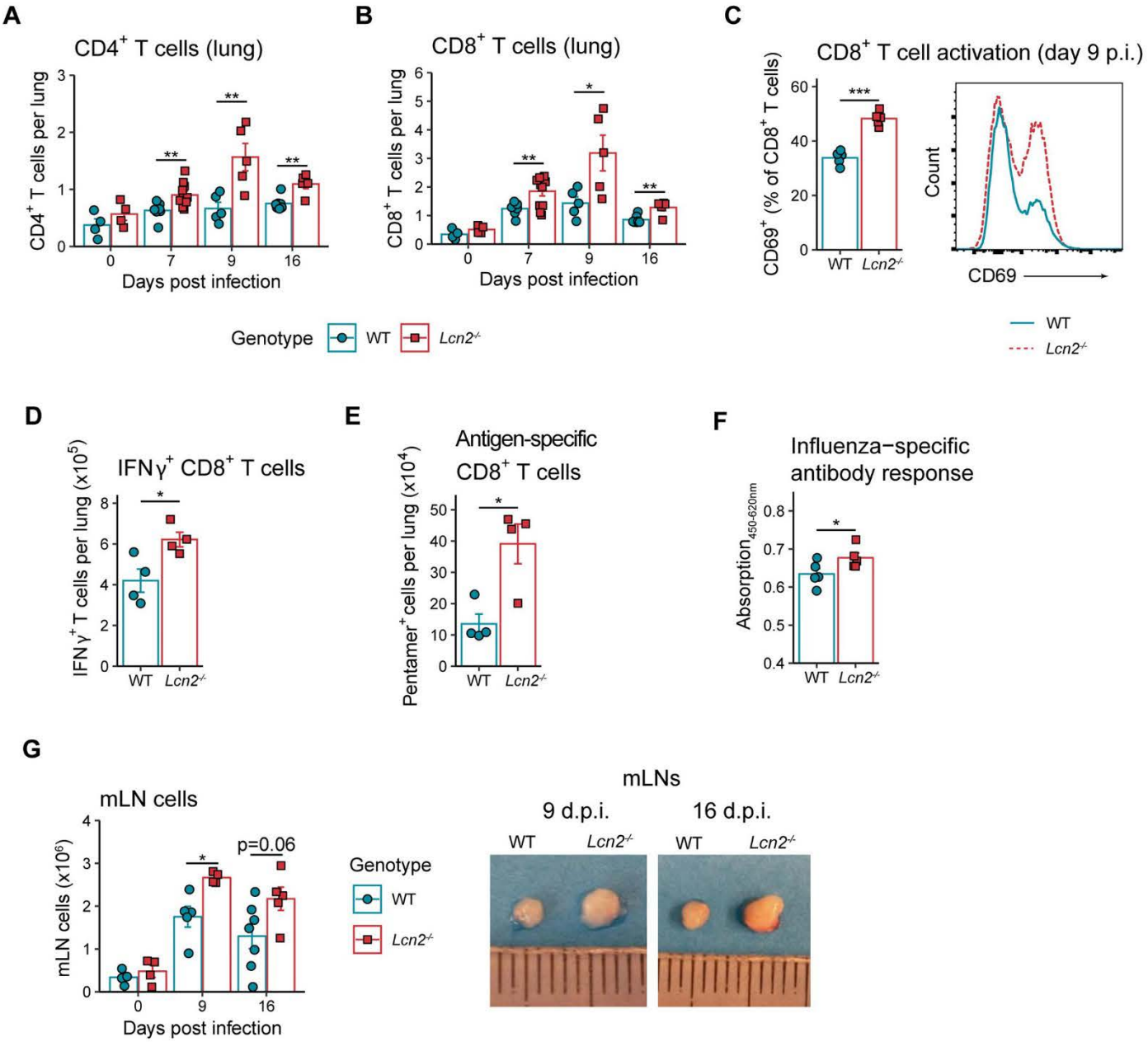

Fig 2. LCN2 reduces lung T cell numbers and mediastinal lymph node size during influenza infection. (A, B) $CD4^+$ (A) and $CD8^+$ T cell counts (B) in lungs of WT and *Lcn2*$^{-/-}$ mice at baseline (d0) or at indicated timepoints after infection with 10 PFU PR/8. n = 4 (baseline), 7–10 (day 7), 5 (day 9) and 5–7 (day 16 post infection) per genotype. Data are representative of two independent experiments. (C) Percent of activated ($CD69^+$) $CD8^+$ lung T cells 9 days post infection. Quantification and representative histograms of are shown. n = 5 per genotype. (D) Number of $IFN\gamma^+$ lung $CD8^+$ T cells. *n = 4 per genotype*. *(E)* Number of antigen-specific (PR8 $pentamer^+$) lung $CD8^+$ T cells. *n = 4 per genotype*. (F) Total influenza-specific IgG levels in serum collected from mice 16 days after influenza infection. n = 5 per genotype. (G) Mediastinal lymph node (mLN) leukocyte counts and representative images of mLNs 9 and 16 days after influenza infection. n = 4 (baseline), 4–5 (day 9 post infection) and 5–7 (day 16 post infection) per genotype. Bar diagrams show group means +/- SEM. Statistical significance for comparisons between genotypes for was assessed using Student's t test. $^*p < 0.05$, $^{**}p < 0.01$, $^{***}p < 0.001$.

https://doi.org/10.1371/journal.ppat.1009487.g002

mice into $CD45.1^+$ WT recipients, and subsequent influenza infection (2 days after transfer, Fig 3F). Nine days after influenza infection of engrafted $CD45.1^+$ mice, we observed comparable numbers of $CD45.2^+$ GFP^+ (WT) and GFP^- (*Lcn2*$^{-/-}$) lung (Fig 3G) and mLN (Fig 3H) T

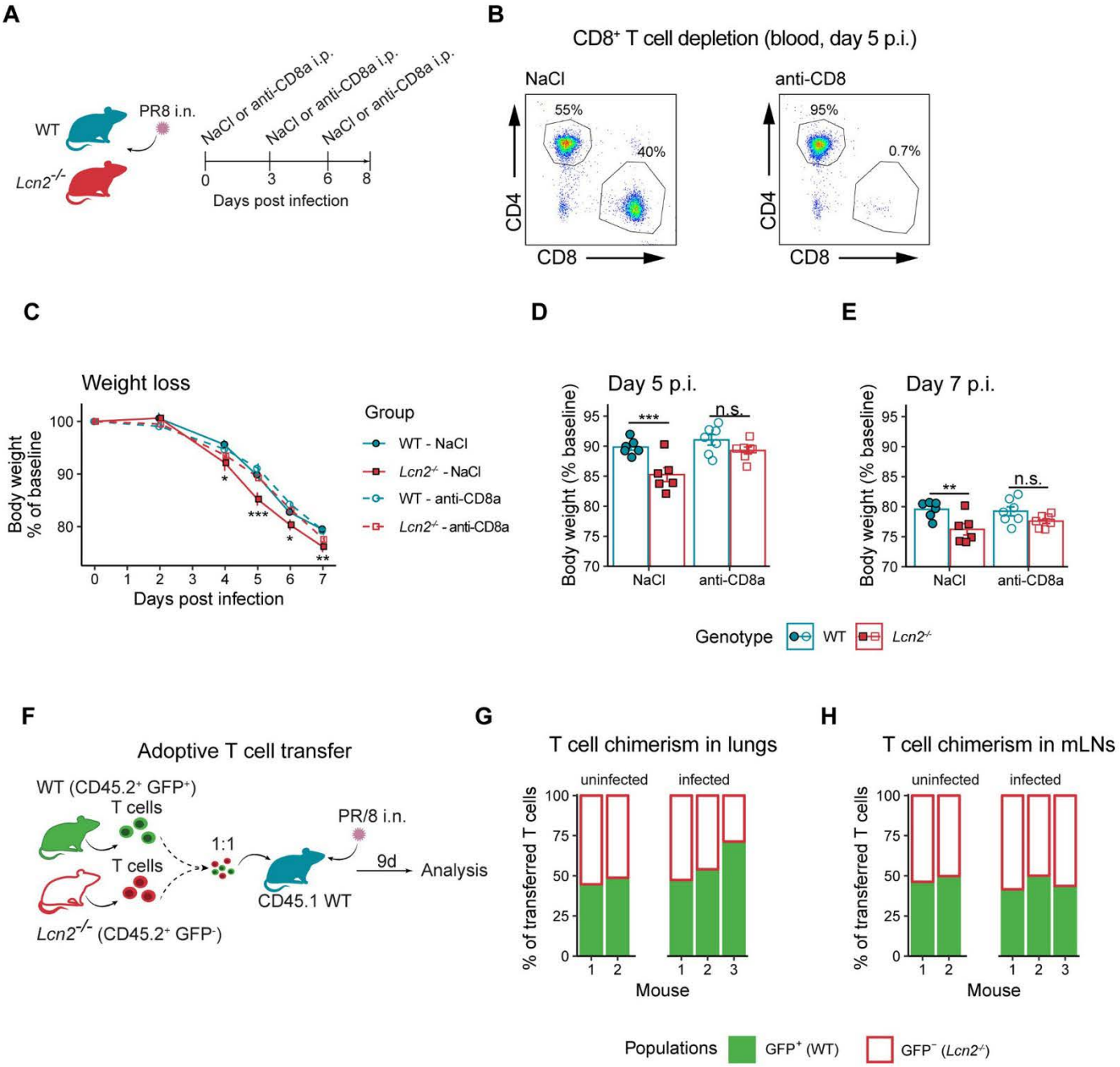

Fig 3. LCN2 protects from excessive weight loss by reducing lung CD8$^+$ T cell numbers but does not affect T cell intrinsic proliferation potential. (A) Experimental layout to assess the contribution of CD8$^+$ T cells to LCN2-related effects on weight loss during influenza infection. WT and *Lcn2*$^{-/-}$ mice were treated with anti-CD8a or vehicle (NaCl) on day 0, 3 and 6 post influenza infection (p.i.). Weight loss was monitored and the experiment was stopped meeting pre-defined endpoint criteria. (B) Representative FACS plots illustrating CD8$^+$ T cell depletion after anti-CD8a treatment on day 5 post infection/start of treatment. Cells are pre-gated single, live, CD45$^+$, CD19$^-$ and CD3$^+$ cells. (C) Weight curves after influenza infection. Asterisks below the curves denote statistical significance for the comparison between NaCl-treated WT *vs.* *Lcn2*$^{-/-}$ mice, asterisks above the curve for the comparison between anti-CD8a treated mice. n = 6–7 per group (D, E) Relative body weight (compared to baseline day 0) on day 5 (D) and day 7 (E) after influenza infection. (F) Experimental layout to assess the proliferative potential of WT and *Lcn2*$^{-/-}$ T cells. 50:50 ratio of splenic WT (GFP$^+$) and *Lcn2*$^{-/-}$ (GFP$^-$) T cells were transferred to CD45.1$^+$ mice and infected with PR/8. CD45.2$^+$ GFP$^+$ and CD45.2$^+$ GFP$^-$ T cells (indicative of transferred WT or *Lcn2*$^{-/-}$ genotype, respectively) were assessed nine days later in lungs and mesenteric lymph nodes (mLNs). (G, H) Relative abundance of GFP$^+$ (WT) and GFP$^-$ (*Lcn2*$^{-/-}$) cells among CD45.2$^+$ CD3$^+$ T cells derived from lungs (G) and mLNs (H) 9 days post infection. Columns represent samples collected from individual mice. Bar diagrams and error bars (C-E) show group means +/- SEM. Statistical significance for comparisons between genotypes for (C-E) was assessed using estimated marginal mean comparison after 2-way ANOVA. $^*p < 0.05$, $^{**}p < 0.01$, $^{***}p < 0.001$.

https://doi.org/10.1371/journal.ppat.1009487.g003

cells. These results prove that LCN2 does not influence the intrinsic proliferative potential of T cells.

Another reason for the increased T cell numbers in *Lcn2*$^{-/-}$ mice could be an altered antigen-presentation process. The proliferation of CD8$^+$ T cells during influenza infection is driven by cross-presentation of viral antigens by lung-resident DCs, which migrate from the infected lung to the mLNs [16]. To compare the potential of WT and *Lcn2*$^{-/-}$ DCs to induce CD8$^+$ T cell proliferation, we used an antigen presentation assay utilizing a genetically modified PR/8 strain expressing an ovalbumin peptide (PR/8-Ova) [22] in combination with OT-I CD8$^+$ T cells (derived from mice which possess exclusively ovalbumin-specific CD8$^+$ T cells [23]). Sixty hours after infection with PR/8-Ova, CD103$^+$ DCs and CD8$^+$ DCs were sorted from mediastinal lymph nodes and then incubated with OT-I T cells (Fig 4A). Using this approach, we observed increased CD8$^+$ T cell proliferation upon incubation with *Lcn2*$^{-/-}$ CD103$^+$ DCs (Fig 4B and 4C). This LCN2-related effect was limited to CD103$^+$ DCs, which are considered the dominant antigen cross-presenting DCs in the lung [16,24,25], and was not observed for CD8a$^+$ DCs (S3A and S3B Fig). To further dissect the effect of LCN2 on DCs in antiviral immunity, we compared the transcriptome of WT and *Lcn2*$^{-/-}$ CD103$^+$ DCs collected from mLNs 60 hours after influenza infection and observed separation of samples according to genotype, suggesting robust LCN2 effects on the CD103$^+$ DC transcriptome during infection (Fig 4D). Among 106 upregulated and 63 downregulated genes in *Lcn2*$^{-/-}$ CD103$^+$ DCs (Fig 4E), only very few (one and four genes, respectively) showed similar regulation in cells isolated from homeostatic lungs (S3D Fig), indicating specific differentially regulated gene sets during homeostasis and infection. The most significantly impacted KEGG pathway in CD103$^+$ DCs isolated from infected *Lcn2*$^{-/-}$ mice was *intestinal immune network for IgA production* (Fig 4F). Differentially expressed genes mapping to this pathway included *Ccr9*, *Icosl* and *Cd40*, the latter two of which are involved in interactions between DCs and T cells [26,27], and *H2–Eb1* and *H2–Aa* which encode subunits of the MHC II complex (Fig 4G). These two genes were also associated with the KEGG pathway *antigen processing and presentation*, which was also significantly affected (Fig 4F and 4G). Further genes linked to this pathway were *H2-M2*, which encodes an MHC class Ib antigen, and *Ciita*, a transcriptional coactivator that regulates MHC class I and II genes [28]. Taken together, these results show that LCN2 negatively regulates antigen presentation of CD103$^+$ DCs to CD8$^+$ T cells during influenza infection, possibly by influencing the expression of specific functionally important gene sets.

The microbiome is shaped by LCN2 and influences the immune response to influenza infection

Having shown that LCN2 protects from influenza-associated disease severity by modulating DC-driven T cell activation during infection, we wanted to investigate potential mechanisms that could link those observations. To this end, we generated DCs from bone marrow (BMDCs) of WT and *Lcn2*$^{-/-}$ mice and investigated their antigen presentation potential *in vitro*. Interestingly, ovalbumin-pulsed WT and LCN2-deficient BMDCs were similarly proficient inducers of OT-I CD8$^+$ T cell proliferation (S3D Fig). Additionally, pre-incubation of BMDC with recombinant LCN2 during antigen pulsing did not alter the antigen presentation capacity (S3E Fig). In line with these results, we considered direct effects of LCN2 on DC antigen presentation rather unlikely, and decided to explore potential indirect mechanisms. Since it is known that LCN2 modulates the availability of microbial nutrients [4] and that the microbiome can influence antiviral immunity [29,30], we tested if LCN2 availability might alter the microbiome. We therefore compared commensal intestinal and pulmonary bacterial communities in WT and *Lcn2*$^{-/-}$ mice. While microbiome analysis of F2 generation offspring of

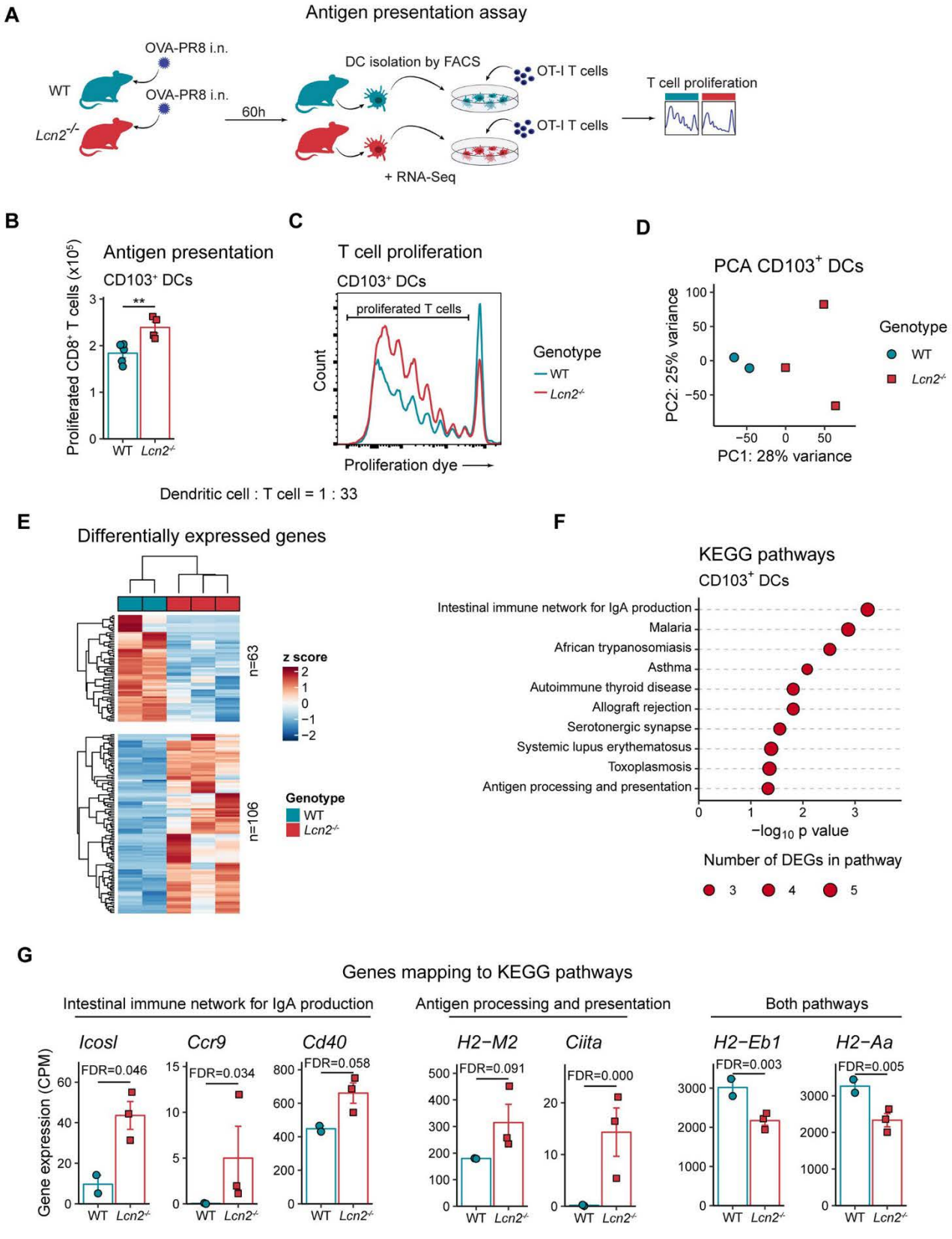
A
Antigen presentation assay
OVA-PR8 i.n.
WT
OVA-PR8 i.n.
Lcn2-/-
60h
DC isolation by FACS
OT-I T cells
OT-I T cells
+ RNA-Seq
T cell proliferation
B
Antigen presentation
CD103+ DCs
Proliferated CD8+ T cells (x10^5)
**
WT
Lcn2-/-
C
T cell proliferation
CD103+ DCs
proliferated T cells
Count
Proliferation dye
Genotype
WT
Lcn2-/-
D
PCA CD103+ DCs
PC2: 25% variance
PC1: 28% variance
Genotype
WT
Lcn2-/-
Dendritic cell : T cell = 1 : 33
E
Differentially expressed genes
n=63
n=106
z score
Genotype
WT
Lcn2-/-
F
KEGG pathways
CD103+ DCs
Intestinal immune network for IgA production
Malaria
African trypanosomiasis
Asthma
Autoimmune thyroid disease
Allograft rejection
Serotonergic synapse
Systemic lupus erythematosus
Toxoplasmosis
Antigen processing and presentation
−log10 p value
Number of DEGs in pathway
G
Genes mapping to KEGG pathways
Intestinal immune network for IgA production
Antigen processing and presentation
Both pathways
Icosl
Ccr9
Cd40
H2−M2
Ciita
H2−Eb1
H2−Aa
FDR=0.046
FDR=0.034
FDR=0.058
FDR=0.091
FDR=0.000
FDR=0.003
FDR=0.005
Gene expression (CPM)
WT
Lcn2-/-

Fig 4. *Lcn2*$^{-/-}$ CD103^{+} DCs are more proficient in presenting antigen to CD8^{+} T cells and have an altered transcriptome after influenza infection. (A) Experimental layout for antigen presentation assay. CD103^{+} and CD8^{+} DCs were sorted from mediastinal lymph nodes (mLNs) of WT and *Lcn2*$^{-/-}$ mice 60h after PR/8-OVA infection, followed by co-culture with splenic OT-I T cells. (B) CD8^{+} T cell proliferation of 96h co-culture with WT or *Lcn2*$^{-/-}$ CD103^{+} DCs at 1: 33 (DC: T cell) ratio. Technical replicates (n = 2–4) of two pools (pooled DCs from 6–7 mice per genotype) are shown (data of CD8^{+} DCs are in S3 Fig). (C) Representative histograms of (B). (D) Principal component analysis of transcriptomic profiles of mLN-derived CD103^{+} DCs from WT and *Lcn2*$^{-/-}$ mice 60 hours after infection with PR/8-OVA. (E) Heatmap of all differentially expressed genes (DEGs) in CD103^{+} DCs. Read counts are *rlog* transformed, followed by z-score scaling. (F) Top ten KEGG pathways with lowest SPIA (Signaling Pathway Impact Analysis) p values in CD103^{+} DCs isolated from mLNs of PR/8-OVA-infected mice. Circle sizes indicate the number of DEGs associated with the respective pathway. (G) Normalized expression (counts per million mapped reads) of differentially expressed genes (FDR < 0.1) mapping to either *intestinal immune network for IgA production* or *antigen processing and presentation*, or both KEGG pathways. Bar diagrams (B), (G) show group means +/- SEM. Statistical significance for (B) was assessed using nested ANOVA. *p < 0.05, **p < 0.01.

https://doi.org/10.1371/journal.ppat.1009487.g004

heterozygous breeding pairs by 16S rRNA gene sequencing (Fig 5A) showed that the BAL microbial profile of WT and *Lcn2*$^{-/-}$ animals was similar, we observed highly different LCN2-dependent compositions of ileum luminal and mucosal, cecal and stool microbial communities (Fig 5B–5F). Shannon diversity was comparable between genotypes for all sampled sites, but we observed trends towards decreased amplicon sequencing variant (ASV) richness in cecal and stool samples (S4A and S4B Fig). The bacterial phyla *Proteobacteria*, *Bacteroidetes* and *Actinobacteria* were increased in stool samples from *Lcn2*$^{-/-}$ mice, whereas *Tenericutes* were decreased (S4C Fig). While phylum level differences in microbial composition were limited to stool samples, we observed differences for multiple ASVs for all sample sites throughout the intestinal tract (S4D Fig and S3 Table). As such, an ASV identified as segmented filamentous bacteria (SFB), which accounted for up to 90% of all bacterial sequencing reads in the ileal mucosa of WT mice, was absent in *Lcn2*$^{-/-}$ mice (S4D Fig). In summary, our data show that LCN2 shapes the intestinal microbiome in a site-specific manner.

We next aimed to determine whether the LCN2-related microbiome differences play a role in the dysregulated antiviral immune response in *Lcn2*$^{-/-}$ mice. To deplete the intestinal microbiome, we treated WT and *Lcn2*$^{-/-}$ mice with antibiotics (vancomycin, metronidazole, ampicillin and gentamicin) in glucose-supplemented drinking water for 4 weeks prior to influenza infection (Fig 5G). While mock-treated *Lcn2*$^{-/-}$ mice (receiving glucose-supplemented water) exhibited increased pulmonary T cell and mediastinal lymph node cell counts as previously observed, microbiome depletion equalized these differences to WT mice (Fig 5H–5J). In addition, antibiotic treatment abolished differences in the antigen presentation potential of *Lcn2*$^{-/-}$ and WT CD103^{+} DCs (S5A and S5B Fig). To further study the role of the microbiome, we co-housed WT and *Lcn2*$^{-/-}$ mice for 4 weeks prior to PR/8 infection (Fig 5K) to partially hybridize microbial profiles by passive transfer of microbiota [31,32]. Confirming the effectivity of this approach, co-housing led to similar levels of the bacterial phylum *Bacteroidetes* in WT and *Lcn2*$^{-/-}$ animals, while significantly different in separately housed mice (S4C Fig). Finally, co-housing decreased lung CD8^{+} T cell differences between influenza-infected WT and *Lcn2*$^{-/-}$ mice (Fig 5L and 5M), while mLN size was unaffected (Fig 5N). Taken together, these results indicate that LCN2 modulated the antiviral immune response and prevented exaggerated CD8^{+} T cell immunity during influenza infection in a microbiome-dependent mechanism.

Discussion

Previous studies provided evidence for the immunomodulatory potential of LCN2 [7–10]. We here extend and substantiate these observations by showing that LCN2 skewed the transcriptome of lung myeloid cells during homeostasis and dampened T cell responses upon influenza infection, resulting in diminished disease-related morbidity and mortality independent of viral clearance. We succeeded in linking the effects of LCN2 to the magnitude of CD8^{+} T cell responses via altered CD103^{+} DC functionalities. Finally, the LCN2-driven

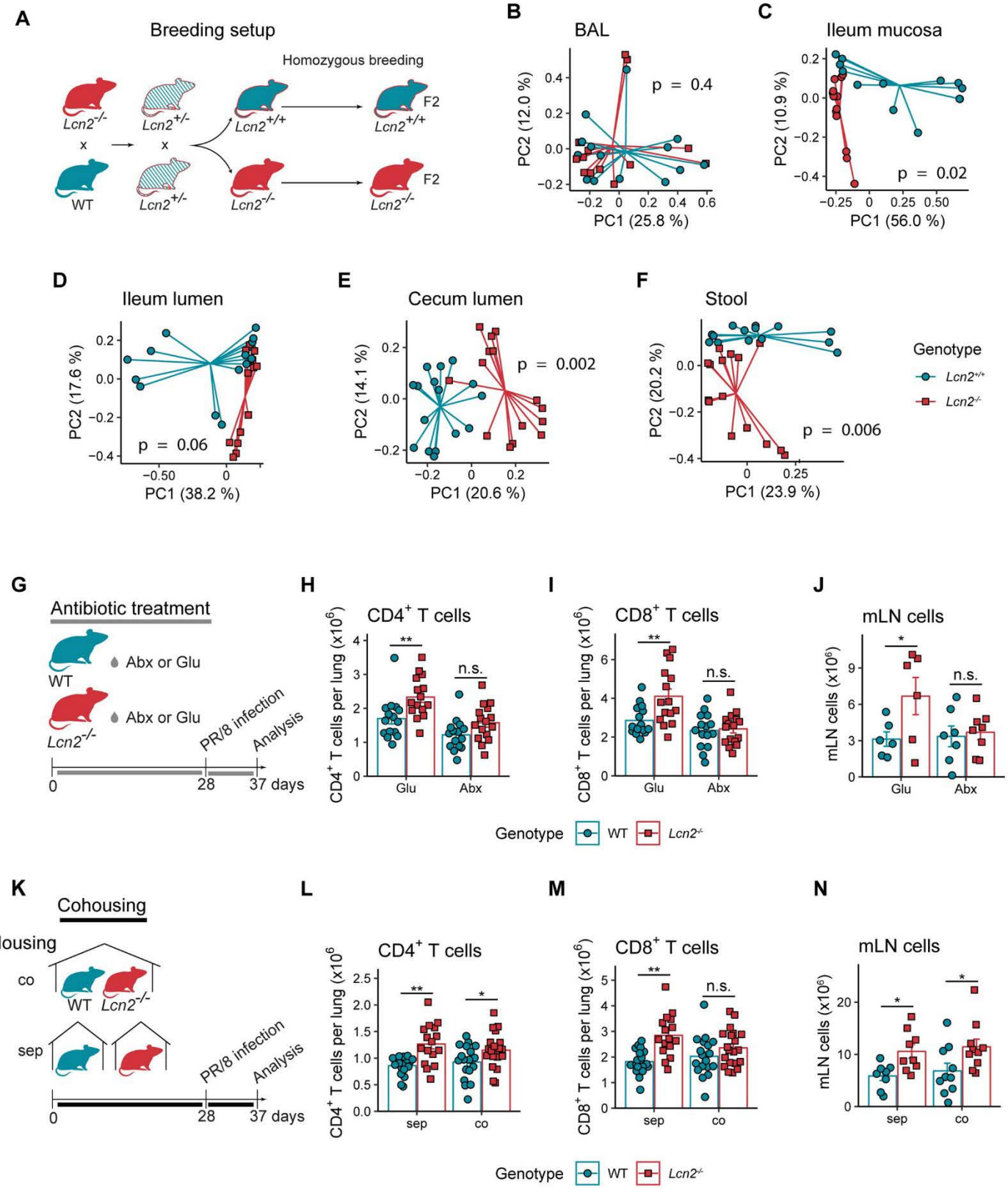
A
Breeding setup
Homozygous breeding
Lcn2-/-
Lcn2+/-
Lcn2+/+
F2
WT
B
BAL
p = 0.4
PC2 (12.0 %)
PC1 (25.8 %)
C
Ileum mucosa
p = 0.02
PC2 (10.9 %)
PC1 (56.0 %)
D
Ileum lumen
p = 0.06
PC2 (17.6 %)
PC1 (38.2 %)
E
Cecum lumen
p = 0.002
PC2 (14.1 %)
PC1 (20.6 %)
F
Stool
p = 0.006
PC2 (20.2 %)
PC1 (23.9 %)
Genotype
Lcn2+/+
Lcn2-/-
G
Antibiotic treatment
Abx or Glu
WT
Lcn2-/-
PR/8 infection
Analysis
0
28
37 days
H
CD4+ T cells
CD4+ T cells per lung (x10^6)
n.s.
Glu
Abx
I
CD8+ T cells
CD8+ T cells per lung (x10^6)
J
mLN cells
mLN cells (x10^6)
Genotype
WT
Lcn2-/-
K
Cohousing
Housing
co
sep
L
CD4+ T cells
M
CD8+ T cells
N
mLN cells

Fig 5. Effect of LCN2 on antiviral immunity is dependent on the microbiome. (A) Breeding setup for microbiome analysis of WT *or* *Lcn2*$^{-/-}$ mice. (B-F) Principal coordinate analyses on Bray-Curtis distances (with PERMANOVA p-values for genotype, controlling for cage) for bronchoalveolar lavage (BAL), ileal mucosa, ileal lumen, cecum and stool samples derived from 12 weeks old WT and *Lcn2*$^{-/-}$ mice. n = 13–16 mice per genotype. (G) Experimental setup for experiments involving antibiotic treatment prior to influenza infection. (H-J) Lung CD4$^+$ T cells (H), CD8$^+$ T cells (I) and total mediastinal lymph node (mLN) cell counts (J) 9 days after PR/8 infection for WT and *Lcn2*$^{-/-}$ antibiotics-treated and control mice. Data from two pooled experiments are shown in (H-I). Total n per genotype and treatment = 15–16 for (H-I) or 6–7 (J). (K) Experimental setup for co-housing experiments. WT and *Lcn2*$^{-/-}$ mice were separately- (sep) or co-housed (co) for four weeks prior to influenza infection. (L-N) Lung CD4$^+$ T (L) and CD8$^+$ T cell counts (M) and total mLN cell counts (N) 9 days after PR/8 infection for co- or separately-housed WT and *Lcn2*$^{-/-}$. Data from two pooled experiments are shown in (L-M), total n per genotype and treatment = 16–20 for (L-M) or 8–10 (N). Bar diagrams show group means +/- SEM, and statistical significance for comparisons between genotypes for (H-J) and (L-N) was assessed using estimated marginal mean comparison after 2-way ANOVA. n.s. not significant, $^*p < 0.05$, $^{**}p < 0.01$.

https://doi.org/10.1371/journal.ppat.1009487.g005

immunomodulation did not occur directly, but relied on LCN2's impact on the microbiome composition, which we verified by experiments using antibiotics or cohousing approaches.

Influenza infection-related pathology in humans, non-human primates and mice is predominantly caused by exaggerated antiviral and hyper-inflammatory responses, rather than direct cytopathic effects of the virus [12,33–35]. While critical for viral clearance and immunological memory, pro-inflammatory cytokine production and cytolytic activity by CD4$^+$ and CD8$^+$ T cells, respectively, importantly contribute to immunopathology [36,37]. Our data indicate that excessive T cell proliferation, resulting from more potent antigen presentation by CD103$^+$ DCs to CD8$^+$ T cells, mediate increased morbidity in *Lcn2*$^{-/-}$ mice. Our study identifies LCN2 as an important modulator of antiviral immunity and suggests that LCN2 fine-tunes DC activity during homeostasis and to prevent excessive T cell expansion and immunopathology during viral infections. Of note, tissue damage due to aberrant immune activation is not restricted to influenza infections, but has been suggested to play an important role in COVID-19 mortality [13]. While we here focused on influenza infection, LCN2-regulated inflammation and immunopathology might also importantly influence the course of other viral infections [15].

Recent research highlights the critical effect of microbiome compositions on maturation and functionality of the immune system [11]. As such, the gut microbiome was reported to influence DC migration to draining lymph nodes and T cell priming during influenza infection by providing signals leading to pro-IL1β and pro-IL18 expression at steady state and inflammasome activation upon influenza infection [29]. While antibiotic treatment interfered with these signals, intranasal or intrarectal injection of TLR ligands was sufficient to restore the microbiome dependent effects. Furthermore, sensing of host microbiota via TLR5 was found to facilitate antibody responses to influenza vaccines by promoting plasma cell differentiation [38]. Additionally, microbial metabolites such as desaminotyrosine and short-chain fatty acids were discovered to regulate antiviral immunity and to protect from influenza associated disease morbidity [39,40]. We here observed that LCN2-deficiency was associated with an altered site-specific intestinal microbial composition and that microbiome disruption by antibiotics abrogated LCN2-related differences in anti-influenza immunity. While we did not identify which specific features of the microbiota mediated the observed effects on host immunity, we identified several candidates. Among the multiple ASVs with differential abundance in ileal, cecal or stool samples, SFB (which were among the most abundant ASVs in the ileal mucosa of WT mice) were completely absent in *Lcn2*$^{-/-}$ mice. This common bacterial strain is involved in host-microbiome crosstalk as it can induce Th17 cells in the gut [41], and its abundance is affected by influenza infection [42].

Two previous studies have set out to assess the effect of LCN2 on stool microbial composition. Singh *et al.* reported distinct bacterial communities in *Lcn2*-deficient mice, which were linked to exacerbated colitis or neutralization of IL10 [43]. In agreement with our findings, this study found increased *Bacteroidetes* and *Proteobacteria* phyla and a decreased *Tenericutes*

phylum in stool samples of *Lcn2*$^{-/-}$ mice. In contrast, Moschen *et al.* reported that LCN2 exclusively affects the intestinal microbiome in mice lacking IL-10 leading to colitis and spontaneous emergence of right sided colonic tumors [44]. These discrepancies could be explained by altered baseline microbiota due to differences in animal housing or the lower number of experimental animals with differences in statistical power in the study by Moschen *et al.* (4 *vs* 13–16 mice per genotype in the present study).

Several cell surface receptors for LCN2 have been identified: both SLC22A17 (also named 24p3R) and megalin bind LCN2 and mediate its cellular uptake [45,46]. Furthermore, LCN2 can bind to and signal through MC4R in the hypothalamus [3]. We conclude from our results that the effects of LCN2 on influenza-associated T cell responses are primarily dependent on the microbiome. While LCN2 exposure of DCs did not alter their antigen presentation potential *in vitro*, we cannot completely rule out that direct effects of LCN2 on immune cells contribute to the immune-regulatory properties of LCN2 *in vivo*. Further research is needed to fully elucidate these mechanisms. Considering its drastic immunomodulatory effects, variable LCN2 levels in human subjects [47] could have important clinical consequences. For instance, decreased LCN2 levels might identify patients at risk of exaggerated responses to inflammatory triggers such as viral infections, and, on the other hand, supraphysiological LCN2 levels might prevent proper function of the adaptive immune system. Recent evidence suggests a beneficial effect of chronically increased LCN2 levels in patients with obesity or type 2 diabetes [48,49], as it assists in counteracting obesity-induced glucose intolerance by reducing appetite and driving beta-cell proliferation [50]. Interestingly, diabetes and obesity are also associated with increased susceptibility to severe influenza infection [51,52], but the potential correlation between LCN2 levels and disease outcome in humans is not known. Considering the dampening effects of LCN2 on adaptive immunity and influenza-specific antibody levels, elevated LCN2 levels could be a reason for the poor vaccination responses observed in obese individuals [53]. While these observations can be interpreted as potential therapeutic scenarios, further research is required to test the applicability and translational feasibility of such LCN2-related treatment strategies.

Materials and methods

Ethics statement

All mouse experiments were performed in accordance with Austrian law after approval by the Austrian Ministry of Sciences (protocol ID BMWFW-66.009/0285_WF/V/3b/2014 and BMBWF-66.009/0084-V/3b/2018).

Mice

Experiments were conducted using specific opportunistic pathogen free (SOPF) age-matched 8- to 12-week-old C57BL/6J WT, *Lcn2*$^{-/-}$[4], CD45.1 [54] and B6-GFP mice [55]. *Lcn2*$^{-/-}$ mice were provided by S. Akira (University of Osaka, Osaka, Japan), and backcrossed to C57BL/6J mice for 10 generations. OT-I transgenic (C57BL/6-Tg(TcraTcrb)1100Mfb/J)) mice [23] were obtained from Maria Sibilia (Medical University of Vienna). Apart from survival experiments, which were conducted in male mice, all experimental procedures were carried out in female mice. To analyze the effect of LCN2 on the gut and lung microbiome, we utilized a breeding scheme based on recommendations by Mamantopoulos *et al.* [56]. Briefly, WT and *Lcn2*$^{-/-}$ mice with a C57BL/6 background were intercrossed, generating *Lcn2*$^{+/-}$ mice. By breeding these mice, we generated *Lcn2*$^{+/+}$ and *Lcn2*$^{-/-}$ littermates (F1 generation from heterozygous mice), which were bred separately. The offspring of these mice (F2 generation) were used for microbiome analysis.

Influenza virus strains

Purified influenza A/PR/8/34 (PR/8) virus was obtained from Charles River, diluted 1:10 in sterile PBS, aliquoted and stored at -80˚C. PR/8-OVA [22] was provided by Adolfo García-Sastre (Icahn School of Medicine at Mount Sinai, New York). Viral titers were determined by plaque forming assay using MDCK cells [57]. One day before the assay, $1x10^6$ cells/well were seeded in 6-well plates and grown overnight in Dulbecco's Modified Eagle Medium (DMEM; Sigma), supplemented with 10% fetal calf serum (FCS; Sigma), 100 U/ml penicillin and 100 μg/ml streptomycin, to obtain monolayers with >90% confluency. Cells were then washed with PBS and serial 1:10 dilutions of virus in DMEM (without FCS and antibiotics) were added to the cells for 1 hour at 37˚C (each dilution in duplicates). Inoculates were aspirated and overlay medium, consisting of DMEM with antibiotics supplemented with 0.005% DEAE-Dextran (Sigma), 0.2% endotoxin-free bovine serum albumin (Fisher Scientific), 0.2% TPCK-treated trypsin (Sigma) and 1% agarose (Biozym), was added. 3 days later, plaques were visualized by staining with 0.03% neutral red (Sigma) for 3 hours and quantified.

Mouse model of influenza infection

For influenza infection, female mice were intranasally infected with 10–12.5 PFU PR/8 in 50 μl sterile injection-grade (sterile and endotoxin-free) 0.9% NaCl solution. For survival experiments, male mice received 15 PFU PR/8 in 50 μl. Mice were monitored daily and graded according to an internally developed scoring sheet, which assessed appearance, posture, change in body weight and body temperature, natural behavior and clinical signs. Animals with a combined score of >5 or individual scores (in one of the categories) of >3, which could result from hunched posture, more than 30% body weight loss, >5 degrees of body temperature drop, squeaking, self-mutilation or inactive behavior and visible signs of unrelated infections or bleeding, were euthanized. In some planned end-point experiments, bronchoalveolar lavage was performed by inserting a tracheal cannula (Venflon, BD Bioscience) and flushing the lungs with 1 ml NaCl. Otherwise, lungs were flushed by injecting 5 ml of endotoxin-free PBS (Gibco) into the left ventricle, removed under sterile conditions and processed. For plaque assay or RT-PCR, lung tissue was homogenized using a Precellys 24 homogenizer (Peqlab). For plaque assays, homogenates where directly stored at -80˚C, whereas for RT-PCR, aliquots of lung homogenates where frozen (-20˚C) in RA1 buffer (Macherey-Nagel) with 10% beta-mercaptoethanol (Calbiochem).

Determination of viral load by qPCR

RNA was isolated using the NucleoSpin® RNA II kit (Macherey-Nagel), reverse transcription was performed using 700ng of isolated RNA and the iScript cDNA Synthesis Kit (Biorad), according to manufacturer's protocol. Real-time PCR was performed with SYBR Green Master Mix reagents (Applied Biosystems) on a StepOnePlus Real-Time PCR System (Applied Biosystems). Primer sequences targeting the influenza M gene [58] were *CATGGAATGGCTAAAGACAAGACC* (forward) or *CCATTAAGGGCATTTTGGACA* (reverse). The reference gene HPRT was quantified using the sequences *GTTAAGCAGTACAGCCCCAAAATG* (forward) and *AAATCCAACAAAGTCTGGCCTGTA* (reverse).

Multiplex immunoassay for measurement of BAL cytokines

BAL cytokines were measured using a custom multiplex immunoassay (eBioscience), according to the manufacturer's protocol. Briefly, magnetic beads where incubated with undiluted BAL (performed with 1ml sterile and endotoxin-free 0.9% NaCl solution) samples in a 96-well

plate for two hours, followed by washing and incubation with detection antibody (30 minutes). After washing, incubation with streptavidin-PE and another washing step, the plate was read on a Luminex 200 instrument (R&D Systems).

Cell suspension preparation and flow cytometry

For flow cytometry analysis of lung tissue samples, representative pieces of each pulmonary lobe were weighed and homogenized using the lung dissociation kit (Miltenyi Biotec), according to the manufacturer's protocol. Tissue was digested for 30 minutes at 37˚C using DNAse I (12 U/ml; Sigma) and Collagenase I (160 U/ml; Gibco). Next, suspensions were filtered using 70 μM cell strainers (BD Biosciences), red blood cells were lysed using ACK lysis buffer (150 mM NH_4Cl, 10 mM $KHCO_3$, 0.1 mM Na_2EDTA, pH 7.2–7.4; all chemicals from Sigma) and suspensions were again filtered through 40 μM strainers. PBS with 0.5% bovine serum albumin (BSA; BDA, cat. no. 8076.3) was used to stop red blood cell lysis and as buffer for all subsequent steps. In experiments assessing T cell antigen specificity, single cell suspensions were incubated with fluorescently labelled recombinant PR8 pentamer (ProImmune, dilution 1:5) for 10 minutes at room temperature. Cells were then incubated with anti-mouse CD16/32 antibody (TruStain fcX; BioLegend, dilution 1:500) to block unspecific binding to Fcγ receptors and viability dye (Fixable Viability Dye eFluor 780; eBioscience, dilution 1:1000) for 20 minutes at 4˚C, followed by staining with fluorescence-labelled antibodies (see S4 Table, 40 minutes, 4˚C). Mediastinal lymph nodes were mashed through 70 μM cell strainers, followed by Fcγ receptor blocking and staining. Cells were fixed using Fix and Perm (Nordic MUbio) reagents, according to the manufacturer's protocol. Analysis was performed using an LSR Fortessa (BD Biosciences) and FlowJo software (FlowJo LLC). Absolute cell numbers for lungs and lymph nodes were determined using counting beads (123 count eBeads, Thermo Fisher Scientific) or a hematocytometer (for spleens).

For intracellular IFNγ staining, lung single cell suspensions were resuspended in RPMI medium containing 10% FCS (both from Sigma), 1% penicillin/streptomycin (Gibco) and 50 μM 2-Mercaptoethanol (Gibco), followed by treatment with phorbol 12-myristate 13-acetate (PMA; 100 ng/ml, Sigma), ionomycin (500 ng/ml, Sigma) and GolgiStop (1:1250, BD Biosciences) for 5 hours. Next, cells were stained for surface markers (as described above), fixed and permeabilized using BD Cytofix/Cytoperm reagents (BD Biosciences), according to manufacturer's instructions, and stained for IFNγ using a fluorescence-labelled antibody (see S4 Table, 40 minutes, 4˚C).

Analysis of influenza specific IgG response

Influenza-specific antibodies were quantified by ELISA, whereby MaxiSorp ELISA plates (Nunc) were coated overnight at 4˚C with UV-inactivated PR/8 (4000 PFU/ml). After blocking of unspecific binding (PBS 1% BSA), 50 μl of 1: 12500 diluted serum samples were added, followed by detection antibody (biotin-conjugated goat anti-mouse IgG, Jackson ImmunoResearch) and horseradish peroxidase-conjugated streptavidin (BD Pharmingen). Signal emitted by TMB liquid substrate (Sigma) was detected at 450 nm (620 nm reference) using a Sunrise plate reader (Tecan).

CD8+ T cell depletion

To deplete $CD8^+$ T cells, WT and $Lcn2^{-/-}$ mice where intraperitoneally injected with 200 μg of anti-CD8a (clone YTS 169.4) in 200 μl NaCl on the day of infection with 12.5 PFU PR/8, and on day 3 and day 6 post infection [59]. Control mice received sterile PBS (carrier) injections

on the same timepoints. Depletion of $CD8^+$ T cells was assessed by FACS analysis of blood samples collected on days 2 and 5 post infection from the retro-orbital vein.

Adoptive T cell transfer

Single cell suspensions were prepared from GFP^+ WT and $Lcn2^{-/-}$ (CD45.2 background for both) mouse spleens as described above, and incubated with biotinylated antibodies directed against mouse MHC-II (clone M5/114.15.2, BioLegend, diluted 1:100), B220 (clone RA3-6B2; BioLegend, diluted 1:50), CD11c (clone N418; BioLegend, diluted 1:100) and CD11b (clone M1/70, BioLegend, diluted 1:100) for 20 minutes. Spleen T cells were enriched by subsequent removal of B cells, DCs and macrophages by streptavidin magnetic beads (BD Imag system, BD Biosciences), according to the manufacturer's protocol. The remaining enriched T cells were washed, counted with a hematocytometer, and 10^6 T cells were injected intravenously into CD45.1 mice, followed by intranasal infection with PR/8 48 hours later. Mice were sacrificed 9 days after infection, and $CD45.2^+$ GFP^+ and GFP^- $CD3^+$ T cells from lungs and mediastinal lymph nodes were quantified using flow cytometry.

Bone marrow derived dendritic cells (BMDCs)

Bone marrow was isolated by flushing sterilized mouse femurs with 10 ml of RPMI medium. Bone marrow cells were cultured in tissue-culture-treated 6-well plates (Corning), in 4ml RPMI medium containing 10% FCS, 1% penicillin/streptomycin and 25 ng/ml murine GM-CSF (PeproTech), at a density of 10^6 cells per ml. On day 2, half of the medium was replaced with fresh medium containing 25 ng/ml murine GM-CSF. On day 3, the complete medium (containing non-adherent cells) was replaced with fresh medium containing 25 ng/ml murine GM-CSF. Non-adherent cells were harvested on day 6 by gentle washing with sterile endotoxin-free PBS (Sigma) and incubated with biotinylated anti-mouse CD11c (clone N418; BioLegend). $CD11c^+$ cells (BMDCs) were purified by magnetic separation using streptavidin-coated magnetic beads (IMag Cell Separation System; BD). Isolated BMDCs were pulsed with ovalbumin (Grade V, Sigma, 100 μg/ml) for 16 hours. For some experiments, recombinant LCN2 (BioLegend) was added during the pulsing step at indicated concentrations. Ovalbumin-pulsed BMDCs were used for antigen presentation assays as described below.

Antigen-presentation assay

Mice where intranasally infected with 10000 PFU of PR/8-OVA in 50 μl. Sixty hours after infection, mediastinal lymph nodes were harvested. To maximize DC yield, lymph nodes were digested in RPMI medium supplemented with 5% FCS, DNAse I (43.3 U/ml, Sigma) and Liberase TL (12.5 μg/ml, Roche) for 25 minutes at 37˚C, followed by mashing through 70 μm strainers. Obtained single cell suspensions where incubated with anti-mouse CD16/32, followed by biotinylated anti-CD3 (clone 17A2, BioLegend), anti-CD19 and anti-B220 antibodies (dilution 1:100 for each). Next, samples were incubated with streptavidin coated magnetic beads (20min, 4˚C), and B and T lymphocytes were depleted using magnetic cell sorting (negative selection, BD Imag system) according to manufacturer's instructions. The remaining cells were washed, stained with viability dye, anti-mouse CD11b-Pe-Cy7, CD8a-FITC, CD103-BV421, CD45-eVolve 605 and CD11c-PE (see S4 Table for details) and live $CD103^+$ or $CD8a^+$ DCs were sorted on a FACSAria Fusion cytometer (BD Biosciences). To obtain OT-I transgenic $CD8^+$ T cells, single cell suspensions were prepared from spleens as described above, and incubated with biotinylated antibodies directed against mouse CD19 (clone 6D45, BioLegend), B220, CD4 (clone GK1.5; BioLegend), CD11c and Ly6G, followed by negative selection with streptavidin-coated magnetic beads (BD Imag system). The remaining enriched

$CD8^+$ T cell suspension was labelled using Cell Proliferation Dye eFluor 450 (eBioscience), according to the manufacturer's protocol. Labelled OT-I transgenic $CD8^+$ T cells were co-cultured with sorted DCs, at 1:100 or 1:33 DC:T cell ratios, or with ovalbumin-pulsed BMDCs (see above), 1:10 DC:T cell ratio, in RPMI medium supplemented with 10% FCS, 1% penicillin/streptomycin, 1% MEM Non-Essential Amino Acids Solution, 10 mM HEPES, 50 μM 2-mercaptoethanol and 1 mM Sodium Pyruvate (all Gibco). After 96 hours, cells were washed, labelled with fluorescent antibodies (see S4 Table) and live, $CD45^+/CD3^+/CD8^+$/proliferation dye-low (indicating proliferation) cells were quantified by flow cytometry.

RNA sequencing

To quantify DC or AM gene expression, 200 alveolar macrophages (defined as single/live/$CD45^+/Ly6G^-/CD11c^+/SiglecF^+$) or $CD103^+$ DCs (defined as single/live/$CD45^+/Ly6G^-$/$SiglecF^-/F4/80^-/CD11c^+/MHCII^+/CD103^+$ [lung] or single/live/$CD45^+/CD11c^+/CD8^-$/$CD11b^-/CD103^+$ [lymph node]) were FACS-sorted from mouse lung or lymph node single cell suspensions (prepared as indicated above) into 4μ μl cell lysis buffer (nuclease-free H2O [Life Technologies, cat. no. AM9930] with 0.2% Triton X-100 [Sigma] and RNase Inhibitor [2 U/μl, Takara/Clonentech]) using a FACSAria Fusion cytometer (BD Biosciences). Cell lysates were stored at -80˚C until library preparation according to the Smart-Seq2 protocol [60]. Pooled libraries were sequenced using the 50 bp single-read setup on the Illumina HiSeq 2000/2500 at the Biomedical Sequencing Facility of CeMM and the Medical University of Vienna.

RNA sequencing data analysis

Sequencing reads were adapter-trimmed using Trimmomatic [61] and aligned to the *mm10* reference genome (*STAR aligner* [62]). Reads mapping to genes were counted using the *summarizeOverlaps* function (*Bioconductor* R package *GenomicAlignments* [63]). Differential gene expression was assessed using *DESeq2* [64], whereby separate models per cell type and condition (lung-homeostasis, lymph node-infection) were formulated for all pairwise comparisons between genotypes. Genes were filtered using independent hypothesis weighting (*ihw* R package [65]). Impact of differential expression on KEGG pathways was assessed using Signaling Pathway Impact Analysis (SPIA, *SPIA* R package [66]). Genes with an FDR-adjusted p value of < 0.1 were considered differentially expressed.

Bacterial DNA collection, extraction, library preparation and sequencing

Sterile surgical tools were used for collection of microbial samples from mice. For lung samples, BAL was performed 10 times with 1 ml NaCl (aliquots were subsequently pooled) as described above. Next, the abdomen of the animal was sterilized using 70% EtOH and the peritoneal cavity was opened. Ileal samples were collected by cutting a 2.5 cm long piece of the terminal ileum 2 cm distal of the ileo-cecal valve. Cecal samples were collected by dissecting the whole cecum. From ileum and cecum, luminal samples were collected in a sterile microcentrifuge tube (Eppendorf Biopur) by gently squeezing out content from the distal end of the dissected intestinal segment. For collection of mucosal samples, the ileal segments where flushed with 10 ml NaCl to remove all luminal content, cut open longitudinally and scraping biopsies where collected using sterile glass slides. Bacterial DNA was isolated using the QIAamp DNA Microbiome Kit (Qiagen) according to the manufacturer's protocol and isolated DNA was eluted in 50 μl of DEPC-treated water (Roth). To control for contaminations introduced during sample collection, two harvest controls (NaCl used to flush cannulas inserted into mouse tracheas, without performing BAL), one isolation control and one PCR control were prepared identically to BAL samples and sequenced. Similarly, another PCR control sample was

prepared for ileal mucosa samples. Isolated bacterial DNA from samples and controls was amplified using barcoded, Illumina adaptor-linked PCR primers that target the V1-V2 hypervariable region of the bacterial 16S rRNA gene [67]. Each sample was amplified using the Accuprime Taq DNA Polymerase High Fidelity kit (Invitrogen) with the following cycling parameters: Initial denaturation for 2 min at 94˚C, followed by amplification cycles starting with 30 sec denaturation at 94˚C, 30 sec annealing at 56˚C, and 60 sec elongation at 68˚C, with a final extension at 68˚C for 7 min. An initial enrichment PCR reaction (10 amplification cycles) was performed, followed by the amplification PCR. The number of cycles performed for amplification PCR varied between sampling sites: Stool: 20 cycles; ileum lumen: 25 cycles; cecum lumen: 35 cycles; ileum mucosa: 40 cycles. For BAL, two amplification PCRs were performed, with 40 (first reaction) and 35 (second reaction) cycles. The ideal number of amplification cycles for each sampling site was determined by increasing the number of cycles by five (starting from 20), until samples were sufficiently amplified (i.e. presence of a visible band by automated electrophoresis using an Agilent 4200 TapeStation system). All PCR reactions contained 2.5 μl of 10x AccuPrime buffer II, 0.5 μl of each 10 mM forward and reverse primers and 0.1 μl of AccuPrime Taq DNA Polymerase, to which 1 μl of template DNA and 20.4 μl of ultrapure water (for the enrichment PCR reaction) or 2 μl of the enrichment PCR reaction and 19.4 μl of ultrapure water (for the amplification PCR reaction) were added. PCR products were screened for sufficient amplification and quantified using automated electrophoresis. Finally, libraries containing pooled equimolar PCR products and spiked with 40% phiX (Illumina) were sequenced using Illumina MiSeq technology in the 2x 350bp configuration (MiSeq Reagent kit v3) at the Biomedical Sequencing Facility of CeMM and the Medical University of Vienna.

16S rRNA gene sequencing data processing and analysis

Raw sequences were demultiplexed using qiime [68] commands *split_libraries.py* with options-r 999 -n 999 -q 0 -p 0.0001 (to prevent quality filtering at this stage) and split_sequence_file_on_sample_ids.py. ASVs (amplicon sequence variants) were selected using dada2 [69]. Forward and reverse reads were trimmed to a length of 225 bp and filtered using parameters *maxN = 0*, *maxEE = c(2,2)* and *truncQ = 2*. Potential contaminants within unique ASVs were identified with the *decontam* R package [69] using prevalence of ASVs in control samples (for ileal mucosa and BAL samples) and correlation of ASV frequency with DNA concentration after PCR amplification as identification methods. Following contaminant removal, taxonomy was assigned against the SILVA 16s rRNA database [70] and ASVs which could not be assigned to kingdom *Bacteria* were removed from the dataset. One ASV was identified as belonging to genus *Candidatus_Arthromitus*. Since the misclassification of mammalian segmented filamentous bacteria (SFB) as *Candidatus_Arthromitus* (which would not be expected to be found in mammalian guts) is well described [71], we refer to this ASV as SFB. Next, samples with a total ASV count of less than 10000 were excluded from further analysis. The remaining samples were rarefied to the smallest library size above 10000 ASVs for the sampling site (between 10033 for stool samples and 27693 for cecal samples). Shannon diversity and Chao 1 ASV richness were calculated using the *vegan* R package [72]. Differences between genotypes (controlling for cage effects) were assessed using the *nested.npmanova* function (*biodiversityR* package) on ASV counts normalized to sample library size (relative abundances). Statistical comparisons of Chao1 richness and Shannon diversity were carried out with linear mixed models using the *lme4* and *lmerTest* R packages [73,74], while cage association was entered as a random factor. Linear mixed models were also used to determine which ASVs were differentially abundant according to genotype, after transforming ASV counts with a centralized log ratio (clr) transformation.

Antibiotic treatment and cohousing

For experiments involving microbiome perturbation by antibiotics, female WT or *Lcn2*$^{-/-}$ mice were treated with a mix of metronidazole ('Kabi', Fresenius), vancomycin (Vancocin, Baxter), ampicillin (Standacilin, Sandoz) and gentamicin (Braun, concentration of each 500 mg/l) in drinking water supplemented with 0.4% D-glucose (Sigma) starting at 5–6 weeks of age. Control mice received drinking water supplemented with 0.4% D-glucose. After 4 weeks of antibiotic treatment, mice were infected with 10 PFU PR/8. Antibiotic treatment was continued until the end of the experiment. For co-housing experiments, 4 weeks old WT or *Lcn2*$^{-/-}$ mice were housed together at equal ratios for 4 weeks prior to influenza infection. Control WT or *Lcn2*$^{-/-}$ mice were housed separately. As with antibiotic treatments, housing conditions were maintained throughout the infection period.

Quantification of bacterial classes using qPCR

Bacterial DNA from stool of separately housed and co-housed WT and *Lcn2*$^{-/-}$ animals was isolated using the QIAamp DNA Mini Kit (Qiagen) according to the manufacturer's recommendations. Perfecta SYBR Green SuperMix (Quanta) on a StepOnePlus Real-Time PCR System (Applied Biosystems) were used for real-time qPCR. Primer sequences for *Bacteroidetes* were CRAACAGGATTAGATACCCT (forward) or GGTAAGGTTCCTCGCGTAT (reverse) [75]. The conserved bacterial (pan-bacteria) 16S-gene was quantified using the sequences TCC TACGGGAGGCAGCAGT (forward) and GGACTACCAGGGTATCTAATCTT (reverse) and used for calculation of $\log_2$ fold changes.

Statistical analysis

Comparisons between two groups were performed using Student's t test, except where noted otherwise. In experiments involving two grouping factors (e.g. genotype and antibiotic treatment), 2-way ANOVA was conducted, and group means were compared using the *emmeans* R package. Survival curves were compared using the asymptotic two-sample logrank test, as implemented in the *coin* R package [76]. In antigen presentation assays, technical replicates of biological replicates were analyzed. To avoid pseudo-replication, nested ANOVA was conducted in these experiments. Where appropriate, p values were corrected for multiple testing using the false-discovery rate approach [77]. Single p values below 0.05 or FDR-corrected p values below 0.1 (RNA-Seq and 16S rRNA gene sequencing) were considered statistically significant.

Supporting information

S1 Fig. Myeloid cell transcriptome and lung viral load in WT and *Lcn2*$^{-/-}$ mice. (A-B) Alveolar macrophages (AMs) and CD103^{+} DCs were isolated from lungs of WT and *Lcn2*$^{-/-}$ animals by FACS and prepared for RNA sequencing. Heatmaps of differentially expressed genes (DEGs) for AMs (A) and CD103^{+} DCs (B). Read counts are *rlog* transformed, followed by z-score scaling. (C) Venn diagrams illustrating overlaps in up- or down-regulated genes according to genotype between AMs and CD103^{+} DCs. (D) Significantly perturbed KEGG pathways (p value < 0.05) with lowest SPIA (Signaling Pathway Impact Analysis) p values in AMs isolated from mediastinal lymph nodes of PR/8-OVA-infected mice. Circle sizes indicate the number of DEGs associated with the respective pathway. (E) Lung viral load, as measured by qPCR, for WT and *Lcn2*$^{-/-}$ mice, at indicated timepoints after PR/8 infection. (F) Heatmaps of indicated bronchoalveolar lavage (BAL) cytokines on day 3 or day 6 post infection. Cytokine concentrations are log-transformed after addition of half of the non-zero minimum (to

account for zeros prior to log-transformation), followed by z-score scaling. (A-B; F) Columns represent samples collected from individual mice. Statistical significance for comparisons between genotypes for (F) was assessed using Student's t test, and p values were adjusted for multiple testing using the FDR approach. *adjusted $p < 0.05$, **adjusted $p < 0.01$.
(TIF)

S2 Fig. FACS gating strategy and pulmonary immune cell counts. (A) FACS gating strategy for identification of lung cell populations. (B) Percent of activated ($CD69^+$) $CD4^+$ lung T cells 9 days post infection in WT and *Lcn2*$^{-/-}$ mice. (C-E) Neutrophil (C), alveolar macrophage (AM) (D) or B cell (E) counts per lung at indicated timepoints after infection. n = 4 (baseline), 5 (day 9 post infection) and 4–7 (day 16 post infection) per genotype. Bar diagrams show group means +/- SEM, and statistical significance for comparisons between genotypes for (B-D) was assessed using Student's t test. *$p < 0.05$.
(TIF)

S3 Fig. Antigen presentation capacity of $CD103^+$ and $CD8a^+$ DCs, overlap of differentially expressed genes in $CD103^+$ DCs from infected and uninfected mice and *in vitro* effects of LCN2 deficiency and supplementation. (A-B) $CD8^+$ T cell proliferation (assessed by antigen presentation assay, as in Fig 3A) after co-culture with WT or *Lcn2*$^{-/-}$ $CD103^+$or $CD8a^+$ DCs at 1: 100 (DC: T cell) ratio. Replicates of 2 pools per genotype (each consisting of 6–7 mice) are shown. (C) Venn diagram illustrating overlaps in genes up- or downregulated in *Lcn2*$^{-/-}$ DCs from infected mediastinal lymph nodes or uninfected lungs. (D) Antigen presentation assay showing numbers of proliferated (proliferation dye^{low}) OT-I-specific $CD8^+$ T cells after 3 days of co-culture with ovalbumin-pulsed WT or *Lcn2*$^{-/-}$ BMDCs. (E) Antigen presentation assay showing numbers of proliferated (proliferation dye^{low}) OT-I-specific $CD8^+$ T cells after 3 days of co-culture with WT BMDCs, which were pulsed with ovalbumin in presence of recombinant LCN2 at indicated concentrations. Bar diagrams show group means +/- SEM. Statistical significance for (A-B) was assessed using nested ANOVA. Statistical significance for (D-E) was assessed using Student's t test. n.s. not significant; *$p < 0.05$.
(TIF)

S4 Fig. Effects of LCN2 on microbial richness and diversity. (A-D) Microbiome analysis of bronchoalveolar lavage (BAL), ileal mucosa, ileal lumen, cecum and stool samples derived from 12 weeks old WT and *Lcn2*$^{-/-}$ mice, n = 13–16 per genotype. Shannon diversity (A) and Chao 1 amplicon sequencing variant (ASV) richness (B) for microbial samples from indicated sites. Linear mixed model p values, controlling for cage, are shown. (C) Bacterial phyla with significantly (FDR < 0.1) differential abundance in WT and *Lcn2*$^{-/-}$ stool samples. (D) ASVs with significantly (FDR < 0.1) differential abundance between WT and *Lcn2*$^{-/-}$ samples from indicated sites along the intestinal tract. SFB: Segmented filamentous bacteria. Boxplots are indicative of median (horizontal line), interquartile range (box) and range (whiskers). Statistical significance for comparisons between genotypes was assessed using linear mixed models on centralized log ratio transformed data, controlling for housing cage.
(TIF)

S5 Fig. Antigen presentation after antibiotic treatment and co-housing effects on on the microbiome. (A) Experimental layout for the antigen presentation assay. WT and *Lcn2*$^{-/-}$ mice were treated with broad-spectrum antibiotics in drinking water. After four weeks treatment, mice were infected with PR/8-OVA and $CD103^+$ DCs were sorted (60 hours post infection) from mediastinal lymph nodes (mLNs), followed by co-culture with purified splenic OT-I T cells. (B) Numbers of proliferated (proliferation dye^{low}) $CD8^+$ T cells after 96h co-culture (1:100 DC: T cell ratio) with WT or *Lcn2*$^{-/-}$ $CD103^+$ DCs derived from antibiotics-treated

mice. Replicates of 3 pools per genotype (each consisting of 6–7 mice) are shown. (C) Experimental setup for co-housing experiments. WT and *Lcn2*$^{-/-}$ mice were separately- (sep) or co-housed (co) for four weeks prior to stool sample collection. (D) Log_2 fold change between the phylum *Bacteroidetes* and total bacteria in stool samples, measured by qPCR. Statistical significance for (B) was assessed using nested ANOVA, and for (C) using Student's t test. n.s. not significant, $^{**}p < 0.01$.
(TIF)

S1 Table. Signaling Pathway Impact Analysis (SPIA) results for CD103$^+$ DCs. CD103$^+$ DCs were isolated by FACS and processed for RNA sequencing. Related to Fig 1D. This table gives an overview of KEGG pathways associated with differentially expressed genes map, ranked by their global p values. DEG: Differentially expressed gene, tA: net perturbation accumulation, FDR: False discovery rate; FWER: Family-wise error rate.
(XLSX)

S2 Table. Signaling Pathway Impact Analysis (SPIA) results for AMs. AMs were isolated by FACS and processed for RNA sequencing. This table gives an overview of KEGG pathways associated with differentially expressed genes map, ranked by their global p values. DEG: Differentially expressed gene, tA: net perturbation accumulation, FDR: False discovery rate; FWER: Family-wise error rate.
(XLSX)

S3 Table. 16 rRNA Gene Amplicon Sequencing Variants. Overview of all detected amplicon sequencing variants (ASVs), and their p values for comparisons of ASV abundance between WT and *Lcn2*$^{-/-}$ samples. BAL: Bronchoalveolar lavage; NA: not applicable.
(XLSX)

S4 Table. Antibodies used for flow cytometry and cell sorting.
(XLSX)

Acknowledgments

We are grateful to Maria Sibilia for providing us with OT-I mice, to Adolfo García-Sastre for generously providing us with the PR/8-Ova virus and to Alessandra Riva, Claus Pelikan and David Berry for help with 16S rRNA gene sequencing data analysis. We further thank the animal technicians of the Department of Biomedical Research at the Medical University of Vienna, Thomas Krausgruber and the staff at the BSF for assistance with sequencing, Dieter Prinz for FACS-sorting, and Céline Pattaroni and Ben Marsland for valuable discussions and advice regarding data analysis.

Author Contributions

Conceptualization: Martin L. Watzenboeck, Barbara Drobits, Philipp Starkl, Sylvia Knapp.

Formal analysis: Martin L. Watzenboeck, Barbara Drobits, Philipp Starkl.

Funding acquisition: Martin L. Watzenboeck, Sylvia Knapp.

Investigation: Martin L. Watzenboeck, Barbara Drobits, Sophie Zahalka, Anna-Dorothea Gorki, Asma Farhat, Federica Quattrone, Anastasiya Hladik, Karin Lakovits, Gabriel M. Richard, Therese Lederer, Philipp Starkl.

Methodology: Martin L. Watzenboeck, Barbara Drobits, Anna-Dorothea Gorki, Birgit Strobl, Gijs A. Versteeg, Philipp Starkl, Sylvia Knapp.

Project administration: Anastasiya Hladik, Karin Lakovits, Sylvia Knapp.

Resources: Birgit Strobl, Gijs A. Versteeg, Louis Boon, Sylvia Knapp.

Supervision: Philipp Starkl, Sylvia Knapp.

Visualization: Martin L. Watzenboeck, Sophie Zahalka.

Writing – original draft: Martin L. Watzenboeck, Philipp Starkl, Sylvia Knapp.

Writing – review & editing: Martin L. Watzenboeck, Barbara Drobits, Sophie Zahalka, Anna-Dorothea Gorki, Asma Farhat, Federica Quattrone, Anastasiya Hladik, Karin Lakovits, Gabriel M. Richard, Therese Lederer, Birgit Strobl, Gijs A. Versteeg, Philipp Starkl, Sylvia Knapp.

References

1. Kjeldsen L, Cowland JB, Borregaard N (2000) Human neutrophil gelatinase-associated lipocalin and homologous proteins in rat and mouse. Biochim Biophys Acta 1482: 272–283. https://doi.org/10.1016/s0167-4838(00)00152-7 PMID: 11058768
2. Xiao X, Yeoh BS, Vijay-Kumar M (2017) Lipocalin 2: An Emerging Player in Iron Homeostasis and Inflammation. Annu Rev Nutr 37: 103–130. https://doi.org/10.1146/annurev-nutr-071816-064559 PMID: 28628361
3. Mosialou I, Shikhel S, Liu JM, Maurizi A, Luo N, et al. (2017) MC4R-dependent suppression of appetite by bone-derived lipocalin 2. Nature 543: 385–390. https://doi.org/10.1038/nature21697 PMID: 28273060
4. Flo TH, Smith KD, Sato S, Rodriguez DJ, Holmes MA, et al. (2004) Lipocalin 2 mediates an innate immune response to bacterial infection by sequestrating iron. Nature 432: 917–921. https://doi.org/10.1038/nature03104 PMID: 15531878
5. Chan YR, Liu JS, Pociask DA, Zheng M, Mietzner TA, et al. (2009) Lipocalin 2 is required for pulmonary host defense against Klebsiella infection. J Immunol 182: 4947–4956. https://doi.org/10.4049/jimmunol.0803282 PMID: 19342674
6. Cowland JB, Borregaard N (1997) Molecular characterization and pattern of tissue expression of the gene for neutrophil gelatinase-associated lipocalin from humans. Genomics 45: 17–23. https://doi.org/10.1006/geno.1997.4896 PMID: 9339356
7. Srinivasan G, Aitken JD, Zhang B, Carvalho FA, Chassaing B, et al. (2012) Lipocalin 2 deficiency dysregulates iron homeostasis and exacerbates endotoxin-induced sepsis. J Immunol 189: 1911–1919. https://doi.org/10.4049/jimmunol.1200892 PMID: 22786765
8. Kang SS, Ren Y, Liu CC, Kurti A, Baker KE, et al. (2018) Lipocalin-2 protects the brain during inflammatory conditions. Mol Psychiatry 23: 344–350. https://doi.org/10.1038/mp.2016.243 PMID: 28070126
9. Ye D, Yang K, Zang S, Lin Z, Chau HT, et al. (2016) Lipocalin-2 mediates non-alcoholic steatohepatitis by promoting neutrophil-macrophage crosstalk via the induction of CXCR2. J Hepatol 65: 988–997. https://doi.org/10.1016/j.jhep.2016.05.041 PMID: 27266617
10. Warszawska JM, Gawish R, Sharif O, Sigel S, Doninger B, et al. (2013) Lipocalin 2 deactivates macrophages and worsens pneumococcal pneumonia outcomes. J Clin Invest 123: 3363–3372. https://doi.org/10.1172/JCI67911 PMID: 23863624
11. Belkaid Y, Harrison OJ (2017) Homeostatic Immunity and the Microbiota. Immunity 46: 562–576. https://doi.org/10.1016/j.immuni.2017.04.008 PMID: 28423337
12. Damjanovic D, Small CL, Jeyanathan M, McCormick S, Xing Z (2012) Immunopathology in influenza virus infection: uncoupling the friend from foe. Clin Immunol 144: 57–69. https://doi.org/10.1016/j.clim.2012.05.005 PMID: 22673491
13. Cao X (2020) COVID-19: immunopathology and its implications for therapy. Nat Rev Immunol 20: 269–270. https://doi.org/10.1038/s41577-020-0308-3 PMID: 32273594
14. Braciale TJ, Sun J, Kim TS (2012) Regulating the adaptive immune response to respiratory virus infection. Nat Rev Immunol 12: 295–305. https://doi.org/10.1038/nri3166 PMID: 22402670
15. Rouse BT, Sehrawat S (2010) Immunity and immunopathology to viruses: what decides the outcome? Nat Rev Immunol 10: 514–526. https://doi.org/10.1038/nri2802 PMID: 20577268

16. Helft J, Manicassamy B, Guermonprez P, Hashimoto D, Silvin A, et al. (2012) Cross-presenting CD103 + dendritic cells are protected from influenza virus infection. J Clin Invest 122: 4037–4047. https://doi.org/10.1172/JCI60659 PMID: 23041628

17. Kopf M, Schneider C, Nobs SP (2015) The development and function of lung-resident macrophages and dendritic cells. Nat Immunol 16: 36–44. https://doi.org/10.1038/ni.3052 PMID: 25521683

18. Kalter SS, Berg G, Prier JE, Jochheim KA, McKenna JM (1955) Virus proliferation in the mouse. I. Growth curves of influenza (mouse-adapted PR 8) and Theiler's mouse encephalomyelitis (GD VII) viruses. J Immunol 75: 410–416. PMID: 13271763

19. Aulakh GK, Suri SS, Singh B (2014) Angiostatin inhibits acute lung injury in a mouse model. Am J Physiol Lung Cell Mol Physiol 306: L58–68. https://doi.org/10.1152/ajplung.00368.2012 PMID: 24213918

20. Wattiez R, Falmagne P (2005) Proteomics of bronchoalveolar lavage fluid. J Chromatogr B Analyt Technol Biomed Life Sci 815: 169–178. https://doi.org/10.1016/j.jchromb.2004.10.029 PMID: 15652807

21. Hufford MM, Kim TS, Sun J, Braciale TJ (2015) The effector T cell response to influenza infection. Curr Top Microbiol Immunol 386: 423–455. https://doi.org/10.1007/82_2014_397 PMID: 25033753

22. Jenkins MR, Webby R, Doherty PC, Turner SJ (2006) Addition of a prominent epitope affects influenza A virus-specific CD8+ T cell immunodominance hierarchies when antigen is limiting. J Immunol 177: 2917–2925. https://doi.org/10.4049/jimmunol.177.5.2917 PMID: 16920927

23. Hogquist KA, Jameson SC, Heath WR, Howard JL, Bevan MJ, et al. (1994) T cell receptor antagonist peptides induce positive selection. Cell 76: 17–27. https://doi.org/10.1016/0092-8674(94)90169-4 PMID: 8287475

24. Desch AN, Gibbings SL, Clambey ET, Janssen WJ, Slansky JE, et al. (2014) Dendritic cell subsets require cis-activation for cytotoxic CD8 T-cell induction. Nat Commun 5: 4674. https://doi.org/10.1038/ncomms5674 PMID: 25135627

25. del Rio ML, Rodriguez-Barbosa JI, Kremmer E, Forster R (2007) CD103- and CD103+ bronchial lymph node dendritic cells are specialized in presenting and cross-presenting innocuous antigen to CD4+ and CD8+ T cells. J Immunol 178: 6861–6866. https://doi.org/10.4049/jimmunol.178.11.6861 PMID: 17513734

26. Wikenheiser DJ, Stumhofer JS (2016) ICOS Co-Stimulation: Friend or Foe? Front Immunol 7: 304. https://doi.org/10.3389/fimmu.2016.00304 PMID: 27559335

27. Ma DY, Clark EA (2009) The role of CD40 and CD154/CD40L in dendritic cells. Semin Immunol 21: 265–272. https://doi.org/10.1016/j.smim.2009.05.010 PMID: 19524453

28. Devaiah BN, Singer DS (2013) CIITA and Its Dual Roles in MHC Gene Transcription. Front Immunol 4: 476. https://doi.org/10.3389/fimmu.2013.00476 PMID: 24391648

29. Ichinohe T, Pang IK, Kumamoto Y, Peaper DR, Ho JH, et al. (2011) Microbiota regulates immune defense against respiratory tract influenza A virus infection. Proc Natl Acad Sci U S A 108: 5354–5359. https://doi.org/10.1073/pnas.1019378108 PMID: 21402903

30. Hagan T, Cortese M, Rouphael N, Boudreau C, Linde C, et al. (2019) Antibiotics-Driven Gut Microbiome Perturbation Alters Immunity to Vaccines in Humans. Cell 178: 1313–1328 e1313. https://doi.org/10.1016/j.cell.2019.08.010 PMID: 31491384

31. Robertson SJ, Lemire P, Maughan H, Goethel A, Turpin W, et al. (2019) Comparison of Co-housing and Littermate Methods for Microbiota Standardization in Mouse Models. Cell Rep 27: 1910–1919 e1912. https://doi.org/10.1016/j.celrep.2019.04.023 PMID: 31067473

32. Franklin CL, Ericsson AC (2017) Microbiota and reproducibility of rodent models. Lab Anim (NY) 46: 114–122. https://doi.org/10.1038/laban.1222 PMID: 28328896

33. Mauad T, Hajjar LA, Callegari GD, da Silva LF, Schout D, et al. (2010) Lung pathology in fatal novel human influenza A (H1N1) infection. Am J Respir Crit Care Med 181: 72–79. https://doi.org/10.1164/rccm.200909-1420OC PMID: 19875682

34. Baskin CR, Bielefeldt-Ohmann H, Tumpey TM, Sabourin PJ, Long JP, et al. (2009) Early and sustained innate immune response defines pathology and death in nonhuman primates infected by highly pathogenic influenza virus. Proc Natl Acad Sci U S A 106: 3455–3460. https://doi.org/10.1073/pnas.0813234106 PMID: 19218453

35. Alberts R, Srivastava B, Wu H, Viegas N, Geffers R, et al. (2010) Gene expression changes in the host response between resistant and susceptible inbred mouse strains after influenza A infection. Microbes Infect 12: 309–318. https://doi.org/10.1016/j.micinf.2010.01.008 PMID: 20114087

36. Teijaro JR, Njau MN, Verhoeven D, Chandran S, Nadler SG, et al. (2009) Costimulation modulation uncouples protection from immunopathology in memory T cell responses to influenza virus. J Immunol 182: 6834–6843. https://doi.org/10.4049/jimmunol.0803860 PMID: 19454679

37. Duan S, Thomas PG (2016) Balancing Immune Protection and Immune Pathology by CD8(+) T-Cell Responses to Influenza Infection. Front Immunol 7: 25. https://doi.org/10.3389/fimmu.2016.00025 PMID: 26904022

38. Oh JZ, Ravindran R, Chassaing B, Carvalho FA, Maddur MS, et al. (2014) TLR5-mediated sensing of gut microbiota is necessary for antibody responses to seasonal influenza vaccination. Immunity 41: 478–492. https://doi.org/10.1016/j.immuni.2014.08.009 PMID: 25220212

39. Steed AL, Christophi GP, Kaiko GE, Sun L, Goodwin VM, et al. (2017) The microbial metabolite desaminotyrosine protects from influenza through type I interferon. Science 357: 498–502. https://doi.org/10.1126/science.aam5336 PMID: 28774928

40. Trompette A, Gollwitzer ES, Pattaroni C, Lopez-Mejia IC, Riva E, et al. (2018) Dietary Fiber Confers Protection against Flu by Shaping Ly6c(-) Patrolling Monocyte Hematopoiesis and CD8(+) T Cell Metabolism. Immunity 48: 992–1005 e1008. https://doi.org/10.1016/j.immuni.2018.04.022 PMID: 29768180

41. Ivanov II, Littman DR(2010) Segmented filamentous bacteria take the stage. Mucosal Immunol 3: 209–212. https://doi.org/10.1038/mi.2010.3 PMID: 20147894

42. Deriu E, Boxx GM, He X, Pan C, Benavidez SD, et al. (2016) Influenza Virus Affects Intestinal Microbiota and Secondary Salmonella Infection in the Gut through Type I Interferons. PLoS Pathog 12: e1005572. https://doi.org/10.1371/journal.ppat.1005572 PMID: 27149619

43. Singh V, Yeoh BS, Chassaing B, Zhang B, Saha P, et al. (2016) Microbiota-inducible Innate Immune, Siderophore Binding Protein Lipocalin 2 is Critical for Intestinal Homeostasis. Cell Mol Gastroenterol Hepatol 2: 482–498 e486. https://doi.org/10.1016/j.jcmgh.2016.03.007 PMID: 27458605

44. Moschen AR, Gerner RR, Wang J, Klepsch V, Adolph TE, et al. (2016) Lipocalin 2 Protects from Inflammation and Tumorigenesis Associated with Gut Microbiota Alterations. Cell Host Microbe 19: 455–469. https://doi.org/10.1016/j.chom.2016.03.007 PMID: 27078067

45. Devireddy LR, Gazin C, Zhu X, Green MR (2005) A cell-surface receptor for lipocalin 24p3 selectively mediates apoptosis and iron uptake. Cell 123: 1293–1305. https://doi.org/10.1016/j.cell.2005.10.027 PMID: 16377569

46. Hvidberg V, Jacobsen C, Strong RK, Cowland JB, Moestrup SK, et al. (2005) The endocytic receptor megalin binds the iron transporting neutrophil-gelatinase-associated lipocalin with high affinity and mediates its cellular uptake. FEBS Lett 579: 773–777. https://doi.org/10.1016/j.febslet.2004.12.031 PMID: 15670845

47. Janas RM, Ochocinska A, Snitko R, Dudka D, Kierkus J, et al. (2014) Neutrophil gelatinase-associated lipocalin in blood in children with inflammatory bowel disease. J Gastroenterol Hepatol 29: 1883–1889. https://doi.org/10.1111/jgh.12597 PMID: 24720485

48. Eilenberg W, Stojkovic S, Piechota-Polanczyk A, Kaider A, Kozakowski N, et al. (2017) Neutrophil gelatinase associated lipocalin (NGAL) is elevated in type 2 diabetics with carotid artery stenosis and reduced under metformin treatment. Cardiovasc Diabetol 16: 98. https://doi.org/10.1186/s12933-017-0579-6 PMID: 28789657

49. Wang Y, Lam KS, Kraegen EW, Sweeney G, Zhang J, et al. (2007) Lipocalin-2 is an inflammatory marker closely associated with obesity, insulin resistance, and hyperglycemia in humans. Clin Chem 53: 34–41. https://doi.org/10.1373/clinchem.2006.075614 PMID: 17040956

50. Mosialou I, Shikhel S, Luo N, Petropoulou PI, Panitsas K, et al. (2020) Lipocalin-2 counteracts metabolic dysregulation in obesity and diabetes. J Exp Med 217. https://doi.org/10.1084/jem.20191261 PMID: 32639539

51. Morgan OW, Bramley A, Fowlkes A, Freedman DS, Taylor TH, et al. (2010) Morbid obesity as a risk factor for hospitalization and death due to 2009 pandemic influenza A(H1N1) disease. PLoS One 5: e9694. https://doi.org/10.1371/journal.pone.0009694 PMID: 20300571

52. Allard R, Leclerc P, Tremblay C, Tannenbaum TN (2010) Diabetes and the severity of pandemic influenza A (H1N1) infection. Diabetes Care 33: 1491–1493. https://doi.org/10.2337/dc09-2215 PMID: 20587722

53. Sheridan PA, Paich HA, Handy J, Karlsson EA, Hudgens MG, et al. (2012) Obesity is associated with impaired immune response to influenza vaccination in humans. Int J Obes (Lond) 36: 1072–1077. https://doi.org/10.1038/ijo.2011.208 PMID: 22024641

54. Janowska-Wieczorek A, Majka M, Kijowski J, Baj-Krzyworzeka M, Reca R, et al. (2001) Platelet-derived microparticles bind to hematopoietic stem/progenitor cells and enhance their engraftment. Blood 98: 3143–3149. https://doi.org/10.1182/blood.v98.10.3143 PMID: 11698303

55. Okabe M, Ikawa M, Kominami K, Nakanishi T, Nishimune Y (1997) 'Green mice' as a source of ubiquitous green cells. FEBS Lett 407: 313–319. https://doi.org/10.1016/s0014-5793(97)00313-x PMID: 9175875

56. Mamantopoulos M, Ronchi F, McCoy KD, Wullaert A (2018) Inflammasomes make the case for littermate-controlled experimental design in studying host-microbiota interactions. Gut Microbes 9: 374–381. https://doi.org/10.1080/19490976.2017.1421888 PMID: 29672197

57. Shukla P, Vogl C, Wallner B, Rigler D, Muller M, et al. (2015) High-throughput mRNA and miRNA profiling of epithelial-mesenchymal transition in MDCK cells. BMC Genomics 16: 944. https://doi.org/10.1186/s12864-015-2036-9 PMID: 26572553

58. Rosenberger CM, Podyminogin RL, Askovich PS, Navarro G, Kaiser SM, et al. (2014) Characterization of innate responses to influenza virus infection in a novel lung type I epithelial cell model. J Gen Virol 95: 350–362. https://doi.org/10.1099/vir.0.058438-0 PMID: 24243730

59. Vashist N, Trittel S, Ebensen T, Chambers BJ, Guzman CA, et al. (2018) Influenza-Activated ILC1s Contribute to Antiviral Immunity Partially Influenced by Differential GITR Expression. Front Immunol 9: 505. https://doi.org/10.3389/fimmu.2018.00505 PMID: 29623077

60. Picelli S, Faridani OR, Bjorklund AK, Winberg G, Sagasser S, et al. (2014) Full-length RNA-seq from single cells using Smart-seq2. Nat Protoc 9: 171–181. https://doi.org/10.1038/nprot.2014.006 PMID: 24385147

61. Bolger AM, Lohse M, Usadel B (2014) Trimmomatic: a flexible trimmer for Illumina sequence data. Bioinformatics 30: 2114–2120. https://doi.org/10.1093/bioinformatics/btu170 PMID: 24695404

62. Dobin A, Davis CA, Schlesinger F, Drenkow J, Zaleski C, et al. (2013) STAR: ultrafast universal RNA-seq aligner. Bioinformatics 29: 15–21. https://doi.org/10.1093/bioinformatics/bts635 PMID: 23104886

63. Lawrence M, Huber W, Pages H, Aboyoun P, Carlson M, et al. (2013) Software for computing and annotating genomic ranges. PLoS Comput Biol 9: e1003118. https://doi.org/10.1371/journal.pcbi.1003118 PMID: 23950696

64. Love MI, Huber W, Anders S (2014) Moderated estimation of fold change and dispersion for RNA-seq data with DESeq2. Genome Biol 15: 550. https://doi.org/10.1186/s13059-014-0550-8 PMID: 25516281

65. Ignatiadis N, Klaus B, Zaugg JB, Huber W (2016) Data-driven hypothesis weighting increases detection power in genome-scale multiple testing. Nat Methods 13: 577–580. https://doi.org/10.1038/nmeth.3885 PMID: 27240256

66. Tarca AL, Draghici S, Khatri P, Hassan SS, Mittal P, et al. (2009) A novel signaling pathway impact analysis. Bioinformatics 25: 75–82. https://doi.org/10.1093/bioinformatics/btn577 PMID: 18990722

67. Rapin A, Pattaroni C, Marsland BJ, Harris NL (2017) Microbiota Analysis Using an Illumina MiSeq Platform to Sequence 16S rRNA Genes. Curr Protoc Mouse Biol 7: 100–129. https://doi.org/10.1002/cpmo.29 PMID: 28628218

68. Caporaso JG, Kuczynski J, Stombaugh J, Bittinger K, Bushman FD, et al. (2010) QIIME allows analysis of high-throughput community sequencing data. Nat Methods 7: 335–336. https://doi.org/10.1038/nmeth.f.303 PMID: 20383131

69. Callahan BJ, McMurdie PJ, Rosen MJ, Han AW, Johnson AJ, et al. (2016) DADA2: High-resolution sample inference from Illumina amplicon data. Nat Methods 13: 581–583. https://doi.org/10.1038/nmeth.3869 PMID: 27214047

70. Quast C, Pruesse E, Yilmaz P, Gerken J, Schweer T, et al. (2013) The SILVA ribosomal RNA gene database project: improved data processing and web-based tools. Nucleic Acids Res 41: D590–596. https://doi.org/10.1093/nar/gks1219 PMID: 23193283

71. Thompson CL, Mikaelyan A, Brune A (2013) Immune-modulating gut symbionts are not "Candidatus Arthromitus". Mucosal Immunol 6: 200–201. https://doi.org/10.1038/mi.2012.91 PMID: 23013646

72. Dixon P (2003) VEGAN, a package of R functions for community ecology. Journal of Vegetation Science 14: 927–930.

73. Bates D, Machler M, Bolker BM, Walker SC (2015) Fitting Linear Mixed-Effects Models Using lme4. Journal of Statistical Software 67: 1–48.

74. Kuznetsova A, Brockhoff PB, Christensen RHB (2017) lmerTest Package: Tests in Linear Mixed Effects Models. Journal of Statistical Software 82: 1–26.

75. Raetz M, Hwang SH, Wilhelm CL, Kirkland D, Benson A, et al. (2013) Parasite-induced TH1 cells and intestinal dysbiosis cooperate in IFN-gamma-dependent elimination of Paneth cells. Nat Immunol 14: 136–142. https://doi.org/10.1038/ni.2508 PMID: 23263554

76. Hothorn T, Hornik K, van de Wiel MAV, Zeileis A (2008) Implementing a Class of Permutation Tests: The coin Package. Journal of Statistical Software 28: 1–23. https://doi.org/10.18637/jss.v028.i07 PMID: 27774042

77. Benjamini Y, Hochberg Y (1995) Controlling the False Discovery Rate—a Practical and Powerful Approach to Multiple Testing. Journal of the Royal Statistical Society Series B-Statistical Methodology 57: 289–300.

2.2 Multi-omics profiling predicts allograft function after lung transplantation

In the second part of this chapter, I will present the paper “Multi-omics profiling predicts allograft function after lung transplantation”. Here, we investigated the temporal dynamics of the BAL microbiome, metabolome and lipidome was well as the major myeloid cell populations after lung transplantation. We found distinct kinetics for each of the investigated datasets. Interestingly, alpha-diversity in the lung showed a rapid increase within the first week after transplantation, which was followed by a more gradual increase and ultimate stability. By comparing microbial composition to the respective donors, we observed a rapid replacement of the donor microbiome, which indicates that recipient associated factors, rather than the donor microbiome, determine the established lung microbiome in lung transplant recipients. When looking at those factors, we found that the underlying disease (i.e. indication for transplantation) continued to be a predictor of the microbial composition even after the transplantation of a new organ. We further identified individual bacterial species and genera associated with certain transplant indications. Finally, we used a machine learning model to predict FEV1 (which is the most important clinical parameter for the diagnosis of CLAD) dynamics, and observed that the microbiome could predict short-term dynamics in lung function with a high accuracy.

Multi-omics profiling predicts allograft function after lung transplantation

Martin L. Watzenboeck[1,2,7], Anna-Dorothea Gorki[1,2,7], Federica Quattrone[1,2,7], Riem Gawish[1,2,7], Stefan Schwarz[3,7], Christopher Lambers[3], Peter Jaksch[3], Karin Lakovits[1,2], Sophie Zahalka[1,2], Nina Rahimi[1,3], Philipp Starkl[1,2], Dörte Symmank[1,2], Tyler Artner[1,2], Céline Pattaroni[4], Nikolaus Fortelny[2], Kristaps Klavins[2], Florian Frommlet[5], Benjamin J. Marsland[4], Konrad Hoetzenecker[3], Stefanie Widder[1,2,6,8] and Sylvia Knapp[1,2,8]

[1]Research Laboratory of Infection Biology, Dept of Medicine I, Medical University of Vienna, Vienna, Austria. [2]CeMM, Research Center for Molecular Medicine of the Austrian Academy of Sciences, Vienna, Austria. [3]Division of Thoracic Surgery, Dept of Surgery, Medical University of Vienna, Vienna, Austria. [4]Dept of Immunology and Pathology, Monash University, Melbourne, Australia. [5]Institute of Medical Statistics, Center for Medical Statistics, Informatics and Intelligent Systems, Medical University of Vienna, Vienna, Austria. [6]Konrad Lorenz Institute for Evolution and Cognition Research, Klosterneuburg, Austria. [7]These authors contributed equally. [8]S. Widder and S. Knapp contributed equally to this article as lead authors and supervised the work.

Corresponding author: Sylvia Knapp (Sylvia.knapp@meduniwien.ac.at)

Shareable abstract (@ERSpublications)
Broncho-alveolar microbiome, cellular composition, metabolome and lipidome show specific temporal dynamics after lung transplantation. The post-transplantation lung microbiome can predict future changes in lung function with high precision. https://bit.ly/3iFlp1u

Cite this article as: Watzenboeck ML, Gorki A-D, Quattrone F, *et al*. Multi-omics profiling predicts allograft function after lung transplantation. *Eur Respir J* 2022; 59: 2003292 [DOI: 10.1183/13993003.03292-2020].

Received: 27 Aug 2020
Accepted: 09 June 2021

Abstract

Rationale Lung transplantation is the ultimate treatment option for patients with end-stage respiratory diseases but bears the highest mortality rate among all solid organ transplantations due to chronic lung allograft dysfunction (CLAD). The mechanisms leading to CLAD remain elusive due to an insufficient understanding of the complex post-transplant adaptation processes.

Objectives To better understand these lung adaptation processes after transplantation and to investigate their association with future changes in allograft function.

Methods We performed an exploratory cohort study of bronchoalveolar lavage samples from 78 lung recipients and donors. We analysed the alveolar microbiome using 16S rRNA sequencing, the cellular composition using flow cytometry, as well as metabolome and lipidome profiling.

Measurements and main results We established distinct temporal dynamics for each of the analysed data sets. Comparing matched donor and recipient samples, we revealed that recipient-specific as well as environmental factors, rather than the donor microbiome, shape the long-term lung microbiome. We further discovered that the abundance of certain bacterial strains correlated with underlying lung diseases even after transplantation. A decline in forced expiratory volume during the first second (FEV_1) is a major characteristic of lung allograft dysfunction in transplant recipients. By using a machine learning approach, we could accurately predict future changes in FEV_1 from our multi-omics data, whereby microbial profiles showed a particularly high predictive power.

Conclusion Bronchoalveolar microbiome, cellular composition, metabolome and lipidome show specific temporal dynamics after lung transplantation. The lung microbiome can predict future changes in lung function with high precision.

Introduction

Lung transplantation is the ultimate, life-saving treatment for patients with end-stage respiratory failure. Despite substantial medical advances, the 5-year survival rate remains at only 54%, which is the lowest among all solid organ recipients [1]. This grim prognosis is a consequence of a range of pathologies that prevent the transplanted lung from maintaining normal function, which are summarised under the umbrella

term chronic lung allograft dysfunction (CLAD). The most frequent manifestation of CLAD is bronchiolitis obliterans syndrome (BOS), which is characterised by the development of airflow limitation caused by bronchiolitis obliterans [2]. The underlying disease mechanism has been linked to allo- and auto-immunity as well as microbial triggers [3], but the precise pathophysiology is not known and no specific treatment is available.

Once considered a sterile body site, the lungs are now known to harbour a unique microbiome that is critical for respiratory health and immune homeostasis [4]. Recent studies indicate that community-level activities can modulate microbiome pathogenicity [5], myeloid cell responses [6], pulmonary remodelling [7, 8] and CLAD development [9, 10] after lung transplantation. However, host–microbe interplay in the transplanted lung is insufficiently understood and it is unclear to what degree the donor lung microbiome contributes to the post-transplant microbiome and whether this bears relevance for CLAD development.

Innate immune responses are an emerging concept in understanding the events leading to chronic inflammation and CLAD [11]. As such, resident alveolar macrophages (AMs) seem to be instrumental in CLAD development [12], and the higher abundance of neutrophils in transplants is considered detrimental in graft acceptance and survival [11, 13]. These findings clearly suggest a role for myeloid cells in transplant adaptation and function, yet studies investigating the simultaneous coordination of cellular and pulmonary microbial changes are lacking.

Metabolites reflect local metabolic states and can mediate the crosstalk between immune responses and microbiota. In lung transplant recipients, the metabolome composition of bronchoalveolar lavage (BAL) fluid was used to reliably classify the degree of BOS severity [14] and metabolomics/lipidomics of donor lung *ex vivo* lung perfusion fluids were shown to predict primary graft dysfunction [15]. Considering these findings, we hypothesised that the pulmonary metabolome and lipidome might provide important clues to understanding multi-level adaptation after lung transplantation.

A better understanding of the contribution of the pulmonary microbiome, metabolome, lipidome and cellular profiles to the development of CLAD requires a holistic assessment of post-transplant dynamics. In this explorative cohort study, we characterised the reshaping of the pulmonary environment after transplantation with the primary objective to identify time-dependent factors of the process and the secondary objective to describe drivers of lung function decline. Variation of cell composition, microbial diversity, lipid and metabolite profiles, as well as the spirometry parameter FEV_1 (forced expiratory volume during the first second) served as statistical endpoints. We discovered that the microbial composition after lung transplantation was primarily driven by environmental and recipient-specific factors, independent of the donor microbiome, and identified selected microbial species that correlated with transplant indication. Using a computational model enabled us to predict lung function trajectories from multi-omics data sets. The explorative study design entails a descriptive interpretation of p-values and limits conclusions on negative results due to lack of power for small effects.

Ultimately, a more comprehensive knowledge of graft adaptation will enable us to identify novel therapeutic angles to prevent lung allograft dysfunction in the future.

Materials and methods

Detailed descriptions of materials and methods are provided as a supplement.

Patient collective and recruitment

We included all 78 patients who underwent lung transplantation at the Medical University of Vienna between February 2017 and November 2018. The cohort consisted of 76 double lung and two single lung recipients. Donor lung derived BAL samples of sufficiently high quality were available for 23 matched transplant recipients. To obtain a reliable number of donor samples for cross-sectional analyses we included 24 additional high-quality donor BALs without matching recipients. Detailed inclusion and exclusion criteria are stated in the supplementary information. All BAL samples were collected under sterile conditions during routine bronchoscopy, except for one sample that was collected due to acute respiratory symptoms. Routine bronchoscopy was performed before extubation, at four, eight, 12, 26 and 52 weeks after transplantation or whenever medically indicated. The collection of follow-up samples was extended to April 2019. Processing and analyses of BAL samples are described in the supplementary information. Collected patient variables included recipients' age, sex, transplant indication, immunosuppressive therapy, antibiotic and antifungal therapies, serum C-reactive protein (CRP) concentration, lung function (FEV_1) and time after transplantation at the time of sample collection. Detailed patient characteristics are presented in table 1. The study was approved by the ethics committee at

TABLE 1 Patient characteristics

	All	Subset 16S rRNA Seq	Subset FACS	Subset metabolomics/lipidomics
Patients n	78	73	54	36
Age in years at Tx; median (range)	55.5 (17–69)	55 (17–69)	56.5 (17–69)	58.5 (20–69)
Female patients; n (%)	32 (41)	30 (41)	20 (37)	11 (31)
Samples n	164	143	116	70
Donor samples (recipient-matched) n	47 (23)	35 (15)	24 (12)	9 (6)
Recipient samples n	117	108	92	61
Samples per time bin n				
0–7	22	18	18	16
7–30	18	16	15	10
30–75	28	28	24	10
75–400	49	46	35	25
Samples per patient; median (range)	2 (1–6)	1 (1–5)	2 (1–6)	2 (1–6)
Tx indication; samples n/patients n				
COPD	44/25	40/22	35/20	29/15
CF	20/20	19/19	10/9	6/6
IPF	14/9	12/9	12/7	10/5
A1ATD	14/5	14/5	13/5	7/3
PPH	6/6	5/6	5/3	1/1
Other	19/13	18/12	17/10	9/6
Immunosuppressive therapy[#]; samples n/patients n				
Prednisolone	117/56	108/54	92/43	61/33
Ciclosporin	4/2	3/1	4/2	1/1
Tacrolimus	113/55	105/33	88/41	60/32
Mycophenolate/mofetil	50/23	47/22	41/18	29/13
Everolimus	6/3	6/3	4/2	1/1
Antibiotic therapy[#]; samples n/patients n				
Trimethoprim/sulfamethoxazole	76/40	73/40	62/33	34/22
Gentamicin inhalation	26/16	21/16	23/16	20/13
Piperacilin/tazobactam	24/17	19/16	20/15	20/14
Tobramycin inhalation	9/7	9/7	4/3	2/2
Meropenem	9/8	8/8	7/6	2/2
Colistin	8/6	7/6	3/2	1/1
Ciprofloxacin	5/5	5/5	2/2	2/2
Other	32/23	29/20	21/15	15/11

[#]: number of specimens collected from patients while receiving respective drugs at the time of bronchoalveolar lavage. CF: cystic fibrosis; IPF: idiopathic pulmonary fibrosis; A1ATD: alpha-1 antitrypsin deficiency; FACS: fluorescence-activated cell sorting; 16S rRNA Seq: 16S rRNA gene sequencing; PPH: primary pulmonary hypertension; Tx: treatment.

the Medical University of Vienna (EK-Nr:1418/2018) and written informed consent was obtained from all patients.

16S rRNA gene sequencing

Bacterial DNA was isolated using the QIAamp DNA Microbiome kit (Qiagen) according to the manufacturer's protocol. We included sampling controls by flushing sterilised bronchoscopes and negative controls for DNA extraction. Isolated bacterial DNA was amplified using barcoded, adaptor-linked PCR primers targeting the V1–V2 16S rRNA gene region. PCR products were sequenced using Illumina MiSeq technology in the 2×250 bp configuration. Sequencing data were processed using the dada2.R package. A detailed description of bacterial DNA extraction, library preparation, sequencing and sequencing data processing is included in the supplementary information.

Lipidomics and metabolomics

Liquid chromatography–mass spectrometry (LC-MS) analysis was performed using a Vanquish ultra high performance liquid chromatography system combined with an Orbitrap Fusion Lumos Tribrid mass spectrometer for lipidomics or an Orbitrap Q Exactive mass spectrometer for metabolomics. Lipid separation was performed by reversed phase chromatography. The detailed description of lipid extraction, lipid- and metabolite LC-MS analysis, and data processing is included in the supplementary information.

Statistical analyses

Associations of microbial diversity and richness, cell populations, lipid species and metabolites with time after transplantation were analysed by permutational multivariate variance testing and linear mixed-effect models. Time intervals were entered as a factor in the permutational multivariate variance testing, and as a metric covariate together with patient identity as a random effect in the linear mixed-effect models. Factors explaining microbial variation were identified using distance-based redundancy analysis (dbRDA). The association of amplicon sequencing variant (ASV) abundance with time after transplantation and transplant indication was determined using log-transformed linear models on cumulative sum scaling-normalised ASV data (MaAsLin2 R package). Prediction of lung function from omics data sets was done with ridge regression, using a nested cross-validation scheme for hyperparameter tuning and estimation of predictive accuracy. Throughout the manuscript, when applicable, p-values are adjusted for multiple testing using the Benjamini–Hochberg procedure. Due to the exploratory nature of our research, all p-values are to be interpreted in a descriptive manner. Detailed information on the statistical analyses is provided as supplementary material.

Results

Sample stratification and inflammatory parameters

We stratified samples of 78 lung transplant patients into time bins spanning from 0 to 7, 7 to 30, 30 to 75 and >75 days after lung transplantation based on temporal changes in administered medications (immunosuppressive and antimicrobial therapies) (figure S1a) to detect nonlinear associations with time after transplantation. We observed strong associations of serum CRP and blood leukocyte counts ($p<0.001$ for both) with time, indicating decreased systemic inflammation with time after transplantation (figures S1b and c).

Pulmonary microbiome shows temporal dynamics after lung transplantation

By analysing the microbial taxonomic compositions based on 16S rRNA gene sequencing, we found a high diversity between samples at genus and phylum level (figure 1a, figure S2a). Hierarchical clustering of genus-level profiles instantaneously separated samples collected early (<30 days) and late (>30 days) after transplantation (figure 1a). Species-level microbial diversity (Shannon) and richness (Chao 1) (figure 1b, figure S2b) showed highly significant ($p<0.001$) associations with time after transplantation. Using principal coordinate analysis, we observed a tendency of samples to cluster according to time after transplantation (figure 1c, figure S2c and d). We confirmed these visual patterns by permutational multivariate analysis of variance (PERMANOVA; $p<0.05$ for all pairwise comparisons between time groups) (table S1). Donor samples exhibited a microbial profile that was most similar to samples collected within the first week after transplantation, but their composition differed significantly from later timepoints (PERMANOVA $p=0.057$ *versus* 0–7 days after transplantation; $p=0.001$ *versus* any other time bin) (table S1). These results show that lung microbial composition and diversity undergo significant changes from pre-implantation (donor) states to post-transplantation.

Antibiotic therapy and underlying disease explain variation in microbial composition

To identify the key factors that influence the lung microbiome after transplantation, we combined dbRDA with stepwise model building. We included 108 samples from 73 lung recipients that were collected over the entire study period (table 1). The primary objective was to assess dependent covariates and to identify the combination of covariates that best explained microbial variation (figure 1d, figure S2e).

We first analysed all recipient samples (all time bins) and found that the administration of trimethoprim/sulfamethoxazole, the transplant indication, as well as colistin, meropenem and (inhaled) tobramycin together could best explain inter-sample variation (figure 1d, top panel). Next, we separately analysed each time bin after transplantation and observed that only ciprofloxacin during the first week after transplantation accounted for a significant variation between microbiome samples, while none of the tested antibiotics explained inter-sample variation 7–30 or 30–75 days after transplantation (figure 1d, second to fourth panel). Interestingly, out of all tested factors, only transplant indication was significantly associated with microbial composition 30–75 days after transplantation. For samples collected later than 75 days, transplant indication best explained microbial variation, followed by some antibiotics, age and sex (figure 1d, last panel). We also tested the potential impact of immunosuppression on the recipients' lung microbiome, but the very homogenous immunosuppressive therapy scheme received by this cohort (figure S1a) prevented us from identifying clear associations (data not shown). These results suggest that microbial profiles in samples collected early after transplantation are mainly driven by antibiotic therapy, while patient-associated factors including transplant indication, age and sex show significant explanatory power for microbiome samples collected later.

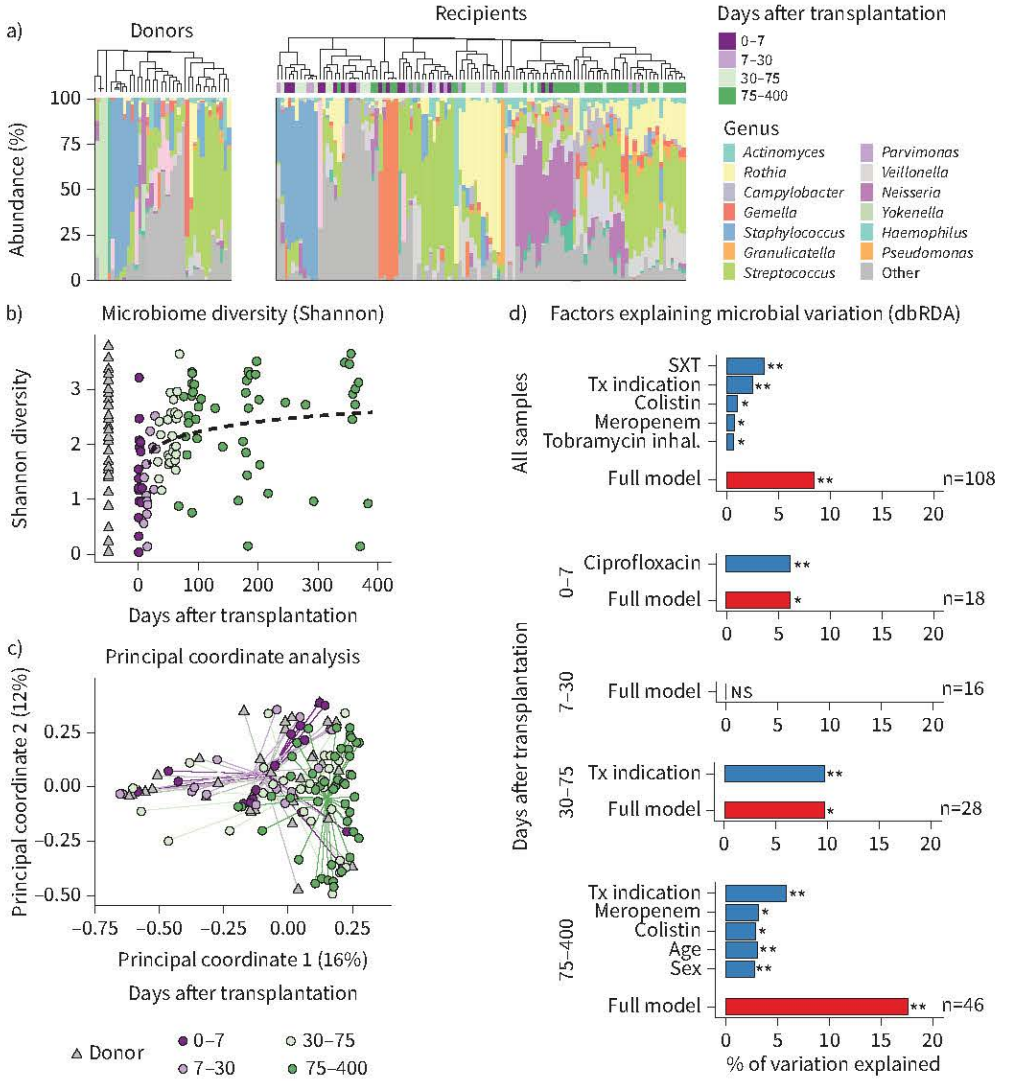

FIGURE 1 Pulmonary microbial dynamics after lung transplantation. a) Relative abundances (genus level) of 16S rRNA gene sequencing amplicons in donor and recipient bronchoalveolar lavage samples. Samples are clustered according to Bray–Curtis distance. Time after transplantation is annotated for recipient samples (heatmap). b) Change in Shannon diversity (species level) with time (linear mixed model $p<0.001$). Samples are coloured according to time after transplantation and shape indicates donor (triangle)/recipient (circle) origin. c) Principal coordinate analysis on Bray–Curtis distances of donor and recipient microbiomes (species level). Every triangle/circle represents a sample and is coloured according to time after transplantation, while shape indicates donor (triangle)/recipient (circle) origin. Lines connect samples to the cluster centroids $p<0.001$, permutational multivariate analysis of variance (PERMANOVA). d) Microbial variation explained by various factors analysed by distance-based redundancy analyses (Bray–Curtis distance). R^2 and significance for multivariate models are shown, whereby the best model was generated by selecting predictors in a stepwise manner, until no further increase in accuracy could be reached. *: $p<0.05$, **: $p<0.01$, PERMANOVA test. SXT: trimethoprim/sulfamethoxazole; dbRDA: distance-based redundancy analysis; Tx: treatment.

Selected strains associate with time and transplant indication

After identifying global associations of time and transplant indication with the pulmonary microbial profile, we tested if individual ASVs differentiated between these associations with time or transplant indication, respectively. In these analyses, we included 108 recipients' samples derived from 73 lung transplant patients with the following indications for lung transplantation: COPD (n=22), cystic fibrosis (CF) (n=19), idiopathic pulmonary fibrosis (IPF) (n=9), alpha-1 antitrypsin deficiency (A1ATD) (n=5), primary pulmonary hypertension (PPH) (n=6) and other (n=12) (table 1). The distribution of underlying diseases is representative of the patient population at our study site (based on 885 patients between 2010

and 2018; data not shown). We found that 33 individual ASVs significantly (false discovery rate (FDR) <0.1) associated with time after transplantation (figure 2a, table S2). Hierarchical clustering separated these strains into three different clusters (figure 2a). Meanwhile, six ASVs associated with transplant indication (figure 2b, table S2). Of these, we detected the strongest association for a strain of *Pseudomonas* (ASV_2, FDR=0.006), which was increased in CF patients, supporting previous reports that showed a predisposition

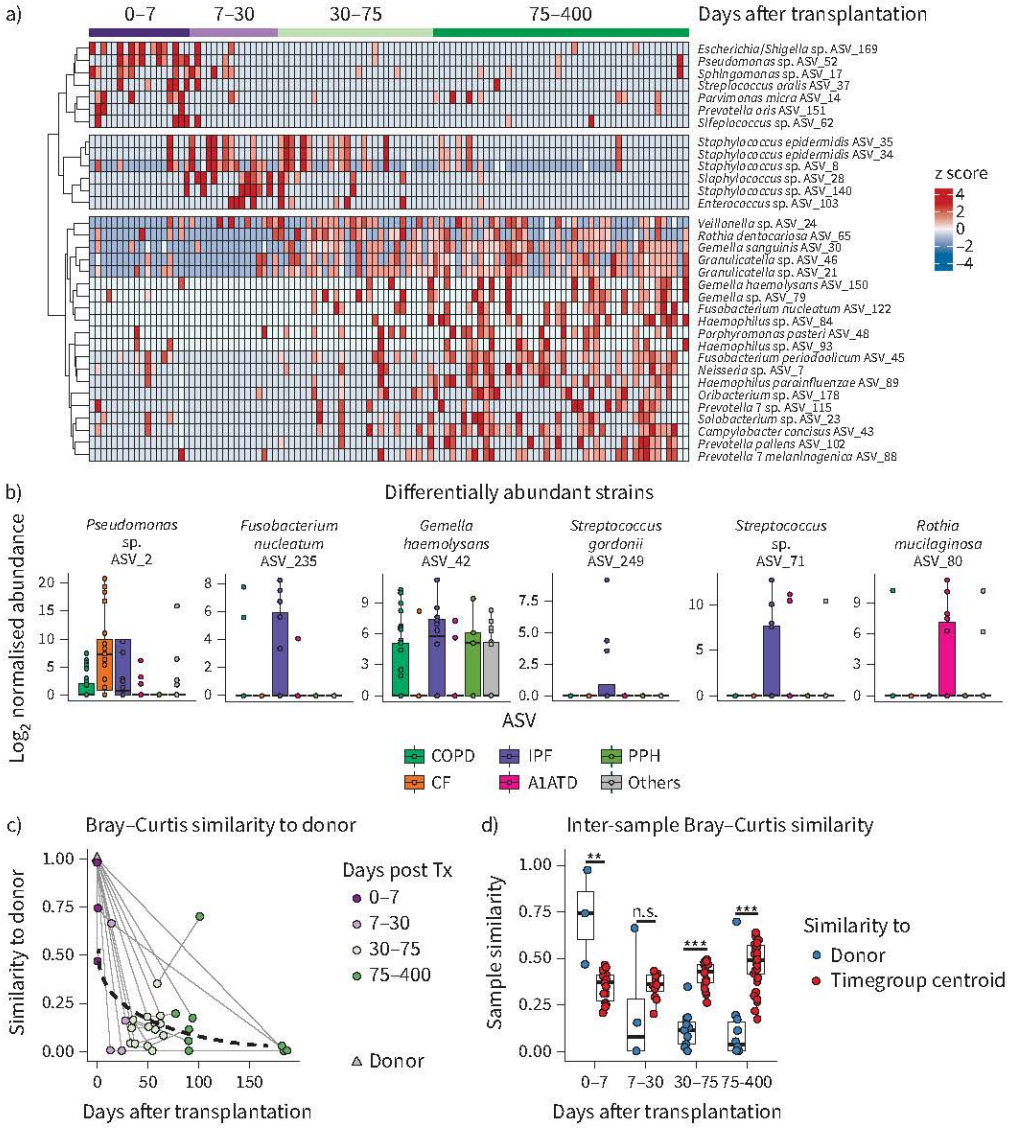

FIGURE 2 Time and underlying disease influence the recipient lung microbiome. a) Heatmap of amplicon sequencing variant (ASVs) showing significant (MaAsLin false discovery rate (FDR)<0.1) association with time after transplantation. Raw counts are cumulative-sum normalised, followed by log-transformation and standardisation (z-score transformation). Samples (columns) are ordered according to time after transplantation. ASVs (rows) are clustered using the "ward.D2" method. The first three branches of the dendrogram are separated for visualisation purposes. b) Boxplots of ASVs showing a significant (MaAsLin FDR<0.1) association with underlying disease. Raw counts are cumulative-sum normalised, followed by log-transformation. Boxplots are indicative of median, interquartile range (IQR) (boxes) and 1.5×IQR (whiskers). CF: cystic fibrosis; IPF: idiopathic pulmonary fibrosis; A1ATD: alpha-1 antitrypsin deficiency; PPH: primary pulmonary hypertension; sp.: species. c) Change of recipient–donor similarity (Bray–Curtis) over time (linear mixed model p<0.001). Connecting lines indicate patient identity; Tx, treatment. d) Comparison between donor–recipient similarity and intersample similarity for various timepoints after transplantation. Boxplots are indicative of median, IQR (boxes) and 1.5×IQR (whiskers). **: p<0.01, ***: p<0.001, Mann–Whitney U-test.

of CF patients to lung allograft colonisation with *Pseudomonas aeruginosa* [16–18]. Furthermore, three strains were almost exclusively found in IPF patients, of which *Fusobacterium nucleatum* (ASV_226) showed the strongest association with transplant indication (FDR=0.01). Another strain identified as *Gemella haemolysans* (ASV_42, FDR=0.03) was rarely encountered in patients with CF or A1ATD, but frequently found in patients with other transplant indications. In addition, *Rothia mucilaginosa* (ASV_80) was preferentially found in patients transplanted due to A1ATD (FDR=0.09). Our results show that transplant indications continuously influence the abundance of certain bacterial strains in the lung after transplantation, in particular in patients with CF, IPF or A1ATD.

Donor lung microbial profiles do not determine the post-transplant microbiome

To determine to what extent the lung allograft microbiome is influenced by the donor lung microbiome, we analysed the similarity between matched donor and recipient microbiomes over time. Bray–Curtis similarity between donors and recipients decreased after transplantation ($p<0.001$) (figure 2c). Similar trends were observed for weighted ($p<0.001$) and unweighted UniFrac similarities ($p<0.01$) (figure S3a and b), which incorporate phylogenetic distances between different organisms. In the first week after transplantation, we found recipient samples to be more similar to matched donor samples than to time-matched recipients (figure 2d). However, at all subsequent timepoints, recipient samples were more similar to samples collected within a comparable timeframe than to their respective donors (figure 2d, figure S3c and d). Thus, the donor microbiome influenced the recipient microbiome only shortly after transplantation, while recipient-associated factors became dominant in shaping the long-term post-transplant pulmonary microbiome.

Pulmonary cellular and molecular profiles change after lung transplantation

The abundance of AMs and inflammatory cells, such as neutrophils, in the BAL correlates with the lung inflammatory state [19]. To investigate alterations in pulmonary cellular profiles after lung transplantation, we conducted flow cytometry of BAL myeloid cell populations (figure S4a). We observed that the numbers of AMs and cells expressing major histocompatibility complex class II (MHCII) but not cluster of differentiation 206 (CD206) were significantly associated with time after transplantation (FDR<0.01 for AMs, FDR<0.001 for $MHCII^+$ $CD206^-$ cells, table S3). While the AM population consistently increased with time (figure 3a), $MHCII^+$ $CD206^-$ cells peaked between 30 and 75 days after transplantation (figure 3b). Concomitantly, myeloid cells ($CD11b^+$) that expressed neither MHCII nor CD206 nor the neutrophil marker CD66b expanded early after transplantation and then declined (FDR<0.05) (figure S4b, table S3). Neutrophils, on average, were surprisingly abundant at all timepoints, but showed high variability between patients (figure 3c). None of the remaining populations significantly associated with time after transplantation (figure S4c and d, table S3) and all investigated cell populations were independent of transplant indication (FDR>0.1 for all) (table S3). Together, we discovered a gradual increase in the proportion of AMs, indicating a transition towards a pattern similar to that observed in healthy lungs [19].

To investigate whether the dynamics of microbial and cellular compositions correlated with BAL metabolic profiles, we performed metabolome and lipidome profiling on a subset of 61 recipients and nine donor samples (table 1). Principal component analysis separated samples according to time after transplantation (figure 3d–e). Samples collected within the first week after transplantation differed most from later samples, suggesting that the most pronounced changes occur early after transplantation (PERMANOVA $p<0.05$ for 0–7 days after transplantation *versus* all other time bins) (tables S4 and S5). To determine whether pre-implantation profiles were more similar to profiles observed early or late after transplantation, we compared donor lavages to recipient lavages. Donor samples differed significantly (PERMANOVA $p<0.05$) from all time bins except the first (0–7 days after transplantation) for both lipids and metabolites (tables S4 and S5), suggesting that lung adaptation after transplantation, rather than the implantation procedure, was responsible for the observed early changes in lipid and metabolite profiles.

Having shown that the global pulmonary lipid and metabolite profile changed after lung transplantation, we next determined which lipid and metabolite species accounted for these changes. Controlling for transplant indication and patient identity, 28 lipid species and eight metabolites showed significant (FDR<0.1) associations with time after transplantation (figure 3f, tables S6 and S7). Of these, 13 lipid species and four metabolites positively correlated with time, whereas 15 lipid species and four metabolites showed a negative correlation with time (figure 3f, figure S4E). None of the tested lipid species were affected by transplant indication (FDR>0.1 for all) (table S6). Transplant indication was significantly associated with leucine concentrations (FDR<0.1), which were higher on average in patients with COPD or A1ATD than in patients receiving transplantation due to other diseases (figure S4f, table S7). These results show that alterations in pulmonary microbial profiles after transplantation were accompanied by changes in intra-alveolar cellular composition and molecular profiles.

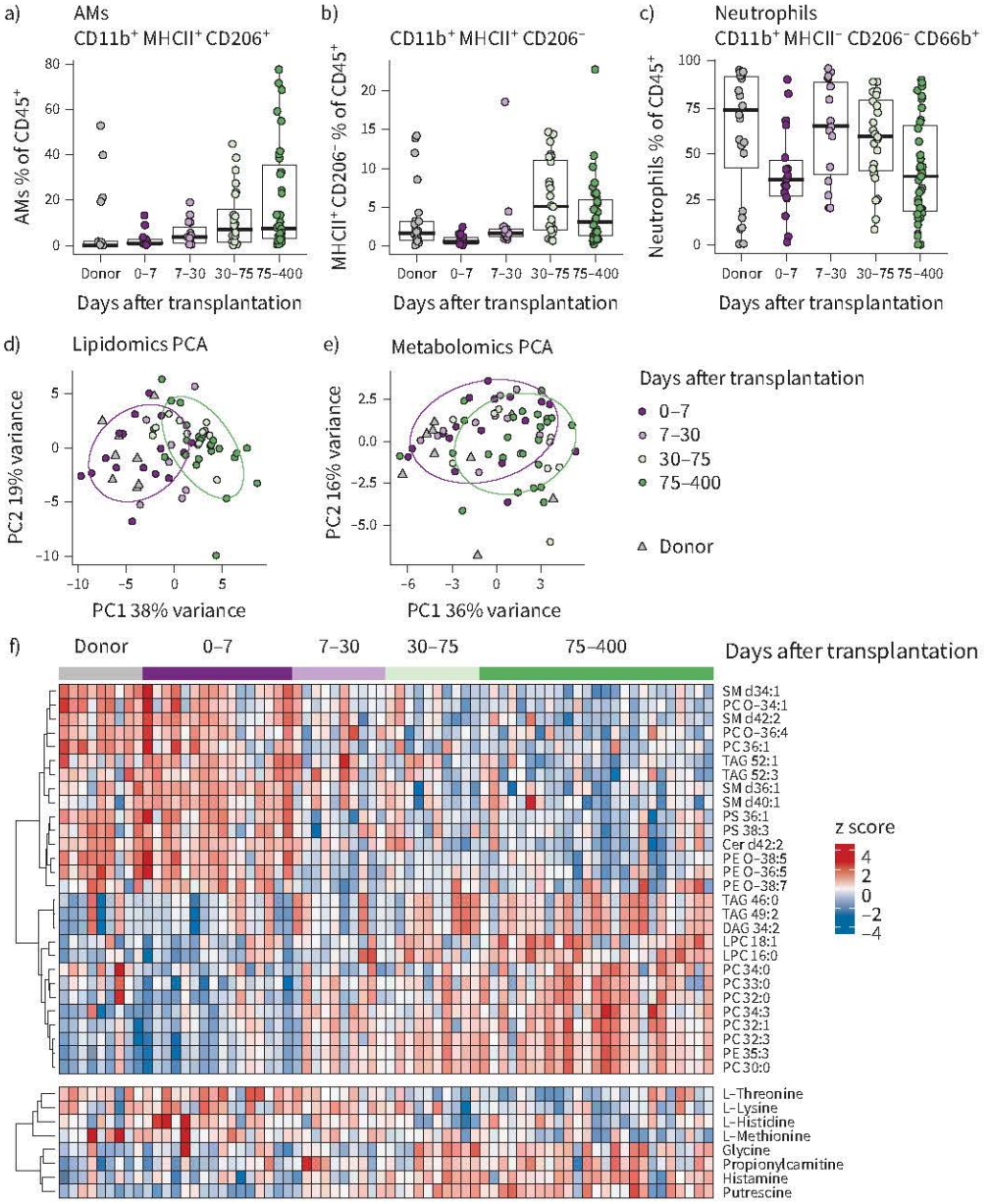

FIGURE 3 Changes in pulmonary cellular and molecular state after lung transplantation. a, b, c) Relative abundance of indicated cell populations in the bronchoalveolar lavage fluid after lung transplantation was assessed by flow cytometry. Boxplots are indicative of median, interquartile range (IQR) (boxes) and 1.5×IQR (whiskers). False discovery rate (FDR)<0.001 for (a), FDR<0.01 (b), FDR>0.1 for (c), linear mixed model. d, e) Principal component analysis (PCA) for lipidome (d) and metabolome (e) data sets. Every triangle/circle represents a sample and is coloured according to time after transplantation, while shape indicates donor (triangle)/recipient (circle) origin. Confidence ellipses (68%) are drawn around samples collected at the earliest (0–7 days after transplantation, purple) and latest (75–400 days after transplantation, green) timepoints. f) Heatmap of lipids and metabolites that show a significant association with time after transplantation (linear mixed model FDR<0.1, controlling for transplant indication and patient identity). AM: alveolar macrophage; MHCII: major histocompatibility complex class II; CD: cluster of differentiation; SM: sphingomyelin; PC: phosphatidylcholine; TAG: triacylglycerol; PS: phosphatidylserine; Cer: ceramide; PE: phosphatidyethanolamine; DAG: diacylglycerol; LPC: lysophosphatidylcholine.

TABLE 2 Characteristics of samples used for prediction of lung function data

	Data sets used for predictions		
	Prediction ΔFEV_1 within 30 days	Prediction ΔFEV_1 within 60 days	Prediction ΔFEV_1 within 90 days
Samples n	32	31	30
Patients n	19	18	17
Females n	8	8	8
Current FEV_1, L; median (range)	2.62 (1.09–4.50)	2.68 (1.09–4.50)	2.70 (1.09–4.50)
Percent change in FEV_1 within X days; median (range)	3 (−7–27)	5 (−18–32)	5 (−29–42)
Age, years; median (range)	59.4 (20.1–68.9)	59.8 (20.1–68.9)	59.4 (20.1–68.9)
CRP, $mg \cdot dL^{-1}$; median (range)	0.17 (0.03–7.46)	0.17 (0.03–7.46)	0.16 (0.03–7.46)

CRP: C-reactive protein; FEV_1: forced expiratory volume during the first second.

Machine learning predicts future lung changes in lung function

CLAD is defined as a persistent decline in FEV_1 of more than 20% compared to the mean of the two best postoperative values (obtained at least three weeks apart) in the absence of other explanations for declining lung function (*e.g.* acute cellular/antibody-mediated rejection, infection, airway stenosis, tracheomalacia) [2]. Several recent studies [3, 20–22] support the importance of the early diagnosis of a decline in lung function, as this knowledge might be utilised to prevent progression and CLAD development. To address this medical need, our secondary objective was to assess whether microbiome, lipidome and metabolome profiles exhibited any predictive value for future changes in FEV_1. We hypothesised that an earlier identification of patients at risk might help in preventing CLAD development and assessed whether the microbiome, lipidome and metabolome profiles exhibited any predictive value for future changes in FEV_1. We included 19 recipients where lung function tests were repeatedly performed over an interval of up to 90 days and all relevant data modalities (microbiome, lipidome, metabolome) and clinical meta-information were available for model building (tables 1 and 2).

Employing a machine learning approach, we trained ridge regression models using clinical metadata, microbiome, metabolome and lipidome data sets as predictors, and changes in FEV_1 at 30, 60 or 90 days after sample collection as response variables (figure 4a). Predictive performance was evaluated using samples collected from patients not included in the training cohort (supplemental methods). To prevent overfitting, we used a nested cross validation scheme by iteratively removing individual patients from the model.

We first tested this approach on individual data sets (*i.e.* microbiome, lipidome or metabolome, respectively) or clinical metadata (sex, age, time after transplantation, current FEV_1 and serum CRP concentration) alone. Doing so, we observed the most accurate short-term predictions of FEV_1 (30 days) when the algorithm was trained on microbiome data (Pearson $r=0.76$, $p<0.001$). For mid-term changes (60 days), microbiome data and clinical metadata performed similarly well (Pearson $r=0.47$, $p<0.01$ for microbiome, $r=0.49$, $p<0.01$ for clinical metadata) while long-term changes (90 days) were most accurately predicted by clinical metadata (Pearson $r=0.42$, $p<0.05$) (figure 4b). Lipidome data performed poorly in comparison to microbiome data, and metabolome data alone could not predict changes in FEV_1. When testing whether combining these individual omics data sets with clinical metadata would improve predictive performance, we found metabolome data in combination with clinical metadata more accurate than any other tested data set in predicting mid-term changes of FEV_1 values (Pearson $r=0.63$, $p<0.001$ for 60 days) (figure 4c). We furthermore evaluated the predictive performance of data sets generated by concatenating individual data modalities (figure 4d), as well as the effect of adding clinical metadata to the combined data sets (figure 4e), which collectively offered superior predictive accuracy over isolated data sets for short- and mid-term changes in FEV_1.

Next, we investigated which specific features contributed to the prediction of FEV_1. The best-performing model for short-term changes in lung function was built on microbiome and metabolome data (Pearson $r=0.78$, $p<0.001$) (figure 4d, f). Analysis of model coefficients showed that *Capnocytophaga gingivalis* received the most positive coefficient (indicating association with improved FEV_1), while *Veillonella dispar* and L-arginine received the most negative coefficients (figure 4f). We observed a tendency towards a higher absolute weight of microbiome *versus* metabolome features (figure S5A). Furthermore, a model built solely on microbiome data performed similarly well (Pearson $r=0.76$, $p<0.001$) (figure 4b, figure

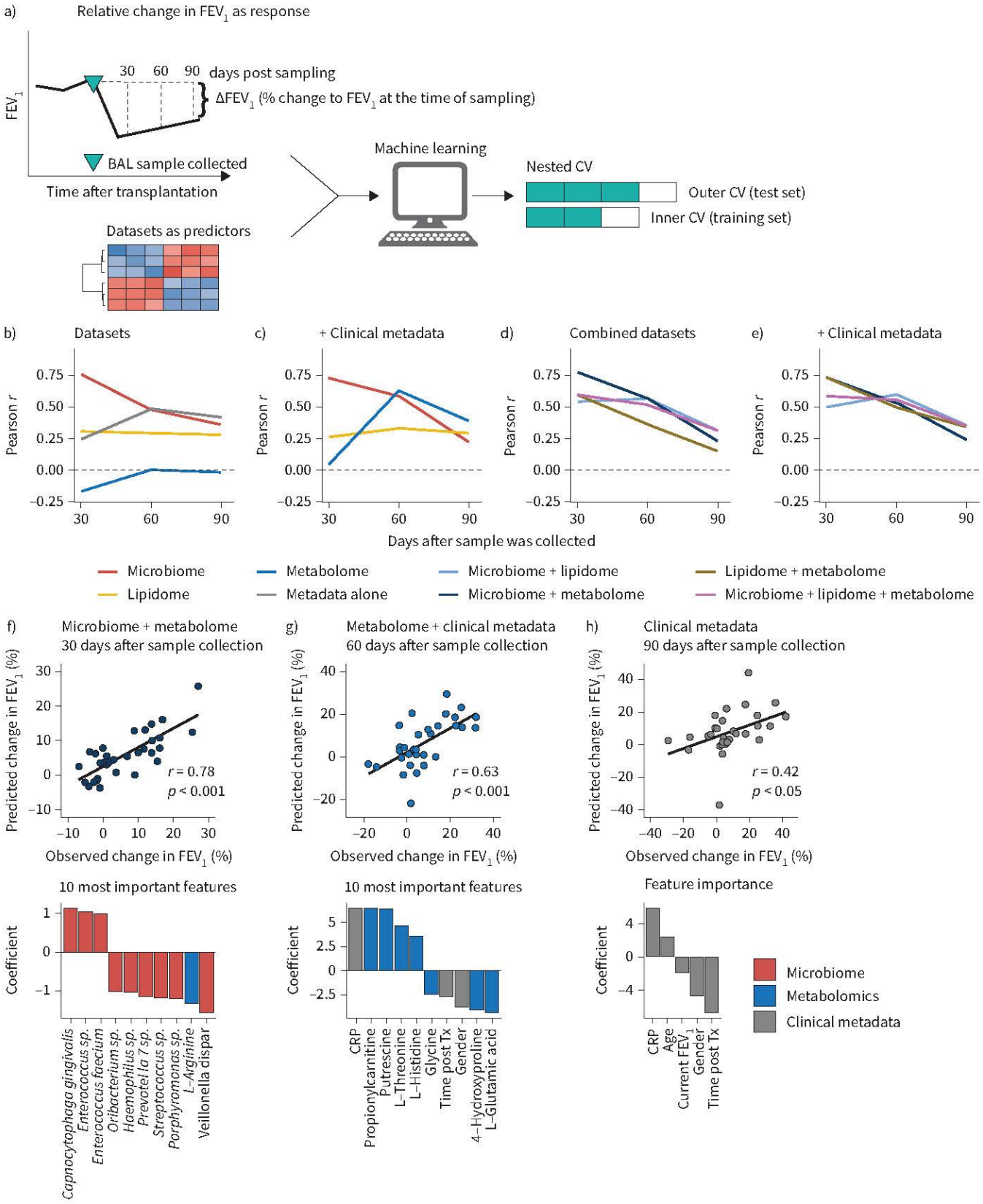

FIGURE 4 Machine learning enables prediction of changes in lung function from multi-omics data. a) Layout of data collection and preparation. Change in forced expiratory volume during the first second (FEV_1) 30, 60 and 90 days after sampling was expressed as percent change to FEV_1 values at the time of sampling. We used our omic data sets to predict these relative changes in FEV_1 using machine learning. To estimate the

performance of our machine learning models on samples which were not included in the data set used to train the model, we employed a nested cross-validation (CV) scheme. b–e) Prediction accuracy (Pearson r between predicted and observed values) for ridge regression models trained on different data sets for changes in FEV_1 at 30, 60 and 90 days after sample collection. Prediction accuracy was evaluated for models trained on specified data sets only (b), on specific data sets plus clinical metadata (age, sex, time after transplantation, serum C-reactive protein (CRP) concentration and current FEV_1) (c), as well as on combined data sets (d) or combined data sets plus clinical metadata (e). f–h) Scatter plots showing observed *versus* predicted changes in FEV_1 and barplots showing the 10 features receiving the highest absolute model coefficients for the best performing models for f) 30, g) 60 and h) 90 days after sample collection. Tx: treatment; sp.: species.

S5b). Intermediate-term changes in lung function were most accurately predicted by a combination of metabolome data and clinical metadata (Pearson r=0.63, p<0.001) with CRP exhibiting the most positive coefficient (figure 4c, g). Finally, for long-term changes in FEV_1, clinical metadata outperformed all other data sets (Pearson r=0.42, p<0.05), with CRP receiving the most positive coefficient, and time after transplantation the most negative (figure 4b, h).

In summary, our data reveal a high predictive power of the lung microbiome for changes in lung function manifesting 30 days after sampling. Surprisingly, clinical metadata including time after transplantation and CRP levels could not match this predictive power for short-term changes, suggesting that effects of the lung microbiome on lung function are independent of time (since transplantation) and systemic inflammation. Long-term changes in FEV_1 were more accurately predicted by clinical metadata, albeit with lower accuracy.

Discussion

Our study provides insight into the pulmonary microbial, cellular and metabolic dynamics after lung transplantation. The analysis of 117 BAL samples from 78 patients together with 47 donor samples makes this one of the largest studies on the human lower respiratory tract microbiome.

We demonstrated that richness and diversity of the microbiome increased rapidly in the first month after lung transplantation and stabilised thereafter, a finding reminiscent of the recently described increase in lung microbiome diversity after birth [23]. Early compositional shifts were linked to antibiotic therapy, in particular trimethoprim/sulfamethoxazole, which is routinely given to prevent infections with *Pneumocystis jirovecii*. Intriguingly, microbial variability at later time points (>30 days after transplantation) showed the strongest association with recipient-specific factors, most notably the transplant indication. We unexpectedly identified several microorganisms that appeared as signature taxa for these lung diseases. While *Pseudomonas* species are the typical pathogens associated with CF, we discovered three bacterial signature strains in IPF patients and one strain associated with A1ATD. Two strains linked to IPF, (*Fusobacterium nucleatum* and *Streptococcus gordonii*), and one strain linked to A1ATD (*Rothia mucilaginosa*) are known colonisers of the oral cavity and upper respiratory tract [24–26]. We hypothesise that these findings may be attributable to recolonisation from the oral flora, which might be altered in IPF or A1ATD patients. Alternatively, altered communication between the upper gastrointestinal tract and the lung (*e.g.* microaspiration) may be responsible, considering the potential association between IPF and reflux disease [27]. While further studies are needed to elucidate the link between IPF or A1ATD and the oral microbiome, we here show specific alterations present in the pulmonary microbiome in IPF and A1ATD patients after lung transplantation.

It is critical to investigate the contribution of the donor microbiome to allograft function, given the fact that non-sterile organs are transplanted to patients. Previous authors suggested that the established lung microbiome after transplantation represents an altered donor microbiome, modified by immigration of microbial species from extrapulmonary sites [28]. This donor microbiome has been proposed as a trigger of pulmonary immune activation, which may contribute to the development of CLAD [3]. In matched samples, we discovered that donor-recipient similarity rapidly decreased after transplantation and that the donor lung microbiome was replaced by a novel bacterial flora in transplanted lungs. These results emphasise that the post-transplantation lung microbiome was independent of the donor microbiome, and that instead a microbial community established that was conserved between patients. Based on these findings, we propose that constant immune activation by the donor microbiome after lung transplantation does not occur.

Early diagnosis of CLAD might enable treatment before irreversible fibrotic remodelling of the lung occurs. Unfortunately, the lack of biomarkers is currently hindering such efforts. Here, using a machine learning approach enabled us to accurately predict changes in FEV_1 based on microbial profiles. Despite

the relatively small-scale sample size used for machine learning, we achieved a highly significant correlation of 0.76 between predicted and observed outcome values. Interestingly, a recent study illustrated the prognostic role of lung microbiota in predicting clinical outcomes, as patients with higher bacterial burdens and the presence of gut-associated taxa were at higher risk of acute respiratory distress syndrome and poor intensive care unit outcome [29]. The authors suggested that translocation of intestinal bacteria to the lung might contribute to lung injury in critically ill patients. Interestingly, we found an abundance of species belonging to the genus *Enterococci*, which are common commensals of the intestinal tract, to be associated with subsequent improvements in FEV_1. This improvement could be linked to adjustments of antibiotic therapy occurring after collection of samples, thereby promoting the elimination of pathogenic bacteria and subsequently improved pulmonary function. Similarly, in predictive models utilising clinical metadata, we observed higher CRP levels to be associated with subsequent improvements in FEV_1, which might seem counterintuitive at first. Elevated serum CRP is a marker of (systemic) inflammation that requires close surveillance and instigates clinicians to initiate proactive treatment. We hypothesise that these activities assist the treatment of potential complications and accelerate resolution, which ultimately leads to improved lung function. Determining whether predictors in our models are beneficial or harmful for lung function is difficult because they are based on associations rather than causality. Beyond CRP, which is a well-understood biomarker, this is particularly true for less well-characterised features such as microbes or metabolites. Our study shares this limitation with any non-interventional approach, which is why clinical trials of targeted therapeutic approaches are required for causal interpretations of host–microbe interplay and lung function to ultimately develop innovative and prophylactic therapies to prevent CLAD.

Acknowledgements: We thank all participating patients, and the medical staff of the Division of Thoracic Surgery, Medical University of Vienna. We thank Thorina Boenke, Martin Senekowitsch, Michael Schuster and Thomas Penz (Biomedical Sequencing Facility, CeMM and Medical University Vienna) for assistance with 16S amplicon sequencing.

Author contributions: M.L. Watzenböck, A.-D. Gorki, F. Quattrone, S. Widder and S. Knapp conceived the project; S. Schwarz, C. Lambers, P. Jaksch, N. Rahimi and K. Hoetzenecker collected samples and clinical data, performed transplantations and managed patient follow-ups; K. Lakovits, F. Quattrone, A.-D. Gorki, R. Gawish, P. Starkl, M.L. Watzenböck, S. Zahalka, D. Symmank and T. Artner processed and analysed samples; K. Klavins performed metabolomic and lipidomic analyses; M.L. Watzenböck analysed data and performed bioinformatics analyses; R. Gawish analysed flow cytometry data; F. Frommlet provided statistical expertise to the study design; C. Pattaroni, N. Fortelny and B.J. Marsland provided technical and analytical support; S. Widder and S. Knapp supervised the project; M.L. Watzenböck, S. Widder and S. Knapp wrote the manuscript. All authors approved the final version of the manuscript.

Conflict of interest: M.L. Watzenböck has nothing to disclose. A.-D. Gorki has nothing to disclose. F. Quattrone has nothing to disclose. R. Gawish has nothing to disclose. S. Schwarz has nothing to disclose. C. Lambers has nothing to disclose. P. Jaksch has nothing to disclose. K. Lakovits has nothing to disclose. S. Zahalka has nothing to disclose. N. Rahimi has nothing to disclose. P. Starkl has nothing to disclose. D. Symmank has nothing to disclose. T. Artner has nothing to disclose. C. Pattaroni has nothing to disclose. N. Fortelny has nothing to disclose. K. Klavins has nothing to disclose. F. Frommlet has nothing to disclose. B.J. Marsland has nothing to disclose. K. Hoetzenecker has nothing to disclose. S. Widder reports grants from Austrian Science Fund (Elise Richter V585-B31), during the conduct of the study. S. Knapp reports grants from FWF, during the conduct of the study.

Support statement: Funding was provided by the Austrian Science Fund (FWF), DK Cell Communication in Health and Disease (W 1205-B09) and the Special Research Program Chromatin Landscapes (L-Mac: F 6104-B21) (to S. Knapp). S. Widder was supported by the Austrian Science Fund (FWF), Elise Richter V585-B31. Funding information for this article has been deposited with the Crossref Funder Registry.

References

1 Yeung JC, Keshavjee S. Overview of clinical lung transplantation. *Cold Spring Harb Perspect Med* 2014; 4: a015628.
2 Verleden GM, Glanville AR, Lease ED, *et al.* Chronic lung allograft dysfunction: definition, diagnostic criteria, and approaches to treatment–A consensus report from the Pulmonary Council of the ISHLT. *J Heart Lung Transplant* 2019; 38: 493–503.
3 Kuehnel M, Maegel L, Vogel-Claussen J, *et al.* Airway remodelling in the transplanted lung. *Cell Tissue Res* 2017; 367: 663–675.
4 Wypych TP, Wickramasinghe LC, Marsland BJ. The influence of the microbiome on respiratory health. *Nat Immunol* 2019; 20: 1279–1290.

5 Dickson RP, Erb-Downward JR, Martinez FJ, *et al.* The microbiome and the respiratory tract. *Annu Rev Physiol* 2016; 78: 481–504.
6 Sharma NS, Wille KM, Athira S, *et al.* Distal airway microbiome is associated with immunoregulatory myeloid cell responses in lung transplant recipients. *J Heart Lung Transplant* 2018, 37: 206–216.
7 Bernasconi E, Pattaroni C, Koutsokera A, *et al.* Airway microbiota determines innate cell inflammatory or tissue remodeling profiles in lung transplantation. *Am J Respir Crit Care Med* 2016; 194: 1252–1263.
8 Mouraux S, Bernasconi E, Pattaroni C, *et al.* Airway microbiota signals anabolic and catabolic remodeling in the transplanted lung. *J Allergy Clin Immunol* 2018; 141: 718–729.e717.
9 Schott C, Weigt SS, Turturice BA, *et al.* Bronchiolitis obliterans syndrome susceptibility and the pulmonary microbiome. *J Heart Lung Transplant* 2018; 37: 1131–1140.
10 Willner DL, Hugenholtz P, Yerkovich ST, *et al.* Reestablishment of recipient-associated microbiota in the lung allograft is linked to reduced risk of bronchiolitis obliterans syndrome. *Am J Respir Crit Care Med* 2013; 187: 640–647.
11 Hsiao HM, Scozzi D, Gauthier JM, *et al.* Mechanisms of graft rejection after lung transplantation. *Curr Opin Organ Transplant* 2017; 22: 29–35.
12 Nayak DK, Zhou F, Xu M, *et al.* Long-term persistence of donor alveolar macrophages in human lung transplant recipients that influences donor-specific immune responses. *Am J Transplant* 2016; 16: 2300–2311.
13 Speck NE, Schuurmans MM, Benden C, *et al.* Plasma and bronchoalveolar lavage samples in acute lung allograft rejection: the potential role of cytokines as diagnostic markers. *Respir Res* 2017; 18: 151.
14 Ciaramelli C, Fumagalli M, Viglio S, *et al.* (1)H NMR to evaluate the metabolome of bronchoalveolar lavage fluid (BALf) in bronchiolitis obliterans syndrome (BOS): toward the development of a new approach for biomarker identification. *J Proteome Res* 2017; 16: 1669–1682.
15 Hsin MK, Zamel R, Cypel M, *et al.* Metabolic profile of *ex vivo* lung perfusate yields biomarkers for lung transplant outcomes. *Ann Surg* 2018; 267: 196–197.
16 Nunley DR, Grgurich W, Iacono AT, *et al.* Allograft colonization and infections with *Pseudomonas* in cystic fibrosis lung transplant recipients. *Chest* 1998; 113: 1235–1243.
17 Beaume M, Kohler T, Greub G, *et al.* Rapid adaptation drives invasion of airway donor microbiota by *Pseudomonas* after lung transplantation. *Sci Rep* 2017; 7: 40309.
18 Walter S, Gudowius P, Bosshammer J, *et al.* Epidemiology of chronic *Pseudomonas aeruginosa* infections in the airways of lung transplant recipients with cystic fibrosis. *Thorax* 1997; 52: 318–321.
19 Meyer KC, Raghu G, Baughman RP, *et al.* An official American Thoracic Society clinical practice guideline: the clinical utility of bronchoalveolar lavage cellular analysis in interstitial lung disease. *Am J Respir Crit Care Med* 2012; 185: 1004–1014.
20 Royer PJ, Olivera-Botello G, Koutsokera A, *et al.* Chronic lung allograft dysfunction: a systematic review of mechanisms. *Transplantation* 2016; 100: 1803–1814.
21 Kneidinger N, Milger K, Janitza S, *et al.* Lung volumes predict survival in patients with chronic lung allograft dysfunction. *Eur Respir J* 2017; 49: 1601315.
22 Todd JL, Neely ML, Finlen Copeland CA, *et al.* Prognostic significance of early pulmonary function changes after onset of chronic lung allograft dysfunction. *J Heart Lung Transplant* 2019; 38: 184–193.
23 Pattaroni C, Watzenboeck ML, Schneidegger S, *et al.* Early-life formation of the microbial and immunological environment of the human airways. *Cell Host Microbe* 2018; 24: 857–865.e854.
24 Han YW. *Fusobacterium nucleatum*: a commensal-turned pathogen. *Curr Opin Microbiol* 2015; 23: 141–147.
25 Krantz AM, Ratnaraj F, Velagapudi M, *et al.* *Streptococcus gordonii* empyema: a case report and review of empyema. *Cureus* 2017; 9: e1159.
26 Maraki S, Papadakis IS. *Rothia mucilaginosa* pneumonia: a literature review. *Infect Dis* 2015; 47: 125–129.
27 Ghisa M, Marinelli C, Savarino V, *et al.* Idiopathic pulmonary fibrosis and GERD: links and risks. *Ther Clin Risk Manag* 2019; 15: 1081–1093.
28 Mitchell AB. The lung microbiome and transplantation. *Curr Opin Organ Transplant* 2019; 24: 305–310.
29 Dickson RP, Schultz MJ, van der Poll T, *et al.* Lung microbiota predict clinical outcomes in critically ill patients. *Am J Respir Crit Care Med* 2020; 201: 555–563

3 Final discussion

Given that the lung is constantly exposed to potential pathogens, its innate and adaptive immune systems are highly organized. However, due to the fragile tissue architecture required for proper organ function, these systems also need to be tightly regulated. The microbiome has been shown to play a key role in the development and regulation of immune responses, and this interplay is linked to multiple pulmonary (patho)physiological processes, such the immune response to influenza infection and the development of CLAD after lung transplantation. Nevertheless, and particularly in light of the fact that this interplay might serve as a target for treatment and/or surveillance of these conditions, our current understanding of this interplay is limited.

In the first part of the study, we investigated the role of LCN2 in the immune response to influenza virus infection. Due to the delicate nature of the tissue, exaggerated immune responses can easily induce immunopathology in the lung. Influenza infection, in particular, is known to be associated with a high degree of immunopathology (Rouse and Sehrawat, 2010). Several different aspects of both innate and adaptive immunity, including dysregulation of the production of proinflammatory cytokines and exuberant activity of cytolytic T cells, are known to be involved in these phenomena. While we observed increases in several proinflammatory cytokines in BAL fluid early (three days) after infection in *Lcn2*$^{-/-}$ mice, no significant differences were detectable after six days, when increased disease morbidity manifested. These kinetics pointed our attention towards the adaptive immune system, which typically is activated later than innate immunity (Chaplin, 2010). Indeed, when conducting flow cytometric analysis of lungs after influenza infection, the most striking finding were drastically increased CD8^{+} T cell counts in the lungs of *Lcn2*$^{-/-}$ mice. By depleting these cells with a specific antibody, we could show that they drive the pronounced morbidity in this mouse model, since CD8^{+} T cell depletion equalized weight loss after influenza infection between WT and *Lcn2*$^{-/-}$ mice.

While our data shows that the effect of LCN2 on lung CD8^{+} T cell responses is dependent on the microbiome, since antibiotic treatment and cohousing led to comparable lung CD8^{+} T cell numbers in WT and *Lcn2*-deficient mice after infection, we cannot completely rule out additional, microbiome-independent effects of LCN2 on antiviral immunity. Several different surface receptors have been described in the literature: LCN2 binds to megalin (Hvidberg et al., 2005) and SLC22A17 (Devireddy et al., 2005), leading to endocytosis. Additionally, LCN2 could be shown to signal through

MC4R, which leads to appetite suppression (Mosialou et al., 2017). Nevertheless, in-vitro, we observed no effects of recombinant LCN2 on antigen presentation. However, we cannot completely rule out the existence of effects of LCN2 on DC function and/or antiviral immunity that might not be adequately recapitulated *in vitro*. For instance, such mechanisms might depend on LCN2´s role in iron homeostasis. Certain viral infections are known to affect the expression of genes involved in iron homeostasis, and iron overload could be shown to negatively affect the prognosis in HIV and hepatitis C virus infections (Drakesmith and Prentice, 2008). Further research on the complex interplay of iron metabolism and antiviral immunity might uncover a potential role of LCN2.

A limitation of our study is that, while our data revealed a dependency of the modulatory effects of LCN2 on antiviral immune responses on the microbiome, we did not identify the precise mechanism via which the dysregulated microbiome in *Lcn2*$^{-/-}$ mice influences the immune response. Given the roles of microbial metabolites, such as SCFAs (Trompette et al., 2018) or desaminotyrosine (Steed et al., 2017) in immune responses against influenza infection, microbial metabolites might also contribute to or drive the effects of LCN2 on antiviral immunity. Large scale metabolomics studies coupled with validation experiments of potential hits would be required to decipher such potential mechanisms. Another possible way of action might be associated with the findings of Ichinohe *et al.*, who observed that microbial signals influence DC migration through inflammasome activation. However, we did not observe increased numbers of DCs in the mediastinal lymph nodes of *Lcn2*$^{-/-}$ mice (Figure 11), suggesting that the increase in lung T cells after influenza infection is not linked to increased DC migration. Also, in our antigen presentation assays, in which we observed increased T cell proliferation after co-culture of *Lcn2*$^{-/-}$ CD103^{+} DCs, equal DC numbers were co-cultured with T cells for both WT and *Lcn2*$^{-/-}$ mice, which proves that, in our model, the observed effects are based on increased cellular potential to induce T cell proliferation, rather than greater DC numbers in the mediastinal lymph nodes, as observed by Ichinohe *et al.*.

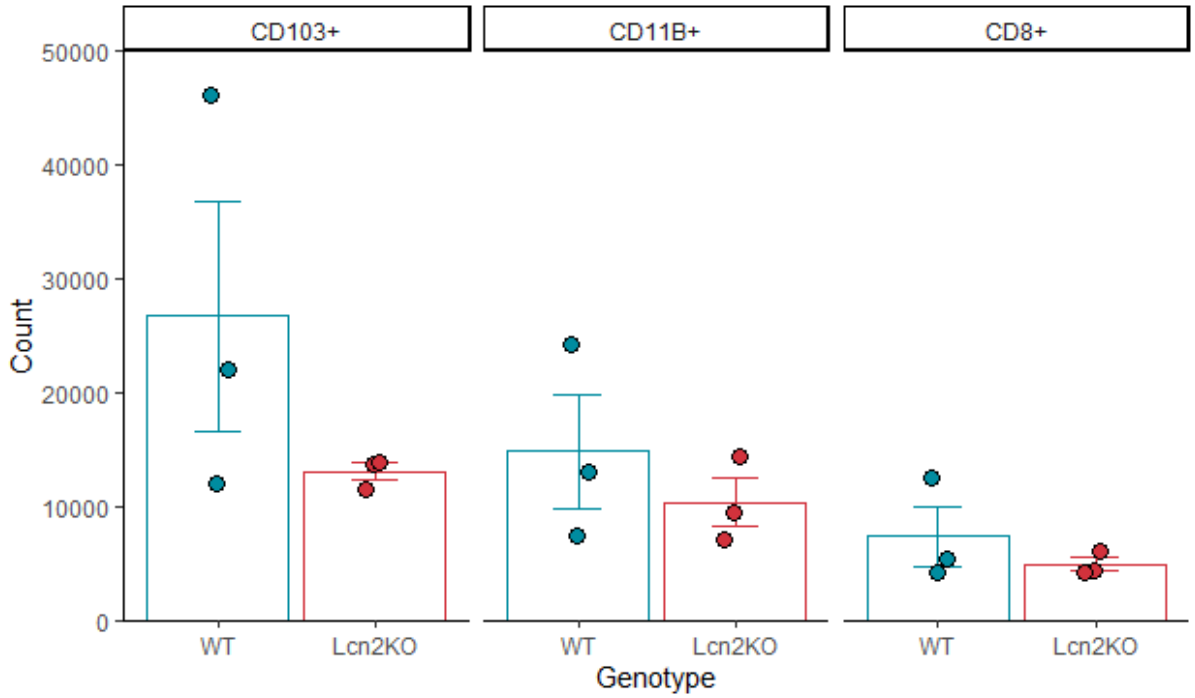

Figure 11: Dendritic cell counts in the mediastinal lymph nodes of WT and *Lcn2*$^{-/-}$ mice 60 hours after infection, quantified using FACS, gated on single/live/CD45^{+}/CD11c^{+}/CD8^{-}/CD11b^{-}/CD103^{+}, single/live/CD45^{+}/CD11c^{+}/CD8^{-}/CD11b^{-}/CD11b^{+} or single/live/CD45^{+}/CD11c^{+}/CD8^{+} cells.

In the second part of this thesis, the lung microbiome, metabolome, lipidome and immune cell compositions in BAL samples collected from lung transplant donors and recipients were investigated. By assessing a total number of 117 BAL samples from recipients, ranging from samples collected within days after transplantation to after the first year after the operation, and 47 donor samples, this study was able to provide unprecedented insights into lung adaption after transplantation. With regards to the lung microbiome, we observed a rapid increase in microbial richness and diversity within the first days after transplantation. Interestingly, these dynamics appear reminiscent of the recently described changes in the respiratory microbiome after birth (Pattaroni et al., 2018). In transplanted patients, these changes may be linked to antibiotic usage, both in the donor prior to transplantation, and the recipient after transplantation. While antibiotic regimes given to brain-dead donors were not accessible to us, we indeed found statistically significant links between the administration of certain antibiotics, in particular trimethoprim/sulfamethoxazole and ciprofloxacin, and microbial composition early (within the first month) after transplantation. Analysis of the individual bacterial strains which showed temporal dynamics after transplantation revealed a cluster of seven bacterial species which

showed a high abundance within the first week after transplantation. Interestingly, this cluster included the known lung pathogens *Pseudomonas sp.*, *Streptococcus sp.* and *Escherichia/Shigella sp*. Another cluster of six bacterial species was particularly dominant between the first week and first month after transplantation. This cluster consisted predominately of different species of *Staphylococcus*. Finally, a cluster of 20 different bacterial species dominated the established lung microbiome after more than 30 days post transplantation. This cluster included *Prevotella sp*., *Veilonella sp*., *Fusobacterium sp*. and *Haemophilus sp.*, which are known to be the main constituents of a healthy lung microbiome. Interestingly, we also observed a high variability in microbial profiles at later stages after transplantation. When assessing potential explanatory factors for these differences, we found that recipient-specific factors, including age, sex, and in particular, transplant indication, were linked to these variations. When comparing recipient microbiomes to the respective donor microbiomes, we found a rapid divergence in their profiles after transplantation. Specifically, after more than one month post transplantation, recipient lung microbiome profiles were more similar to other recipient samples collected within similar time frames after transplantation, than to their respective donor sample. This observation leads to two important conclusions: Firstly, lung adaption after transplantation is associated with conserved changes in microbial profiles, which are likely driven, at least partly, by antimicrobial therapies. Second, the influence of the donor microbiome on the recipient lung microbiome is neglectable after more than one month post transplantation. Immune cell activation by the donor microbiome has been suggested as a factor implicated in the pathogenesis of CLAD (Kuehnel et al., 2017). However, based on our results, the donor microbiome is unlikely to be a persistent trigger of immune cell activation in the transplanted lung.

Similarly to the microbiome, the lung lipidome and metabolome showed significant dynamics after transplantation. This was more pronounced in the lipidome, where more than half of the quantified lipids differed between the investigated time points. Interestingly, the lipidomic and metabolomics profiles found in BALs collected from donors prior to lung explantation did not significantly differ from the profiles observed within the first week after transplantation. Rather, the main compositional shifts in metabolomics and lipidomic profiles occurred after the first week post transplantation. This suggests that adaptation processes, instead of the explantation and implantation procedure, alter the airway metabolism. These dynamics correlated with the

abundance of immune cell types within the BAL: The percentage of alveolar macrophages and monocytes gradually increased, while the relative abundance of neutrophils peaked between the first week and first month after transplantation and subsequently declined, which is most likely linked to an early surge of inflammation after lung transplantation.

Early effective treatment approaches for CLAD are hampered by the lack of sensitive and reliable biomarkers (Tissot et al., 2019). To this date, clinical diagnosis of CLAD is based on pulmonary function tests (PFTs), however, altered pulmonary function can be considered the endpoint of tissue remodeling, and there are no biomarkers accurately predicting subsequent CLAD development. To discern whether multi-omics data could potentially reveal new predictors of lung allograft dysfunction, we developed a machine learning approach, whereby mathematical models were trained to predict subsequent changes in lung function based on the microbial, metabolomics and lipidomic profiles of bronchoalveolar lavage samples after transplantation. These models were benchmarked against models trained on clinical data alone. Interestingly, we found that early changes in lung function (that occurred within 30 days after collection of the representative bronchoalveolar lavage samples), could be accurately predicted by the bronchoalveolar lavage microbial profile. These data highlight the close interplay between the airway microbiome and lung function after transplantation. In this context, it is important to recognize the potential role of airway infections, which are also known to be risk factors for the development of CLAD (Gregson, 2016). However, considering the fact that C-reactive protein (CRP) levels could not predict early changes in lung function as accurately as the airway microbiome, these data provide direct evidence that the lung microbiome is associated with allograft (dys)function beyond clinical infections. While this study was under review, a prospective cohort study, which investigated whether lung bacterial burden or microbial composition in lavage samples collected during surveillance bronchoscopies performed one year after transplantation could predict CLAD development or death (Combs et al., 2021). The authors found that a lower lung bacterial burden was strongly associated with a longer CLAD-free survival. Additionally, they reported community-level differences between patients who developed CLAD or died and those who did not. These data further validate our result and further stress the importance of the lung microbiome in CLAD development.

In summary, the work presented in this thesis increases the understanding of interactions of the pulmonary immune system with the microbiome, by providing evidence for the importance of these interactions for the regulation of antiviral immune responses and allograft function after lung transplantation.

4 References

ABADIA-MOLINA, A. C., JI, H., FAUBION, W. A., JULIEN, A., LATCHMAN, Y., YAGITA, H., SHARPE, A., BHAN, A. K. & TERHORST, C. 2006. CD48 controls T-cell and antigen-presenting cell functions in experimental colitis. *Gastroenterology,* 130**,** 424-34.

ABLASSER, A., POECK, H., ANZ, D., BERGER, M., SCHLEE, M., KIM, S., BOURQUIN, C., GOUTAGNY, N., JIANG, Z., FITZGERALD, K. A., ROTHENFUSSER, S., ENDRES, S., HARTMANN, G. & HORNUNG, V. 2009. Selection of molecular structure and delivery of RNA oligonucleotides to activate TLR7 versus TLR8 and to induce high amounts of IL-12p70 in primary human monocytes. *J Immunol,* 182**,** 6824-33.

ABT, M. C., OSBORNE, L. C., MONTICELLI, L. A., DOERING, T. A., ALENGHAT, T., SONNENBERG, G. F., PALEY, M. A., ANTENUS, M., WILLIAMS, K. L., ERIKSON, J., WHERRY, E. J. & ARTIS, D. 2012. Commensal bacteria calibrate the activation threshold of innate antiviral immunity. *Immunity,* 37**,** 158-70.

ALEXOPOULOU, L., HOLT, A. C., MEDZHITOV, R. & FLAVELL, R. A. 2001. Recognition of double-stranded RNA and activation of NF-kappaB by Toll-like receptor 3. *Nature,* 413**,** 732-8.

ANDREWS, N. C. 2000. Iron homeostasis: insights from genetics and animal models. *Nat Rev Genet,* 1**,** 208-17.

ANTUNES, K. H., FACHI, J. L., DE PAULA, R., DA SILVA, E. F., PRAL, L. P., DOS SANTOS, A. A., DIAS, G. B. M., VARGAS, J. E., PUGA, R., MAYER, F. Q., MAITO, F., ZARATE-BLADES, C. R., AJAMI, N. J., SANT'ANA, M. R., CANDREVA, T., RODRIGUES, H. G., SCHMIELE, M., SILVA CLERICI, M. T. P., PROENCA-MODENA, J. L., VIEIRA, A. T., MACKAY, C. R., MANSUR, D., CABALLERO, M. T., MARZEC, J., LI, J., WANG, X., BELL, D., POLACK, F. P., KLEEBERGER, S. R., STEIN, R. T., VINOLO, M. A. R. & DE SOUZA, A. P. D. 2019. Microbiota-derived acetate protects against respiratory syncytial virus infection through a GPR43-type 1 interferon response. *Nat Commun,* 10**,** 3273.

ASIMAKOPOULOU, A., WEISKIRCHEN, S. & WEISKIRCHEN, R. 2016. Lipocalin 2 (LCN2) Expression in Hepatic Malfunction and Therapy. *Front Physiol,* 7**,** 430.

BAHADORAN, A., LEE, S. H., WANG, S. M., MANIKAM, R., RAJARAJESWARAN, J., RAJU, C. S. & SEKARAN, S. D. 2016. Immune Responses to Influenza Virus and Its Correlation to Age and Inherited Factors. *Front Microbiol,* 7**,** 1841.

BAILEY, C. C., HUANG, I. C., KAM, C. & FARZAN, M. 2012. Ifitm3 limits the severity of acute influenza in mice. *PLoS Pathog,* 8**,** e1002909.

BALACHANDRAN, S., ROBERTS, P. C., BROWN, L. E., TRUONG, H., PATTNAIK, A. K., ARCHER, D. R. & BARBER, G. N. 2000. Essential role for the dsRNA-dependent protein kinase PKR in innate immunity to viral infection. *Immunity,* 13**,** 129-41.

BANERJEE, I., YAMAUCHI, Y., HELENIUS, A. & HORVATH, P. 2013. High-content analysis of sequential events during the early phase of influenza A virus infection. *PLoS One,* 8**,** e68450.

BANKIER, A. A., VAN MUYLEM, A., KNOOP, C., ESTENNE, M. & GEVENOIS, P. A. 2001. Bronchiolitis obliterans syndrome in heart-lung transplant recipients: diagnosis with expiratory CT. *Radiology,* 218**,** 533-9.
BEATY, S. R., ROSE, C. E., JR. & SUNG, S. S. 2007. Diverse and potent chemokine production by lung CD11bhigh dendritic cells in homeostasis and in allergic lung inflammation. *J Immunol,* 178**,** 1882-95.
BELKAID, Y. & HARRISON, O. J. 2017. Homeostatic Immunity and the Microbiota. *Immunity,* 46**,** 562-576.
BERNASCONI, E., PATTARONI, C., KOUTSOKERA, A., PISON, C., KESSLER, R., BENDEN, C., SOCCAL, P. M., MAGNAN, A., AUBERT, J. D., MARSLAND, B. J., NICOD, L. P. & SYS, C. C. 2016. Airway Microbiota Determines Innate Cell Inflammatory or Tissue Remodeling Profiles in Lung Transplantation. *Am J Respir Crit Care Med,* 194**,** 1252-1263.
BOREWICZ, K., PRAGMAN, A. A., KIM, H. B., HERTZ, M., WENDT, C. & ISAACSON, R. E. 2013. Longitudinal analysis of the lung microbiome in lung transplantation. *FEMS Microbiol Lett,* 339**,** 57-65.
BOS, S., VOS, R., VAN RAEMDONCK, D. E. & VERLEDEN, G. M. 2020. Survival in adult lung transplantation: where are we in 2020? *Curr Opin Organ Transplant,* 25**,** 268-273.
BRACIALE, T. J., SUN, J. & KIM, T. S. 2012. Regulating the adaptive immune response to respiratory virus infection. *Nat Rev Immunol,* 12**,** 295-305.
BRADLEY, K. C., FINSTERBUSCH, K., SCHNEPF, D., CROTTA, S., LLORIAN, M., DAVIDSON, S., FUCHS, S. Y., STAEHELI, P. & WACK, A. 2019. Microbiota-Driven Tonic Interferon Signals in Lung Stromal Cells Protect from Influenza Virus Infection. *Cell Rep,* 28**,** 245-256 e4.
BULTE, J. W. M. & SHAKERI-ZADEH, A. 2022. In Vivo MRI Tracking of Tumor Vaccination and Antigen Presentation by Dendritic Cells. *Mol Imaging Biol,* 24**,** 198-207.
BYRNE, D., NADOR, R. G., ENGLISH, J. C., YEE, J., LEVY, R., BERGERON, C., SWISTON, J. R., METS, O. M., MULLER, N. L. & BILAWICH, A. M. 2021. Chronic Lung Allograft Dysfunction: Review of CT and Pathologic Findings. *Radiol Cardiothorac Imaging,* 3**,** e200314.
CAMASCHELLA, C., NAI, A. & SILVESTRI, L. 2020. Iron metabolism and iron disorders revisited in the hepcidin era. *Haematologica,* 105**,** 260-272.
CENTERS FOR DISEASE CONTROL AND PREVENTION. 2021, September 29. *Estimated Flu-Related Illnesses, Medical visits, Hospitalizations, and Deaths in the United States — 2018–2019 Flu Season* [Online]. Available: https://www.cdc.gov/flu/about/burden/2018-2019.html.
CHAN, Y. R., LIU, J. S., POCIASK, D. A., ZHENG, M., MIETZNER, T. A., BERGER, T., MAK, T. W., CLIFTON, M. C., STRONG, R. K., RAY, P. & KOLLS, J. K. 2009. Lipocalin 2 is required for pulmonary host defense against Klebsiella infection. *J Immunol,* 182**,** 4947-56.
CHAPLIN, D. D. 2010. Overview of the immune response. *J Allergy Clin Immunol,* 125**,** S3-23.
CHARLSON, E. S., DIAMOND, J. M., BITTINGER, K., FITZGERALD, A. S., YADAV, A., HAAS, A. R., BUSHMAN, F. D. & COLLMAN, R. G. 2012. Lung-enriched organisms and aberrant bacterial and fungal respiratory microbiota after lung transplant. *Am J Respir Crit Care Med,* 186**,** 536-45.
CLARKE, S. H., STAUDT, L. M., KAVALER, J., SCHWARTZ, D., GERHARD, W. U. & WEIGERT, M. G. 1990. V region gene usage and somatic mutation in the

primary and secondary responses to influenza virus hemagglutinin. *J Immunol,* 144**,** 2795-801.
COMBS, M. P., WHEELER, D. S., LUTH, J. E., FALKOWSKI, N. R., WALKER, N. M., ERB-DOWNWARD, J. R., LAMA, V. N. & DICKSON, R. P. 2021. Lung microbiota predict chronic rejection in healthy lung transplant recipients: a prospective cohort study. *Lancet Respir Med,* 9**,** 601-612.
CORRENTI, C. & STRONG, R. K. 2012. Mammalian siderophores, siderophore-binding lipocalins, and the labile iron pool. *J Biol Chem,* 287**,** 13524-31.
COWLAND, J. B. & BORREGAARD, N. 1997. Molecular characterization and pattern of tissue expression of the gene for neutrophil gelatinase-associated lipocalin from humans. *Genomics,* 45**,** 17-23.
DAWOOD, F. S., IULIANO, A. D., REED, C., MELTZER, M. I., SHAY, D. K., CHENG, P. Y., BANDARANAYAKE, D., BREIMAN, R. F., BROOKS, W. A., BUCHY, P., FEIKIN, D. R., FOWLER, K. B., GORDON, A., HIEN, N. T., HORBY, P., HUANG, Q. S., KATZ, M. A., KRISHNAN, A., LAL, R., MONTGOMERY, J. M., MOLBAK, K., PEBODY, R., PRESANIS, A. M., RAZURI, H., STEENS, A., TINOCO, Y. O., WALLINGA, J., YU, H., VONG, S., BRESEE, J. & WIDDOWSON, M. A. 2012. Estimated global mortality associated with the first 12 months of 2009 pandemic influenza A H1N1 virus circulation: a modelling study. *Lancet Infect Dis,* 12**,** 687-95.
DEKENS, D. W., NAUDE, P. J. W., KEIJSER, J. N., BOEREMA, A. S., DE DEYN, P. P. & EISEL, U. L. M. 2018. Lipocalin 2 contributes to brain iron dysregulation but does not affect cognition, plaque load, and glial activation in the J20 Alzheimer mouse model. *J Neuroinflammation,* 15**,** 330.
DEL RIO, M. L., RODRIGUEZ-BARBOSA, J. I., KREMMER, E. & FORSTER, R. 2007. CD103- and CD103+ bronchial lymph node dendritic cells are specialized in presenting and cross-presenting innocuous antigen to CD4+ and CD8+ T cells. *J Immunol,* 178**,** 6861-6.
DENTON, A. E., DOHERTY, P. C., TURNER, S. J. & LA GRUTA, N. L. 2007. IL-18, but not IL-12, is required for optimal cytokine production by influenza virus-specific CD8+ T cells. *Eur J Immunol,* 37**,** 368-75.
DEVIREDDY, L. R., GAZIN, C., ZHU, X. & GREEN, M. R. 2005. A cell-surface receptor for lipocalin 24p3 selectively mediates apoptosis and iron uptake. *Cell,* 123**,** 1293-305.
DICKSON, R. P., ERB-DOWNWARD, J. R., MARTINEZ, F. J. & HUFFNAGLE, G. B. 2016. The Microbiome and the Respiratory Tract. *Annu Rev Physiol,* 78**,** 481-504.
DOU, D., REVOL, R., OSTBYE, H., WANG, H. & DANIELS, R. 2018. Influenza A Virus Cell Entry, Replication, Virion Assembly and Movement. *Front Immunol,* 9**,** 1581.
DRAKESMITH, H. & PRENTICE, A. 2008. Viral infection and iron metabolism. *Nat Rev Microbiol,* 6**,** 541-52.
DUNNING, J., THWAITES, R. S. & OPENSHAW, P. J. M. 2020. Seasonal and pandemic influenza: 100 years of progress, still much to learn. *Mucosal Immunol,* 13**,** 566-573.
EDINGER, T. O., POHL, M. O. & STERTZ, S. 2014. Entry of influenza A virus: host factors and antiviral targets. *J Gen Virol,* 95**,** 263-277.
ELLER, K., SCHROLL, A., BANAS, M., KIRSCH, A. H., HUBER, J. M., NAIRZ, M., SKVORTSOV, S., WEISS, G., ROSENKRANZ, A. R. & THEURL, I. 2013. Lipocalin-2 expressed in innate immune cells is an endogenous inhibitor of inflammation in murine nephrotoxic serum nephritis. *PLoS One,* 8**,** e67693.

ENAUD, R., PREVEL, R., CIARLO, E., BEAUFILS, F., WIEERS, G., GUERY, B. & DELHAES, L. 2020. The Gut-Lung Axis in Health and Respiratory Diseases: A Place for Inter-Organ and Inter-Kingdom Crosstalks. *Front Cell Infect Microbiol,* 10**,** 9.

FLO, T. H., SMITH, K. D., SATO, S., RODRIGUEZ, D. J., HOLMES, M. A., STRONG, R. K., AKIRA, S. & ADEREM, A. 2004. Lipocalin 2 mediates an innate immune response to bacterial infection by sequestrating iron. *Nature,* 432**,** 917-21.

FLOWER, D. R. 1996. The lipocalin protein family: structure and function. *Biochem J,* 318 (Pt 1)**,** 1-14.

GANZ, T. & NEMETH, E. 2009. Iron sequestration and anemia of inflammation. *Semin Hematol,* 46**,** 387-93.

GAZIT, R., GRUDA, R., ELBOIM, M., ARNON, T. I., KATZ, G., ACHDOUT, H., HANNA, J., QIMRON, U., LANDAU, G., GREENBAUM, E., ZAKAY-RONES, Z., PORGADOR, A. & MANDELBOIM, O. 2006. Lethal influenza infection in the absence of the natural killer cell receptor gene Ncr1. *Nat Immunol,* 7**,** 517-23.

GOETZ, D. H., HOLMES, M. A., BORREGAARD, N., BLUHM, M. E., RAYMOND, K. N. & STRONG, R. K. 2002. The neutrophil lipocalin NGAL is a bacteriostatic agent that interferes with siderophore-mediated iron acquisition. *Mol Cell,* 10**,** 1033-43.

GOETZ, D. H., WILLIE, S. T., ARMEN, R. S., BRATT, T., BORREGAARD, N. & STRONG, R. K. 2000. Ligand preference inferred from the structure of neutrophil gelatinase associated lipocalin. *Biochemistry,* 39**,** 1935-41.

GREGSON, A. L. 2016. Infectious Triggers of Chronic Lung Allograft Dysfunction. *Curr Infect Dis Rep,* 18**,** 21.

HAMMAD, H. & LAMBRECHT, B. N. 2008. Dendritic cells and epithelial cells: linking innate and adaptive immunity in asthma. *Nat Rev Immunol,* 8**,** 193-204.

HARDY, J. D., WEBB, W. R., DALTON, M. L., JR. & WALKER, G. R., JR. 1963. Lung Homotransplantation in Man. *JAMA,* 186**,** 1065-74.

HASHIMOTO, Y., MOKI, T., TAKIZAWA, T., SHIRATSUCHI, A. & NAKANISHI, Y. 2007. Evidence for phagocytosis of influenza virus-infected, apoptotic cells by neutrophils and macrophages in mice. *J Immunol,* 178**,** 2448-57.

HEFTI, H. P., FRESE, M., LANDIS, H., DI PAOLO, C., AGUZZI, A., HALLER, O. & PAVLOVIC, J. 1999. Human MxA protein protects mice lacking a functional alpha/beta interferon system against La crosse virus and other lethal viral infections. *J Virol,* 73**,** 6984-91.

HENTZE, M. W., MUCKENTHALER, M. U. & ANDREWS, N. C. 2004. Balancing acts: molecular control of mammalian iron metabolism. *Cell,* 117**,** 285-97.

HO, A. W., PRABHU, N., BETTS, R. J., GE, M. Q., DAI, X., HUTCHINSON, P. E., LEW, F. C., WONG, K. L., HANSON, B. J., MACARY, P. A. & KEMENY, D. M. 2011. Lung CD103+ dendritic cells efficiently transport influenza virus to the lymph node and load viral antigen onto MHC class I for presentation to CD8 T cells. *J Immunol,* 187**,** 6011-21.

HOLMES, M. A., PAULSENE, W., JIDE, X., RATLEDGE, C. & STRONG, R. K. 2005. Siderocalin (Lcn 2) also binds carboxymycobactins, potentially defending against mycobacterial infections through iron sequestration. *Structure,* 13**,** 29-41.

HOTA, P., DASS, C., KUMARAN, M. & SIMPSON, S. 2018. High-Resolution CT Findings of Obstructive and Restrictive Phenotypes of Chronic Lung Allograft

Dysfunction: More Than Just Bronchiolitis Obliterans Syndrome. *AJR Am J Roentgenol,* 211**,** W13-W21.
HUFFORD, M. M., KIM, T. S., SUN, J. & BRACIALE, T. J. 2011. Antiviral CD8+ T cell effector activities in situ are regulated by target cell type. *J Exp Med,* 208**,** 167-80.
HUGGENVIK, J. I., CRAVEN, C. M., IDZERDA, R. L., BERNSTEIN, S., KAPLAN, J. & MCKNIGHT, G. S. 1989. A splicing defect in the mouse transferrin gene leads to congenital atransferrinemia. *Blood,* 74**,** 482-6.
HUGHES, C. E., BENSON, R. A., BEDAJ, M. & MAFFIA, P. 2016. Antigen-Presenting Cells and Antigen Presentation in Tertiary Lymphoid Organs. *Front Immunol,* 7**,** 481.
HUMAN MICROBIOME PROJECT, C. 2012. A framework for human microbiome research. *Nature,* 486**,** 215-21.
HVIDBERG, V., JACOBSEN, C., STRONG, R. K., COWLAND, J. B., MOESTRUP, S. K. & BORREGAARD, N. 2005. The endocytic receptor megalin binds the iron transporting neutrophil-gelatinase-associated lipocalin with high affinity and mediates its cellular uptake. *FEBS Lett,* 579**,** 773-7.
ICHINOHE, T., PANG, I. K. & IWASAKI, A. 2010. Influenza virus activates inflammasomes via its intracellular M2 ion channel. *Nat Immunol,* 11**,** 404-10.
ICHINOHE, T., PANG, I. K., KUMAMOTO, Y., PEAPER, D. R., HO, J. H., MURRAY, T. S. & IWASAKI, A. 2011. Microbiota regulates immune defense against respiratory tract influenza A virus infection. *Proc Natl Acad Sci U S A,* 108**,** 5354-9.
INCI, I. 2020. Lung transplantation for emphysema. *Ann Transl Med,* 8**,** 1473.
IWASAKI, A. & PILLAI, P. S. 2014. Innate immunity to influenza virus infection. *Nat Rev Immunol,* 14**,** 315-28.
JAKUBZICK, C., TACKE, F., GINHOUX, F., WAGERS, A. J., VAN ROOIJEN, N., MACK, M., MERAD, M. & RANDOLPH, G. J. 2008. Blood monocyte subsets differentially give rise to CD103+ and CD103- pulmonary dendritic cell populations. *J Immunol,* 180**,** 3019-27.
JESTER, B. J., UYEKI, T. M. & JERNIGAN, D. B. 2020. Fifty Years of Influenza A(H3N2) Following the Pandemic of 1968. *Am J Public Health,* 110**,** 669-676.
JIANG, F., RAMANATHAN, A., MILLER, M. T., TANG, G. Q., GALE, M., JR., PATEL, S. S. & MARCOTRIGIANO, J. 2011. Structural basis of RNA recognition and activation by innate immune receptor RIG-I. *Nature,* 479**,** 423-7.
KAMBAYASHI, T. & LAUFER, T. M. 2014. Atypical MHC class II-expressing antigen-presenting cells: can anything replace a dendritic cell? *Nat Rev Immunol,* 14**,** 719-30.
KANG, S. S., REN, Y., LIU, C. C., KURTI, A., BAKER, K. E., BU, G., ASMANN, Y. & FRYER, J. D. 2018. Lipocalin-2 protects the brain during inflammatory conditions. *Mol Psychiatry,* 23**,** 344-350.
KIM, H., WEBSTER, R. G. & WEBBY, R. J. 2018. Influenza Virus: Dealing with a Drifting and Shifting Pathogen. *Viral Immunol,* 31**,** 174-183.
KIM, T. S. & BRACIALE, T. J. 2009. Respiratory dendritic cell subsets differ in their capacity to support the induction of virus-specific cytotoxic CD8+ T cell responses. *PLoS One,* 4**,** e4204.
KIM, T. S., HUFFORD, M. M., SUN, J., FU, Y. X. & BRACIALE, T. J. 2010. Antigen persistence and the control of local T cell memory by migrant respiratory dendritic cells after acute virus infection. *J Exp Med,* 207**,** 1161-72.

KRAMMER, F., SMITH, G. J. D., FOUCHIER, R. A. M., PEIRIS, M., KEDZIERSKA, K., DOHERTY, P. C., PALESE, P., SHAW, M. L., TREANOR, J., WEBSTER, R. G. & GARCIA-SASTRE, A. 2018. Influenza. *Nat Rev Dis Primers,* 4**,** 3.

KUEHNEL, M., MAEGEL, L., VOGEL-CLAUSSEN, J., ROBERTUS, J. L. & JONIGK, D. 2017. Airway remodelling in the transplanted lung. *Cell Tissue Res,* 367**,** 663-675.

LAUDER, S. N., JONES, E., SMART, K., BLOOM, A., WILLIAMS, A. S., HINDLEY, J. P., ONDONDO, B., TAYLOR, P. R., CLEMENT, M., FIELDING, C., GODKIN, A. J., JONES, S. A. & GALLIMORE, A. M. 2013. Interleukin-6 limits influenza-induced inflammation and protects against fatal lung pathology. *Eur J Immunol,* 43**,** 2613-25.

LAWRENCE, C. W. & BRACIALE, T. J. 2004. Activation, differentiation, and migration of naive virus-specific CD8+ T cells during pulmonary influenza virus infection. *J Immunol,* 173**,** 1209-18.

LEVINE, D. J., GLANVILLE, A. R., ABOYOUN, C., BELPERIO, J., BENDEN, C., BERRY, G. J., HACHEM, R., HAYES, D., JR., NEIL, D., REINSMOEN, N. L., SNYDER, L. D., SWEET, S., TYAN, D., VERLEDEN, G., WESTALL, G., YUSEN, R. D., ZAMORA, M. & ZEEVI, A. 2016. Antibody-mediated rejection of the lung: A consensus report of the International Society for Heart and Lung Transplantation. *J Heart Lung Transplant,* 35**,** 397-406.

LI, Y. T., LINSTER, M., MENDENHALL, I. H., SU, Y. C. F. & SMITH, G. J. D. 2019. Avian influenza viruses in humans: lessons from past outbreaks. *Br Med Bull,* 132**,** 81-95.

LIU, Q. & NILSEN-HAMILTON, M. 1995. Identification of a new acute phase protein. *J Biol Chem,* 270**,** 22565-70.

LU, A. & WU, H. 2015. Structural mechanisms of inflammasome assembly. *FEBS J,* 282**,** 435-44.

MADAN, R., CHANSAKUL, T. & GOLDBERG, H. J. 2014. Imaging in lung transplants: Checklist for the radiologist. *Indian J Radiol Imaging,* 24**,** 318-26.

MALLA, M. A., DUBEY, A., KUMAR, A., YADAV, S., HASHEM, A. & ABD ALLAH, E. F. 2018. Exploring the Human Microbiome: The Potential Future Role of Next-Generation Sequencing in Disease Diagnosis and Treatment. *Front Immunol,* 9**,** 2868.

MARCHESI, J. R. & RAVEL, J. 2015. The vocabulary of microbiome research: a proposal. *Microbiome,* 3**,** 31.

MCAULEY, J. L., TATE, M. D., MACKENZIE-KLUDAS, C. J., PINAR, A., ZENG, W., STUTZ, A., LATZ, E., BROWN, L. E. & MANSELL, A. 2013. Activation of the NLRP3 inflammasome by IAV virulence protein PB1-F2 contributes to severe pathophysiology and disease. *PLoS Pathog,* 9**,** e1003392.

MEDZHITOV, R. 2001. Toll-like receptors and innate immunity. *Nat Rev Immunol,* 1**,** 135-45.

MEDZHITOV, R. 2007. Recognition of microorganisms and activation of the immune response. *Nature,* 449**,** 819-26.

MEDZHITOV, R., SCHNEIDER, D. S. & SOARES, M. P. 2012. Disease tolerance as a defense strategy. *Science,* 335**,** 936-41.

MEYER, K. C., RAGHU, G., VERLEDEN, G. M., CORRIS, P. A., AURORA, P., WILSON, K. C., BROZEK, J., GLANVILLE, A. R., COMMITTEE, I. A. E. B. T. F. & COMMITTEE, I. A. E. B. T. F. 2014. An international ISHLT/ATS/ERS clinical practice guideline: diagnosis and management of bronchiolitis obliterans syndrome. *Eur Respir J,* 44**,** 1479-503.

MILLS, C. E., ROBINS, J. M. & LIPSITCH, M. 2004. Transmissibility of 1918 pandemic influenza. *Nature,* 432**,** 904-6.
MONTICELLI, L. A., SONNENBERG, G. F., ABT, M. C., ALENGHAT, T., ZIEGLER, C. G., DOERING, T. A., ANGELOSANTO, J. M., LAIDLAW, B. J., YANG, C. Y., SATHALIYAWALA, T., KUBOTA, M., TURNER, D., DIAMOND, J. M., GOLDRATH, A. W., FARBER, D. L., COLLMAN, R. G., WHERRY, E. J. & ARTIS, D. 2011. Innate lymphoid cells promote lung-tissue homeostasis after infection with influenza virus. *Nat Immunol,* 12**,** 1045-54.
MORENS, D. M. & FAUCI, A. S. 2007. The 1918 influenza pandemic: insights for the 21st century. *J Infect Dis,* 195**,** 1018-28.
MOSCHEN, A. R., GERNER, R. R., WANG, J., KLEPSCH, V., ADOLPH, T. E., REIDER, S. J., HACKL, H., PFISTER, A., SCHILLING, J., MOSER, P. L., KEMPSTER, S. L., SWIDSINSKI, A., ORTH HOLLER, D., WEISS, G., BAINES, J. F., KASER, A. & TILG, H. 2016. Lipocalin 2 Protects from Inflammation and Tumorigenesis Associated with Gut Microbiota Alterations. *Cell Host Microbe,* 19**,** 455-69.
MOSIALOU, I., SHIKHEL, S., LIU, J. M., MAURIZI, A., LUO, N., HE, Z., HUANG, Y., ZONG, H., FRIEDMAN, R. A., BARASCH, J., LANZANO, P., DENG, L., LEIBEL, R. L., RUBIN, M., NICKOLAS, T., CHUNG, W., ZELTSER, L. M., WILLIAMS, K. W., PESSIN, J. E. & KOUSTENI, S. 2017. MC4R-dependent suppression of appetite by bone-derived lipocalin 2. *Nature,* 543**,** 385-390.
MOURAUX, S., BERNASCONI, E., PATTARONI, C., KOUTSOKERA, A., AUBERT, J. D., CLAUSTRE, J., PISON, C., ROYER, P. J., MAGNAN, A., KESSLER, R., BENDEN, C., SOCCAL, P. M., MARSLAND, B. J., NICOD, L. P. & SYS, C. C. 2018. Airway microbiota signals anabolic and catabolic remodeling in the transplanted lung. *J Allergy Clin Immunol,* 141**,** 718-729 e7.
MURPHY, K. & WEAVER, C. 2016. *Janeway's immunobiology,* New York, NY, Garland Science/Taylor & Francis Group, LLC.
NAIRZ, M., SCHROLL, A., HASCHKA, D., DICHTL, S., SONNWEBER, T., THEURL, I., THEURL, M., LINDNER, E., DEMETZ, E., ASSHOFF, M., BELLMANN-WEILER, R., MULLER, R., GERNER, R. R., MOSCHEN, A. R., BAUMGARTNER, N., MOSER, P. L., TALASZ, H., TILG, H., FANG, F. C. & WEISS, G. 2015. Lipocalin-2 ensures host defense against Salmonella Typhimurium by controlling macrophage iron homeostasis and immune response. *Eur J Immunol,* 45**,** 3073-86.
NAIRZ, M., THEURL, I., SCHROLL, A., THEURL, M., FRITSCHE, G., LINDNER, E., SEIFERT, M., CROUCH, M. L., HANTKE, K., AKIRA, S., FANG, F. C. & WEISS, G. 2009. Absence of functional Hfe protects mice from invasive Salmonella enterica serovar Typhimurium infection via induction of lipocalin-2. *Blood,* 114**,** 3642-51.
PANG, I. K., ICHINOHE, T. & IWASAKI, A. 2013. IL-1R signaling in dendritic cells replaces pattern-recognition receptors in promoting CD8(+) T cell responses to influenza A virus. *Nat Immunol,* 14**,** 246-53.
PATTARONI, C., WATZENBOECK, M. L., SCHNEIDEGGER, S., KIESER, S., WONG, N. C., BERNASCONI, E., PERNOT, J., MERCIER, L., KNAPP, S., NICOD, L. P., MARSLAND, C. P., ROTH-KLEINER, M. & MARSLAND, B. J. 2018. Early-Life Formation of the Microbial and Immunological Environment of the Human Airways. *Cell Host Microbe,* 24**,** 857-865 e4.
PETERSEN, C. & ROUND, J. L. 2014. Defining dysbiosis and its influence on host immunity and disease. *Cell Microbiol,* 16**,** 1024-33.

PETES, C., ODOARDI, N. & GEE, K. 2017. The Toll for Trafficking: Toll-Like Receptor 7 Delivery to the Endosome. *Front Immunol,* 8**,** 1075.
PICHLMAIR, A., SCHULZ, O., TAN, C. P., NASLUND, T. I., LILJESTROM, P., WEBER, F. & REIS E SOUSA, C. 2006. RIG-I-mediated antiviral responses to single-stranded RNA bearing 5'-phosphates. *Science,* 314**,** 997-1001.
RATLEDGE, C. & DOVER, L. G. 2000. Iron metabolism in pathogenic bacteria. *Annu Rev Microbiol,* 54**,** 881-941.
ROUSE, B. T. & SEHRAWAT, S. 2010. Immunity and immunopathology to viruses: what decides the outcome? *Nat Rev Immunol,* 10**,** 514-26.
SAIGA, H., NISHIMURA, J., KUWATA, H., OKUYAMA, M., MATSUMOTO, S., SATO, S., MATSUMOTO, M., AKIRA, S., YOSHIKAI, Y., HONDA, K., YAMAMOTO, M. & TAKEDA, K. 2008. Lipocalin 2-dependent inhibition of mycobacterial growth in alveolar epithelium. *J Immunol,* 181**,** 8521-7.
SATO, M., WADDELL, T. K., WAGNETZ, U., ROBERTS, H. C., HWANG, D. M., HAROON, A., WAGNETZ, D., CHAPARRO, C., SINGER, L. G., HUTCHEON, M. A. & KESHAVJEE, S. 2011. Restrictive allograft syndrome (RAS): a novel form of chronic lung allograft dysfunction. *J Heart Lung Transplant,* 30**,** 735-42.
SAVAGE, D. C. 1977. Microbial ecology of the gastrointestinal tract. *Annu Rev Microbiol,* 31**,** 107-33.
SCHOTT, C., WEIGT, S. S., TURTURICE, B. A., METWALLY, A., BELPERIO, J., FINN, P. W. & PERKINS, D. L. 2018. Bronchiolitis obliterans syndrome susceptibility and the pulmonary microbiome. *J Heart Lung Transplant,* 37**,** 1131-1140.
SEALY, R., SURMAN, S., HURWITZ, J. L. & COLECLOUGH, C. 2003. Antibody response to influenza infection of mice: different patterns for glycoprotein and nucleocapsid antigens. *Immunology,* 108**,** 431-9.
SENDER, R., FUCHS, S. & MILO, R. 2016a. Are We Really Vastly Outnumbered? Revisiting the Ratio of Bacterial to Host Cells in Humans. *Cell,* 164**,** 337-40.
SENDER, R., FUCHS, S. & MILO, R. 2016b. Revised Estimates for the Number of Human and Bacteria Cells in the Body. *PLoS Biol,* 14**,** e1002533.
SHANKAR, J., NGUYEN, M. H., CRESPO, M. M., KWAK, E. J., LUCAS, S. K., MCHUGH, K. J., MOUNAUD, S., ALCORN, J. F., PILEWSKI, J. M., SHIGEMURA, N., KOLLS, J. K., NIERMAN, W. C. & CLANCY, C. J. 2016. Looking Beyond Respiratory Cultures: Microbiome-Cytokine Signatures of Bacterial Pneumonia and Tracheobronchitis in Lung Transplant Recipients. *Am J Transplant,* 16**,** 1766-78.
SHARMA, N. S., WILLE, K. M., ATHIRA, S., ZHI, D., HOUGH, K. P., DIAZ-GUZMAN, E., ZHANG, K., KUMAR, R., RANGARAJAN, S., EIPERS, P., WANG, Y., SRIVASTAVA, R. K., RODRIGUEZ DAGER, J. V., ATHAR, M., MORROW, C., HOOPES, C. W., CHAPLIN, D. D., THANNICKAL, V. J. & DESHANE, J. S. 2017. Distal airway microbiome is associated with immunoregulatory myeloid cell responses in lung transplant recipients. *J Heart Lung Transplant*.
SILVA, Y. P., BERNARDI, A. & FROZZA, R. L. 2020. The Role of Short-Chain Fatty Acids From Gut Microbiota in Gut-Brain Communication. *Front Endocrinol (Lausanne),* 11**,** 25.
SILVERMAN, R. H. 2007. Viral encounters with 2',5'-oligoadenylate synthetase and RNase L during the interferon antiviral response. *J Virol,* 81**,** 12720-9.
SINGH, V., YEOH, B. S., CHASSAING, B., ZHANG, B., SAHA, P., XIAO, X., AWASTHI, D., SHASHIDHARAMURTHY, R., DIKSHIT, M., GEWIRTZ, A. & VIJAY-KUMAR, M. 2016. Microbiota-inducible Innate Immune, Siderophore

Binding Protein Lipocalin 2 is Critical for Intestinal Homeostasis. *Cell Mol Gastroenterol Hepatol,* 2**,** 482-498 e6.
SNELL, G., HIHO, S., LEVVEY, B., SULLIVAN, L. & WESTALL, G. 2019. Consequences of donor-derived passengers (pathogens, cells, biological molecules and proteins) on clinical outcomes. *J Heart Lung Transplant,* 38**,** 902-906.
SPREEUWENBERG, P., KRONEMAN, M. & PAGET, J. 2018. Reassessing the Global Mortality Burden of the 1918 Influenza Pandemic. *Am J Epidemiol,* 187**,** 2561-2567.
SRINIVASAN, G., AITKEN, J. D., ZHANG, B., CARVALHO, F. A., CHASSAING, B., SHASHIDHARAMURTHY, R., BORREGAARD, N., JONES, D. P., GEWIRTZ, A. T. & VIJAY-KUMAR, M. 2012. Lipocalin 2 deficiency dysregulates iron homeostasis and exacerbates endotoxin-induced sepsis. *J Immunol,* 189**,** 1911-9.
STEED, A. L., CHRISTOPHI, G. P., KAIKO, G. E., SUN, L., GOODWIN, V. M., JAIN, U., ESAULOVA, E., ARTYOMOV, M. N., MORALES, D. J., HOLTZMAN, M. J., BOON, A. C. M., LENSCHOW, D. J. & STAPPENBECK, T. S. 2017. The microbial metabolite desaminotyrosine protects from influenza through type I interferon. *Science,* 357**,** 498-502.
SUNG, S. S., FU, S. M., ROSE, C. E., JR., GASKIN, F., JU, S. T. & BEATY, S. R. 2006. A major lung CD103 (alphaE)-beta7 integrin-positive epithelial dendritic cell population expressing Langerin and tight junction proteins. *J Immunol,* 176**,** 2161-72.
SYED, S. A., WHELAN, F. J., WADDELL, B., RABIN, H. R., PARKINS, M. D. & SURETTE, M. G. 2016. Reemergence of Lower-Airway Microbiota in Lung Transplant Patients with Cystic Fibrosis. *Ann Am Thorac Soc,* 13**,** 2132-2142.
TATEMATSU, M., NISHIKAWA, F., SEYA, T. & MATSUMOTO, M. 2013. Toll-like receptor 3 recognizes incomplete stem structures in single-stranded viral RNA. *Nat Commun,* 4**,** 1833.
THOMAS, P. G., DASH, P., ALDRIDGE, J. R., JR., ELLEBEDY, A. H., REYNOLDS, C., FUNK, A. J., MARTIN, W. J., LAMKANFI, M., WEBBY, R. J., BOYD, K. L., DOHERTY, P. C. & KANNEGANTI, T. D. 2009. The intracellular sensor NLRP3 mediates key innate and healing responses to influenza A virus via the regulation of caspase-1. *Immunity,* 30**,** 566-75.
TISSOT, A., DANGER, R., CLAUSTRE, J., MAGNAN, A. & BROUARD, S. 2019. Early Identification of Chronic Lung Allograft Dysfunction: The Need of Biomarkers. *Front Immunol,* 10**,** 1681.
TOPHAM, D. J. & DOHERTY, P. C. 1998. Clearance of an influenza A virus by CD4+ T cells is inefficient in the absence of B cells. *J Virol,* 72**,** 882-5.
TROMPETTE, A., GOLLWITZER, E. S., PATTARONI, C., LOPEZ-MEJIA, I. C., RIVA, E., PERNOT, J., UBAGS, N., FAJAS, L., NICOD, L. P. & MARSLAND, B. J. 2018. Dietary Fiber Confers Protection against Flu by Shaping Ly6c(-) Patrolling Monocyte Hematopoiesis and CD8(+) T Cell Metabolism. *Immunity,* 48**,** 992-1005 e8.
VERLEDEN, G. M., GLANVILLE, A. R., LEASE, E. D., FISHER, A. J., CALABRESE, F., CORRIS, P. A., ENSOR, C. R., GOTTLIEB, J., HACHEM, R. R., LAMA, V., MARTINU, T., NEIL, D. A. H., SINGER, L. G., SNELL, G. & VOS, R. 2019. Chronic lung allograft dysfunction: Definition, diagnostic criteria, and approaches to treatment-A consensus report from the Pulmonary Council of the ISHLT. *J Heart Lung Transplant,* 38**,** 493-503.

VERLEDEN, G. M., RAGHU, G., MEYER, K. C., GLANVILLE, A. R. & CORRIS, P. 2014. A new classification system for chronic lung allograft dysfunction. *J Heart Lung Transplant,* 33**,** 127-33.
VERLEDEN, S. E., RUTTENS, D., VANDERMEULEN, E., BELLON, H., DUBBELDAM, A., DE WEVER, W., DUPONT, L. J., VAN RAEMDONCK, D. E., VANAUDENAERDE, B. M., VERLEDEN, G. M., BENDEN, C. & VOS, R. 2016. Predictors of survival in restrictive chronic lung allograft dysfunction after lung transplantation. *J Heart Lung Transplant,* 35**,** 1078-84.
VERLEDEN, S. E., VANAUDENAERDE, B. M., EMONDS, M. P., VAN RAEMDONCK, D. E., NEYRINCK, A. P., VERLEDEN, G. M. & VOS, R. 2017. Donor-specific and -nonspecific HLA antibodies and outcome post lung transplantation. *Eur Respir J,* 50.
VERLEDEN, S. E., VON DER THUSEN, J., ROUX, A., BROUWERS, E. S., BRAUBACH, P., KUEHNEL, M., LAENGER, F. & JONIGK, D. 2020a. When tissue is the issue: A histological review of chronic lung allograft dysfunction. *Am J Transplant,* 20**,** 2644-2651.
VERLEDEN, S. E., VON DER THUSEN, J., VAN HERCK, A., WEYNAND, B., VERBEKEN, E., VERSCHAKELEN, J., DUBBELDAM, A., VANAUDENAERDE, B. M., VOS, R., VERLEDEN, G. M. & LEUVEN LUNG TRANSPLANT, G. 2020b. Identification and characterization of chronic lung allograft dysfunction patients with mixed phenotype: A single-center study. *Clin Transplant,* 34**,** e13781.
VIBOUD, C., SIMONSEN, L., FUENTES, R., FLORES, J., MILLER, M. A. & CHOWELL, G. 2016. Global Mortality Impact of the 1957-1959 Influenza Pandemic. *J Infect Dis,* 213**,** 738-45.
VIVIER, E. & MALISSEN, B. 2005. Innate and adaptive immunity: specificities and signaling hierarchies revisited. *Nat Immunol,* 6**,** 17-21.
VOS, R., VANAUDENAERDE, B. M., OTTEVAERE, A., VERLEDEN, S. E., DE VLEESCHAUWER, S. I., WILLEMS-WIDYASTUTI, A., WAUTERS, S., VAN RAEMDONCK, D. E., NAWROT, T. S., DUPONT, L. J. & VERLEDEN, G. M. 2010. Long-term azithromycin therapy for bronchiolitis obliterans syndrome: divide and conquer? *J Heart Lung Transplant,* 29**,** 1358-68.
WALLACE, D. F. 2016. The Regulation of Iron Absorption and Homeostasis. *Clin Biochem Rev,* 37**,** 51-62.
WARSZAWSKA, J. M., GAWISH, R., SHARIF, O., SIGEL, S., DONINGER, B., LAKOVITS, K., MESTERI, I., NAIRZ, M., BOON, L., SPIEL, A., FUHRMANN, V., STROBL, B., MULLER, M., SCHENK, P., WEISS, G. & KNAPP, S. 2013. Lipocalin 2 deactivates macrophages and worsens pneumococcal pneumonia outcomes. *J Clin Invest,* 123**,** 3363-72.
WATANABE, T., MARTINU, T., CHRUSCINSKI, A., BOONSTRA, K., JOE, B., HORIE, M., GUAN, Z., BEI, K. F., HWANG, D. M., LIU, M., KESHAVJEE, S. & JUVET, S. C. 2019. A B cell-dependent pathway drives chronic lung allograft rejection after ischemia-reperfusion injury in mice. *Am J Transplant,* 19**,** 3377-3389.
WEBSTER, R. G., BEAN, W. J., GORMAN, O. T., CHAMBERS, T. M. & KAWAOKA, Y. 1992. Evolution and ecology of influenza A viruses. *Microbiol Rev,* 56**,** 152-79.
WRAMMERT, J., SMITH, K., MILLER, J., LANGLEY, W. A., KOKKO, K., LARSEN, C., ZHENG, N. Y., MAYS, I., GARMAN, L., HELMS, C., JAMES, J., AIR, G. M., CAPRA, J. D., AHMED, R. & WILSON, P. C. 2008. Rapid cloning of high-

affinity human monoclonal antibodies against influenza virus. *Nature,* 453**,** 667-71.
WU, C., OROZCO, C., BOYER, J., LEGLISE, M., GOODALE, J., BATALOV, S., HODGE, C. L., HAASE, J., JANES, J., HUSS, J. W., 3RD & SU, A. I. 2009. BioGPS: an extensible and customizable portal for querying and organizing gene annotation resources. *Genome Biol,* 10**,** R130.
WYPYCH, T. P., WICKRAMASINGHE, L. C. & MARSLAND, B. J. 2019. The influence of the microbiome on respiratory health. *Nat Immunol,* 20**,** 1279-1290.
YANG, Y., WANG, H., KOUADIR, M., SONG, H. & SHI, F. 2019. Recent advances in the mechanisms of NLRP3 inflammasome activation and its inhibitors. *Cell Death Dis,* 10**,** 128.

CURRICULUM VITAE

DR. MED. UNIV. MARTIN WATZENBÖCK

Geburtsdatum:	22. Oktober 1989
Geburtsort:	Wien
Nationalität:	Österreich
Adresse:	Staudgasse 20/15, 1180 Wien
E-Mail:	martin.watzenboeck@gmail.com
Telefon:	+43 (0)699 10143006

AUSBILDUNG

2020 – derzeit	Facharztausbildung im Sonderfach “Radiologie“ an der Universitätsklinik für Radiologie und Nuklearmedizin der Medizinischen Universität Wien
2015 - derzeit	PhD Studium, Center for Molecular Medicine (CeMM) der österreichischen Akademie der Wissenschaften und Medizinische Universität Wien – Dissertation unter Begutachtung
Oktober 2014	Dr. med. univ., Medizinische Universität Innsbruck
2008 - 2014	Studium der Humanmedizin, Medizinische Universität Innsbruck
2000 – 2008	Bundesgymnasium Vöcklabruck, Matura mit ausgezeichnetem Erfolg

BERUFLICHER WERDEGANG

08/2020 – derzeit	Assistenzarzt in Facharztausbildung im Sonderfach “Radiologie“ an der Universitätsklinik für Radiologie und Nuklearmedizin der Medizinischen Universität Wien
02/2021 – 05/2021	Internistischer Teil der Basisausbildung an Klin. Abteilung für Endokrinologie und Stoffwechsel, Univ. Klinik für Innere Medizin III der Medizinischen Universität Wien
11/2020 – 2/2021	Chirurgischer Teil der Basisausbildung an der Univ. Klinik für Thoraxchirurgie der Medizinischen Universität Wien
03/2015 – 08/2020	PhD Student im FWF-geförderten Doktoratskolleg CCHD (Cell Communication in Health and Disease), Center for Molecular Medicine (CeMM) der österreichischen Akademie der Wissenschaften und Medizinische Universität Wien Titel: *“Immune-microbe interactions in the context of the lungs”* – unter Begutachtung Betreuerin: Prof. Dr. Sylvia Knapp, PhD
09/2018 - 12/2018	Forschungsaufenthalt (3 Monate) im Rahmen des PhD-Studiums im Labor von Prof. Dr. Benjamin Marsland, Department of Immunology and Pathology, Monash University, Melbourne, Australien

10/2017 - 12/2017	Forschungsaufenthalt (3 Monate) im Rahmen des PhD-Studiums im Labor von Prof. Dr. Benjamin Marsland, Service de Pneumologie, Centre Hospitalier Universitaire Vaudois (CHUV), Lausanne, Schweiz
11/2014 – 03/2015	Praktikum im Labor von Prof. DDr. Christoph J. Binder, Center for Molecular Medicine (CeMM) und Institut für Labormedizin (KILM), Medizinische Universität Wien
12/2013 – 02/2014	Studienkoordinator innerhalb der ASTUTE RUBY STUDY - *"Identification and validation of biomarkers of acute kidney injury"* Gemeinsame Einrichtung für Internistische Notfall- und Intensivmedizin, Department Innere Medizin, Medizinische Universität Innsbruck
2013 – 2014	Diplomarbeit - *"Retrospective analysis of the impact of SeptiFast on the chosen antimicrobial strategy in intensive care patients"* Betreuer: Prof. Dr. Michael Joannidis, Leiter der Gemeinsamen Einrichtung für Internistische Notfall- und Intensivmedizin, Department Innere Medizin, Medizinische Universität Innsbruck

PUBLIKATIONEN

M. L. Watzenboeck, B. H. Heidinger, J. Rainer, V. Schmidbauer, B. Ulm, E. Rubesova, D. Prayer, G. Kasprian, F. Prayer#. „*Reproducibility of 2D vs. 3D radiomics for quantitative assessment of fetal lung development: a retrospective fetal MRI study*" – unter Review.

F. Prayer, P. Kienast, A. Strassl, P. Moser, D. Bernitzky, C. Milacek, M. Gyöngyösi, D. Kifjak, S. Röhrich, L. Beer, **M. L. Watzenboeck**, R. I. Milos, C. Wassipaul, D. Gomplemann, C. J. Herold, H. Prosch, B. H. Heidinger#. „*Ultra-high-resolution photon-counting detector vs. high-resolution conventional energy-integrating detector computed tomography for post-Covid lung imaging*" – unter Review.

M. L. Watzenboeck, L. Beer#, D. Kifjak, S. Röhrich, B. H. Heidinger, F. Prayer, R. I. Milos, P. Apfaltrer, G. Langs, P. A. T. Baltzer and H. Prosch. „*Contrast agent dynamics determine CT radiomics profiles and machine-learning-based tumor identification in oncologic imaging"* – unter Review.

F. Prayer, **M. L. Watzenboeck**, B. Heidinger, J. Rainer, V. Schmidbauer, H. Prosch, B. Ulm, E. Rubesova, D. Prayer, G. Kasprian#. "*Standardized in-vivo fetal MRI acquisition allows non-invasive and reproducible extraction of radiomics features from the developing lung for quantitative tissue characterization*" – unter Review.

R. Gawish, B. Maier, G. Obermayer, **M. L. Watzenboeck**, A. D. Gorki, F. Quattrone, A. Farhat, K. Lakovits, A. Hladik, A. Korosec, A. Alimohammadi, I. Mesteri, F. Oberndorfer, F. Oakley, J. Brain, L. Boon, I. Lang, C. Binder, S. Knapp#. "*A neutrophil -B-cell axis governs disease tolerance during sepsis via Cxcr4*" – in Revision.

N. Bayer, B. Hausman, R. Vinay-Pandey, F. Deckert, L. Gail, J. Strobl, P. Pjevac, C. Krall, L. Unterluggaurer, A. Redl, V. Bachmayr, L. Kleissl, M. Nehr, R. Kirkegaard, A. Makristathis, **M. L. Watzenboeck**, R. Nica, C. Staud, L. Hammerl, P. Wohlfarth, R. C. Ecker, S. Knapp5 W. Rabitsch, D. Berry, G. Stary#. "*Disturbances in microbial skin recolonization and cutaneous immune response following allogeneic stem cell transfer*" – in Revision.

S. Zahalka., P. Starkl, **M. L. Watzenboeck**, A. Farhat, M. Radhouani, F. Deckert, A. Hladik, K. Lakovits, F. Oberndorfer, C. Lassnig, B. Strobl, K. Klavins, M. Matsushita, D. E. Sanin, K. Grzes, E. Pearce, A. D. Gorki, S. Knapp#, (2022). "*Trained immunity of alveolar macrophages requires metabolic rewiring and type 1 interferon signalling*". **Mucosal Immunology** (akzeptiert und im Druck). Impact Factor 8,7

A. Benazzo, S. Bozzini, S. Auner, H.O. Berezhinskiy, **M.L. Watzenboeck**, S. Schwarz, T. Schweiger, W. Klepetko, T. Wekerle, K. Hoetzenecker, F. Meloni, P. Jaksch#. *"Differential expression of circulating miRNAs after alemtuzumab induction therapy in lung transplantation"* – **Sci Rep**. 2022 Apr 30;12(1):7072. Impact Factor 5,0

M. L. Watzenboeck, P. Starkl, B. Drobits, A. D. Gorki, S. E. Zahalka, K. Lakovits, A. Hladik and S. Knapp#. *"Lipocalin 2 modulates antiviral immunity in a microbiome dependent manner"* – **PLoS Pathog**. 2021 Apr 27;17(4) Impact Factor 7,42

M. L. Watzenboeck*, A.D. Gorki*, F. Quattrone*, R. Gawish*, S. A. Schwarz*, C. Lambers, P. Jaksch, K. Lakovits, D. Symmank, P. Starkl, S. Zahalka, T. Artner, C. Pattaroni, N. Fortelny, B. J. Marsland, K. Hoetzenecker, S. Knapp*# and S. Widder1,2*#. *"Multi-omics profiling predicts allograft function after lung transplantation."* – **Eur Respir J**. 2021 Jul 8:2003292. Impact Factor 33,8

P. Starkl#, N. Gaudenzio, T. Marichal, L. L. Reber, R. Sibilano, **M. L. Watzenboeck**, F. Fontaine, A. C. Mueller, M. Tsai, S. Knapp, S. J. Galli# (2021). *"IgE antibodies increase honeybee venom responsiveness and detoxification efficiency of mast* cells" – **Allergy**. 2021 Apr 11:10.1111 Impact Factor 14,71

Schwarz*, S., N. Rahimi*, D. Kifjak, M. Muckenhuber, **M. L. Watzenboeck**, A. Benazzo, P. Jaksch, S. Knapp, W. Klepetko, K. Hoetzenecker# and Vienna Lung Transplant Group (2020). *"Comparison of donor scores in bilateral lung transplantation-A large single-center analysis."* **Am J Transplant.** 2021 Jun;21(6):2132-2144 Impact Factor 9,37

Starkl, P#., **M. L. Watzenboeck**, L. M. Popov, S. Zahalka, A. Hladik, K. Lakovits, M. Radhouani, A. Haschemi, T. Marichal, L. L. Reber, N. Gaudenzio, R. Sibilano, L. Stulik, F. Fontaine, A. C. Mueller, M. R. Amieva, S. J. Galli# and S. Knapp# (2020). "IgE Effector Mechanisms, in Concert with Mast Cells, Contribute to Acquired Host Defense against Staphylococcus aureus." **Immunity** 53(6): 1333 Impact Factor 43,47

Pattaroni, C., **M. L. Watzenboeck**, S. Schneidegger, S. Kieser, N. C. Wong, E. Bernasconi, J. Pernot, L. Mercier, S. Knapp, L. P. Nicod, C. P. Marsland, M. Roth-Kleiner and B. J. Marsland# (2018). *"Early-life formation of the microbial and immunological environment of the human airways."* **Cell Host Microbe** 24(6): 857-865 e854. Impact Factor 31,32

Hendrikx, T., **M. L. Watzenboeck**, S. M. Walenbergh, S. Amir, S. Gruber, M. O. Kozma, H. I. Grabsch, G. H. Koek, M. J. Pierik, K. Staufer, M. Trauner, S. C. Kalhan, D. Jonkers, M. H. Hofker, C. J. Binder# and R. Shiri-Sverdlov# (2016). *"Low levels of IgM antibodies recognizing oxidation-specific epitopes are associated with human non-alcoholic fatty liver disease."* **BMC Med** 14(1): 107. Impact Factor 11,15

REVIEWS

R. I. Milos, C. Bartha, S. Röhrich, B. H. Heidinger, F. Prayer, L. Beer, C. Wassipaul, D. Kifjak, M**. L. Watzenboeck**, H. Prosch#. *"Imaging in patients with acute dyspnea"* - in Revision

S. Röhrich, B. H. Heidinger, F. Prayer, D. Kifjak, L. Beer, C. Wassipaul, **M. L. Watzenboeck**, R. I. Milos, H. Prosch#. "*Smoking-related interstitial lung diseases*" - **Radiologie** (Heidelb). 2022 Jun 23.

* AutorInnen trugen gleichermaßen bei, # korrespondierende AutorInnen

REVIEWTÄTIGKEIT

European Radiology

PLOS One

Clinical and Experimental Allergy

LEHRE

Wintersemester 2022/23 KPJ-Mentoring und Famulaturbetreuungen - Universitätsklinik für Radiologie und Nuklearmedizin der Medizinischen Universität Wien

Sommersemester 2022 Famulaturbetreuungen - Universitätsklinik für Radiologie und Nuklearmedizin der Medizinischen Universität Wien

Sommersemester 2022 OSCE-Prüfer „Thoraxröntgen" – Medizinische Universität Wien

Sommersemester 2022 Famulaturbetreuungen - Universitätsklinik für Radiologie und Nuklearmedizin der Medizinischen Universität Wien

Wintersemester 2021/22 Grundkurs Ultraschall – Universitätsklinik für Radiologie und Nuklearmedizin der Medizinischen Universität Wien

KONFERENZEN

10/2021	34. Tagung der österreichischen Gesellschaft für Transplantation, Transfusion und Genetik - AUSTROTRANSPLANT 2021 – eingeladener Sprecher
03/2021	European Congress of Radiology
10/2020	44th Annual Meeting of the Austrian Society of Pneumology and the Austrian Society of Thoracic Surgery – virtuelle Posterpräsentation
09/2020	ISHLTv Webinar: Molecular Mechanisms of Allograft Injury and CLAD – virtuelle Podiumspräsentation
11/2019	ÖGAI Symposium 2019, Graz, Austria – Posterpräsentation
10/2019	3rd AMICI Symposium, Innsbruck, Austria
06/2019	15th YSA PhD-Symposium of the Medical University of Vienna - Podiumspräsentation
06/2018	14th YSA PhD-Symposium of the Medical University of Vienna – Posterpräsentation
02/2018	Cell-Weizmann Institute of Science Symposium – Next Gen Immunology, Tel Aviv, Israel – Posterpräsentation
06/2017	13th YSA PhD-Symposium of the Medical University of Vienna – Podiumspräsentation

04/2017	10th Bridging the Gap Symposium, Vienna, Austria – Posterpräsentation
02/2017	1st AMICI Symposium, Vienna, Austria
06/2016	12th YSA PhD-Symposium of the Medical University of Vienna - Posterpräsentation
02/2016	9th Bridging the Gap Symposium, Vienna, Austria – Posterpräsentation
12/2015	ÖGAI Symposium 2015, Vienna, Austria - Posterpräsentation
09/2015	4th European Congress of Immunology, Vienna, Austria

KURSE

06/2022-07/2022	OIC - Oncologic Imaging Course 2022 (ESOI), Dubrovnik, Kroatien
04/2016 – 06/2016	Computational Methods in Microbial Ecology, Universität Wien
10/2015	FELASA B – Basics of Laboratory Animal Science, Veterinärmedizinische Universität Wien
09/2015	18th International Summer School on Immunology (FEBS), Rabac, Kroatien

MITGLIEDSCHAFT IN FACHGESELLSCHAFTEN

ÖGMBT - Österreichische Gesellschaft für Molekulare Biowissenschaften und Biotechnologie

ÖGAI - Österreichische Gesellschaft für Allergologie und Immunologie

MIC - Medical Imaging Cluster, Medizinische Universität Wien

FÖRDERUNGEN UND PREISE

10/2020	Posterpreis (1. Platz) 44th Annual Meeting of the Austrian Society of Pneumology and the the Austrian Society of Thoracic Surgery
06/2019	Oral Presentation Award 15th YSA PhD-Symposium of the Medical University of Vienna
10/2017	Böhringer Ingelheim Foundation Travel Grant (für dreimonatigen Auslandsaufenthalt in Lausanne)
06/2017	Oral Presentation Award 13th YSA PhD-Symposium of the Medical University of Vienna
2015-2019	PhD Stipendium des CCHD (Cell Communication in Health and Disease) Doktoratskollegs

SPRACHEN und FÄHIGKEITEN

SPRACHEN

- Deutsch Muttersprache
- Englisch C1
- Spanisch A2

EDV

- Programmiersprachen: Python, R, UNIX Shell
- Extraktion und Analyse von multiparametrischen Bilddaten (“Radiomics”)
- Analyse von RNA-Sequencing, Amplicon-Sequencing, Proteomics, Lipidomics und Metabolomics Datensätzen
- Automatisierte Bildanalyse

LABORFERTIGKEITEN

- Molekularbiologie (Zellkultur, DNA/RNA Extraktion, PCR, Western Blot, ELISA)
- Aufbereitung von Next Generation Sequencing Libraries
- Umgang mit Mäusen (i.p und i.v. Injektionen, Blutentahme, intranasale Infektion)
- Durchflusszytometrie